

[illegible]

Manuel Markus Menapace, BSc



Manuel Markus Menapace, BSc

State of the Art of Direct Lignin Liquefaction

MASTER'S THESIS

to achieve the university degree of

Diplomingenieur

Master's degree program: Chemical and Pharmaceutical Engineering

submitted to

Graz University of Technology

Supervisor:

Priv.-Doz. Dipl.-Ing. Dr. techn. Nikolaus Schwaiger

Institute of Chemical Engineering and Environmental Technology

Graz, December 2023

STATUTORY DECLARATION

I declare that I have authored this thesis independently, that I have not used other than the declared sources / resources, and that I have explicitly marked all material which has been quoted either literally or by content from the used sources.

Graz,

(date)

(signature)

Kurzfassung

Lignin, ein Nebenprodukt der Papier- und Zellstoffherstellung, wird derzeit fast ausschließlich verbrannt. Dieses Makromolekül, das sich aus phenolischen Komponenten zusammensetzt, könnte sich als eine wertvolle Quelle für Feinchemikalien erweisen. Die Pyrolyse bietet einen thermo-chemischen Weg zur Fragmentierung von Lignin. In dieser Arbeit wird die Verarbeitung von Lignin durch Flash-Pyrolyse im Rahmen einer Literaturrecherche bewertet. Neben einem Überblick über die Grundlagen der Lignin Pyrolyse, wie technische Parameter, Produktverteilung und chemische Reaktionen, werden der aktuelle Stand der Technik sowie neue Herausforderungen dargestellt. Es wird gezeigt, dass die Wechselwirkungen zwischen Prozessparametern und Reaktionswegen noch Forschungsbedarf in grundlegenden Themen haben. Häufige technische Schwierigkeiten sind Verstopfungen des Beschickungssystems und Agglomeratbildung im Reaktorbett. Die größten bekannten Versuchsanlagen pyrolysieren bis zu 1500 g Lignin bei Raten von maximal 600 g/h mit Pyrolyseölausbeuten von 30-50 %. Die Ausbeute an phenolischen Monomeren liegt im Bereich von 5-10 %. Faktoren, die den Pyrolyseprozess beeinflussen, werden analysiert und auf der Grundlage dieser Faktoren werden Optimierungsmöglichkeiten ermittelt. Der Einsatz von Katalysatoren, die Depolymerisation vor der Pyrolyse und die Co-Pyrolyse mit wasserstoffreichen Substraten sind geeignete Optionen zur Optimierung der Lignin Pyrolyse. Schließlich wird auf der Grundlage der gesammelten Daten ein Verfahren zur Ausfällung von Lignin aus Schwarzlauge mit anschließender Flash-Pyrolyse modelliert. Die Massen- und Energieströme sowie die thermischen und prozesschemischen Kosten werden abgeschätzt. In dem modellierten Prozess, mit einem Einsatz von 100 kt/a Schwarzlauge, werden 2,92 kt/a Pyrolyseöl erzeugt. Als Kosten für das erzeugte Pyrolyseöl werden auf 550 €/t berechnet.

Abstract

Lignin, a by-product of paper and pulp production, is currently almost exclusively incinerated. This macromolecule, which is made up of phenolic components, could contribute to be a valuable source of fine chemicals. Pyrolysis offers a thermo-chemical pathway to lignin fragmentation. In this thesis, the processing of lignin by flash pyrolysis is evaluated in the course of a literature review. In addition to an overview of the basic principles of lignin pyrolysis such as technical parameters, product distribution, and chemical reactions, the current state of the art as well as emerging challenges are presented. It is shown that the interactions between process parameters and reaction pathways still require fundamental scientific research. Common difficulties are blockages of the feed system and agglomerate formation in the reactor bed. The largest known experimental plants pyrolyze up to 1500 g of lignin at rates of around 600 g/h with pyrolysis oil yields of 30-50%. Yields of phenolic monomers are in the range of 5-10 %. Factors influencing the pyrolysis process are analysed and optimisation options are identified on the basis of these factors. The use of catalysts, depolymerisation before pyrolysis, and co-pyrolysis with hydrogen-rich substrates are feasible options for optimising lignin pyrolysis. Finally, based on the data collected, a process for the precipitation of lignin from kraft black liquor with subsequent flash pyrolysis is modelled. The mass and energy flows as well as the thermal and process chemicals-related costs are estimated. In the modelled process with a feed of 100 kt/y of black liquor, 2.92 kt/y of pyrolysis oil is produced. The cost in terms of produced pyrolysis oil is estimated to 550 €/t.

Acknowledgments

The following words are addressed to all those who have supported me so energetically with theoretical knowledge, patience, and kindness in the course of my studies and in particular in the preparation of this thesis. You have made all this possible in the first place.

First of all, I would also like to thank Dipl. Ing. Thomas Timmel, the managing director of BioBase GmbH, who coordinated the cooperation between TU-Graz and BioBase GmbH and always created a pleasant climate for discussion. Thomas brought humour to technical discussions as well as valuable professional input.

My special thanks go to Priv.-Doz. Dipl.-Ing. Dr.techn. Nikolaus Schwaiger. Niki always had an open ear for me, was able to solve every difficult question seemingly effortlessly and, above all, gave me the feeling that I could do anything thanks to his infinite patience and warm-hearted manner. In addition, thesis meetings are particularly instructive, where the peroral incorporation of products from industrial processes that microbiologically upgrade starchy substrates is not only treated in theory.

Special thanks go to my family, who have supported me all these years. You have always believed in me and supported me even in the most difficult times. I would also like to thank my wonderful partner Jelena, who has probably given me the most emotional support in my studies with her loving and caring nature.

Contents

1	Introduction.....	1
1.1	Wooden biomass.....	2
1.1.1	Macro- and microscopic structure of wood.....	2
1.1.2	Cell architecture of wood fibres.....	3
1.1.3	Cellulose.....	5
1.1.4	Hemicellulose.....	7
1.1.5	Lignin.....	9
1.2	Motivation and objectives.....	12
2	Fundamentals.....	13
2.1	Pulping processes.....	13
2.1.1	Sulfate process – Kraft process.....	14
2.1.2	Sulfite process.....	22
2.1.3	Organosolv process.....	25
2.1.4	Comparison of technical lignins.....	27
2.2	Pyrolysis.....	28
2.2.1	Pyrolysis products.....	30
2.2.2	Reactor types.....	33
3	State of the art of lignin pyrolysis.....	41
3.1	Basic information.....	42
3.1.1	Products.....	45
3.1.2	Reactions.....	54
3.2	State of art of lignin pyrolysis.....	63
3.2.1	Challenges of lignin pyrolysis.....	65
3.3	Tuning of lignin pyrolysis.....	68
3.3.1	Biomass.....	69
3.3.2	Isolation of lignin.....	70
3.3.3	Refinement.....	73
3.3.4	Process parameters of pyrolysis.....	82
3.4	Summary.....	89
4	Process modelling.....	92
4.1	Process model parameters and boundaries.....	92
4.2	Mass balance.....	95
4.2.1	Lignin precipitation and drying.....	95
4.2.2	Lignin Pyrolysis.....	96
4.2.3	Chemicals and water consumption.....	97
4.3	Energy consumption.....	99

4.3.1	Drying of lignin	99
4.3.2	Pyrolysis	100
4.3.3	Evaporation of washing water	100
4.3.4	Condensation of pyrolysis vapours	101
4.3.5	Energy supply by process byproducts.....	102
4.3.6	Energy balance.....	103
4.4	Cost estimation.....	104
4.4.1	Cost of process chemicals	104
4.4.2	Thermal energy related costs.....	104
4.4.3	Process costs – summary	105
5	Conclusion	106
6	Appendix	108
6.1	Literature	108
6.2	List of figures	121
6.3	List of tables	124

Symbols and Abbreviations

%	mass percent
°C	degrees centigrade
BFB	bubbling fluidized bed
C	carbon
Ca	catechol, calcium
CFB	circulating fluidized bed
C _p	specific heat capacity
DS	dry substance
EF	entrained flow
FB	fixed bed
g	gram
G	guaiacol
GC	gas chromatography
GC-MS	gas chromatography with mass spectroscopy
h	hour, enthalpy
h _c	enthalpy of condensation
h _p	enthalpy of pyrolysis
h _v	enthalpy of evaporation
H	hydrogen, p-hydroxyphenol
J	Joule
K	Kelvin
kg	kilogram
LCBM	lignocellulosic biomass
MALDI-TOF	matrix-assisted laser desorption time-of-flight

min	minute
M _n	average values of number based molecular size distributions
ms	millisecond
M _w	average values of weight based molecular size distributions
MWL	milled wood lignin
p	pressure
PL	pyrolytic lignin
S	syringol
SEM	scanning electron microscopy
T	temperature
t	metric ton
y	year

1 Introduction

This chapter covers the introduction to woody biomass, especially to the compound lignin. Furthermore, the goals and objectives of this thesis and the cooperation partner BioBase GmbH are presented.

The chemical industry generally strives for optimization in terms of product yield, economical profitability, environmental requirements, and energy demands. Some industrial processes have a higher potential for significant improvement than others. On the one hand, there are novel techniques which are especially prone to fundamental changes due to lack of experience and data from similar projects. On the other hand, there are historically proven processes that have been tried and tested over decades or even more than 100 years. In most cases latter procedures have been optimized to a point where further improvements mainly show up in minor variations in process parameters or in the use of enhanced equipment material. One prominent example which has been proven over time is the “kraft process” patented in 1884 by Carl Ferdinand Dahl [1]. The pulp and paper industry uses the kraft process for pulp production. Wood chips are treated chemically and thermally to separate cellulose from woody biomass. The remaining liquid the so called “black liquor” which is rich in lignin is subsequently concentrated and incinerated to generate process heat and to recycle used chemicals [1,2].

More than 100 years after C.F. Dahl patented the kraft process, many research papers and patents that deal with the topic of extended black liquor utilization were published. The industry started to explore alternatives to burning of black liquor and thus sophisticated lignin separation processes emerged in scientific literature [3,4]. This technical advancement led to larger quantities of available high purity lignin on the market and has thus initiated further research into lignin valorisation.

This thesis deals with a thermochemical processing method of lignin known as pyrolysis. Lignin pyrolysis could fundamentally improve the historically proven kraft process through improved utilisation of the lignin side stream. In the course of this thesis, the state of the art of lignin pyrolysis is evaluated. Finally, a pyrolysis process of kraft lignin is modelled.

1.1 Wooden biomass

This subchapter deals with basic aspects of wooden biomass. The structure of wood is presented, starting at a macroscopic level. The construction of wood cells and fibres is explained in more detail. Finally, an insight is given into the chemistry of the structurally and quantitatively most important components of wooden biomass, namely cellulose, hemicellulose and lignin.

1.1.1 Macro- and microscopic structure of wood

Basic knowledge of the structural composition of wood is essential for understanding the principles and limitations of pulping processes discussed in this thesis. As shown in Figure 1, wood has a complex hierarchical structure [5]. The first part of the figure shows the macroscopic structure of wood. In the centre of the cross-section of the log is the pith from which the annual rings grow radially outwards. New annual rings form in the cambium zone, just beneath the bark and cause the bark to shift outwards [6]. Rapid growth in the early seasons of the year results in larger lumens of the wood cells in the areas of the so called "early wood". In summer and autumn the growth decreases which results in denser areas known as "late wood" [7]. The difference between early wood and late wood is visually presented in the meso-scale section in Figure 1. In the rightmost area of Figure 1 the microscopic structure can be seen, here the lumen and cell walls are clearly visible. Despite different classifications of wood, such as hardwood and softwood, and variations in the visibility of annual ring separation, this basic structure applies to the majority of woody biomass [5]. More detailed insights into the structure of wood cells are given in chapter 1.1.2.

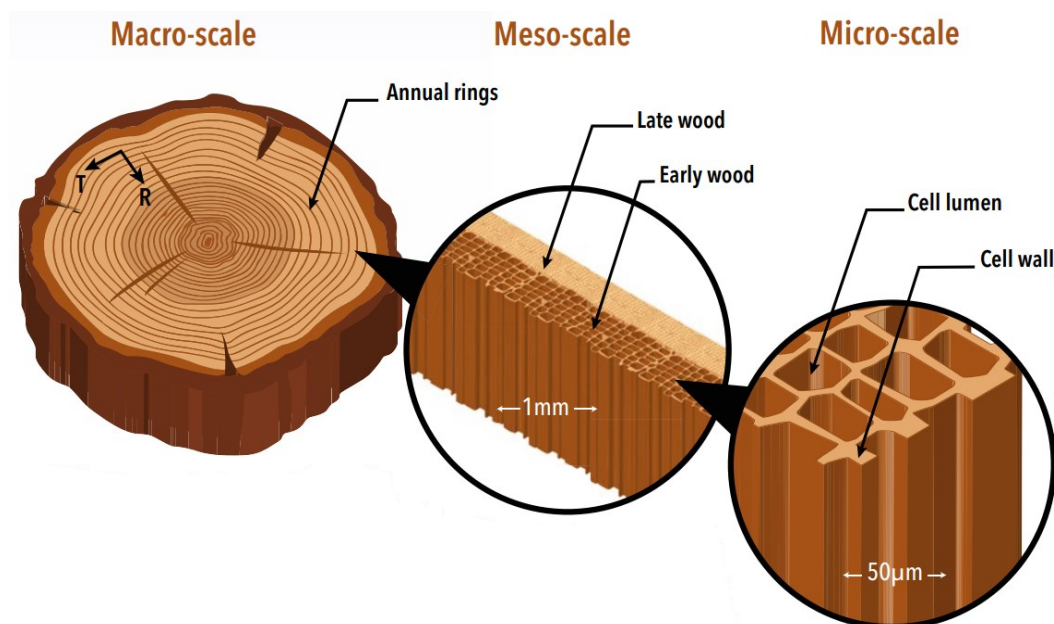


Figure 1: Macro to micro-scale structures of wood [5]

1.1.2 Cell architecture of wood fibres

The first microscopic image of a wood tracheid, in which cell walls and lumen are clearly distinguishable, was made by Bailey and Kerr at Harvard in 1935. A cross section of wood tracheids of the genus *siparuna bifida* is shown in Figure 2 [8].

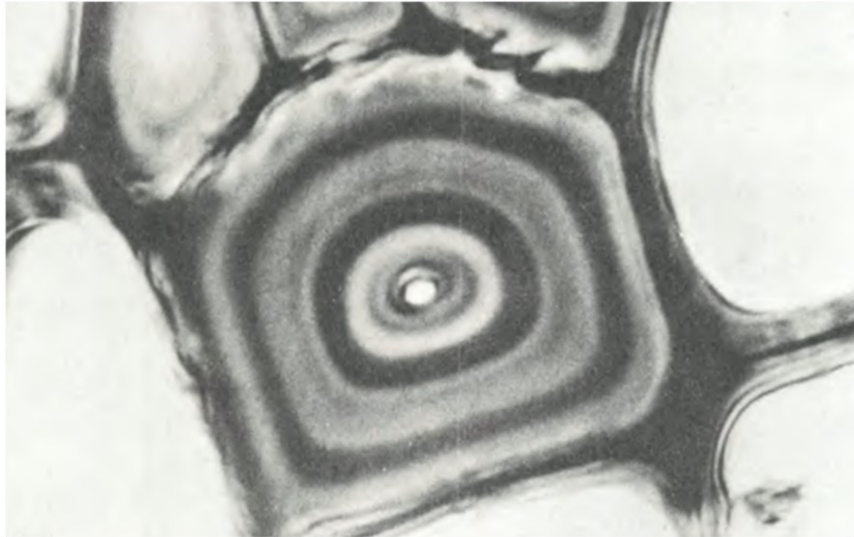


Figure 2: Cross section of a tracheid cell of *siparuna bifida* [8]

The dark area that connects the tracheid to adjacent cells is called middle lamella. The outermost layer of plant cells is the primary wall, from which the secondary walls 1-3 extend inwards. The lumen is in the middle of the cell. A labelled representation of the cell layers mentioned above is given in Figure 3 [9]. The primary wall of adjacent cells in conjunction with the middle lamella separating them is often referred to as compound middle lamella (CML) [10].

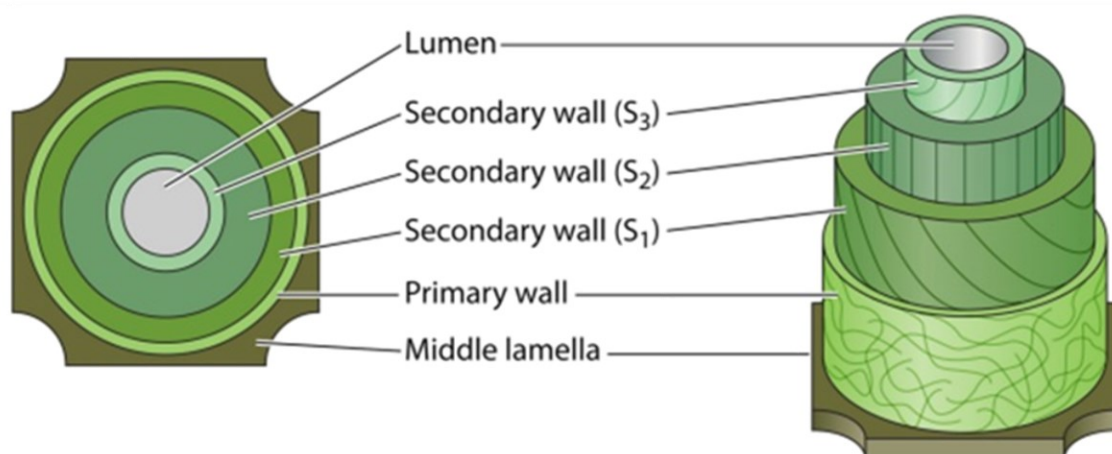


Figure 3: Cell layers of a plant cell - schematic representation [9]

Secondary walls 1-3 (S1-S3), the primary wall and the middle lamella differ in their molecular composition. The three most abundant macromolecules in wood are cellulose, hemicellulose,

and lignin. There are differences in the distribution of these macromolecules between different cell walls of one species and between the same cell wall of different species. The cell wall composition of e.g. S2 can even vary significantly within a plant. [11]. In S2 of *picea mariana*, for example, the lignin content differs from earlywood to latewood from 16 to 18 % whereas a lignin content of 74 % is measured in the CML [10]. The crosslinking of these macromolecules is highly complex, and many aspects thereof are part of current research. As shown in Figure 4, cellulose fibers form the basic framework of macro-molecular crosslinking. Hemicelluloses such as xylan bring flexibility and lignins mostly provide stability to the cell walls by binding the macromolecules glue-like together. Variation in composition of these components allows plants to provide suitable mechanical properties to different parts of their anatomy, such as wood, leaves, branches and bark [6].

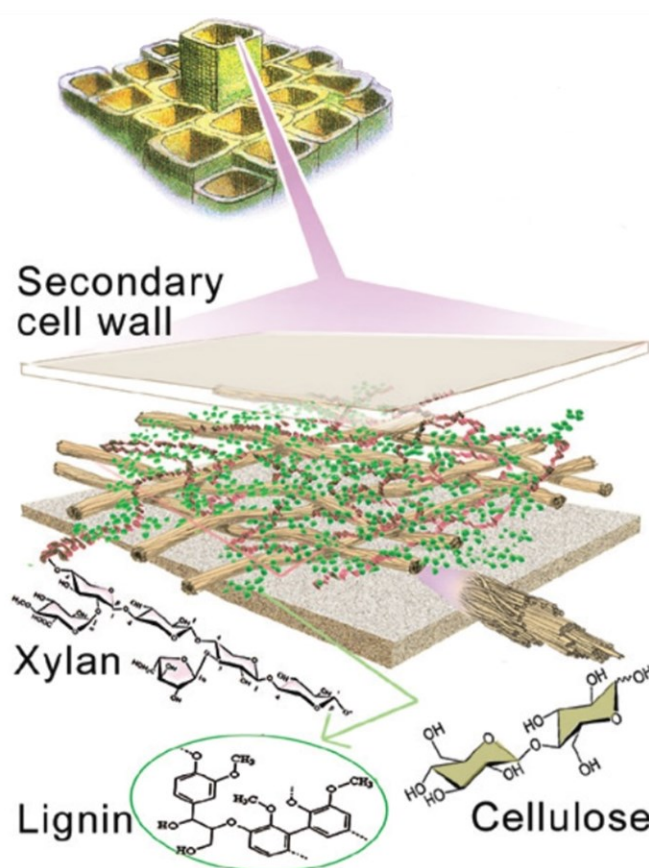


Figure 4: Macromolecular interconnections of cellulose, hemicelluloses and lignin in secondary walls [6]

A challenge to researchers over the last generations has been to develop concepts for efficient separation of wooden biomass into its components. Knowledge of chemical and physical properties of macro-molecules involved is important for designing efficient separation processes. Industrially relevant are pulping processes to isolate cellulose in large quantities, as described in more detail in chapter 2.1.

1.1.3 Cellulose

Cellulose is the most abundant organic compound in the world. With approximately 40 - 45 %, it also makes up the largest constituent of wood [12].

Chemically speaking, cellulose is a macromolecule, specifically a polysaccharide composed of many linked monosaccharide units. The monosaccharide β -D-glucopyranose, a cyclic form of glucose, is this basic building block [12]. Bonds formed by a condensation reaction of the anomeric hydroxy group of one monosaccharide with a hydroxy group of another monosaccharide are called O-glycosidic bonds [13]. In the example of cellulose, the hydroxy group of the hemiacetal at C1 reacts with the hydroxy group of C4 to form a covalent bond, which is termed as β -(1-4)-glycosidic bond. This reaction is a condensation reaction, in which a molecule of water is formed. The repeating disaccharide in cellulose, formed from β -D-glucopyranose by (1-4) glycosidic bonding, is called cellobiose and is shown in Figure 5. Up to about 15 000 glucose units may form one cellulose molecule [14].

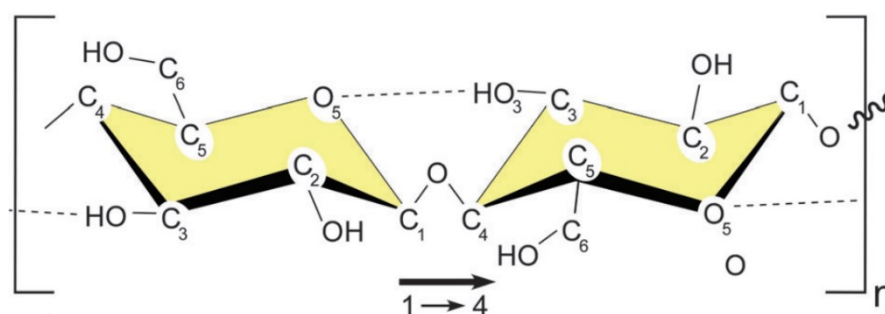


Figure 5: β -(1-4) glycosidic bond of β -D-glucopyranose units [14]

Free OH groups, in cellulose at the C2 and C6 atoms, represent dipoles that generally increase solubility in polar solvents such as water or ethanol. However, cellulose is shown to be insoluble in water and many polar organic solvents [15]. This discrepancy with empirical experience is due to stabilizing hydrogen bonding. Figure 5 shows an intramolecular hydrogen bond between the OH group at C3 and the heteroatom O5. Another intramolecular bond can be formed between the hydroxy groups of C2 and C5. Intermolecular (located between two neighbouring molecules) hydrogen bonds are particularly important for explaining water insolubility. There are several intermolecular bonding possibilities, some of which are shown in Figure 6 [14]. Type, number, and regularity of hydrogen bonds are responsible for the stability, reactivity, hydrophilicity, and solubility of cellulose. They also play a major role in the formation of amorphous and crystalline cellulose substructures. In cellulose fibres, adjacent cellulose chains can be arranged in different regularities. Areas in which there is a high degree of irregularity in the arrangement of adjacent cellulose chains are referred to as amorphous cellulose. In contrast,

highly ordered cellulose chains can form various crystalline structures [16]. The ratio of crystalline cellulose in relation to total cellulose is called crystallinity and is about 0.6 in spruce wood [17].

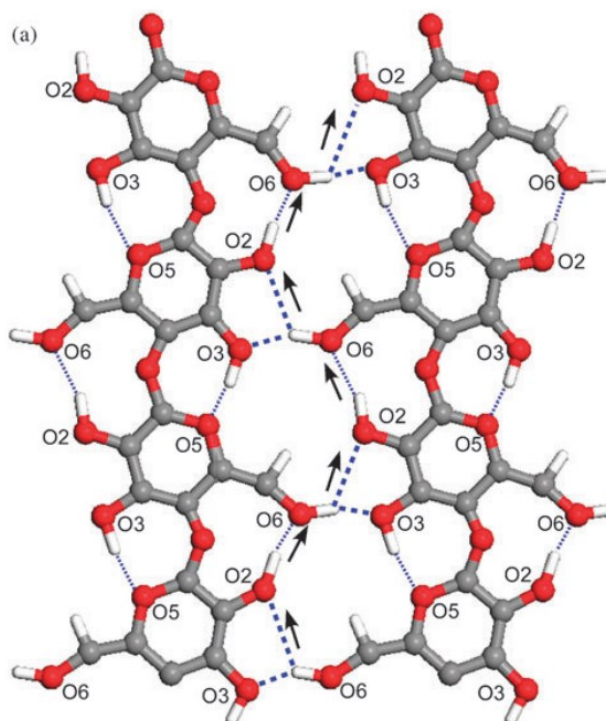


Figure 6: Intramolecular (thin dotted) and intermolecular (dotted) hydrogen bonds of cellulose chains [14]

Figure 7 schematically shows a cellulose microfibril composed of disordered and crystalline areas [14]. The biological importance of cellulose lies mainly in its structure-giving function and in water transportation inside the plant [18,19]. Physio-chemical characteristics of cellulose explained in this chapter are of significant importance for pulping processes hence, the separation of cellulose, hemicellulose, and lignin.

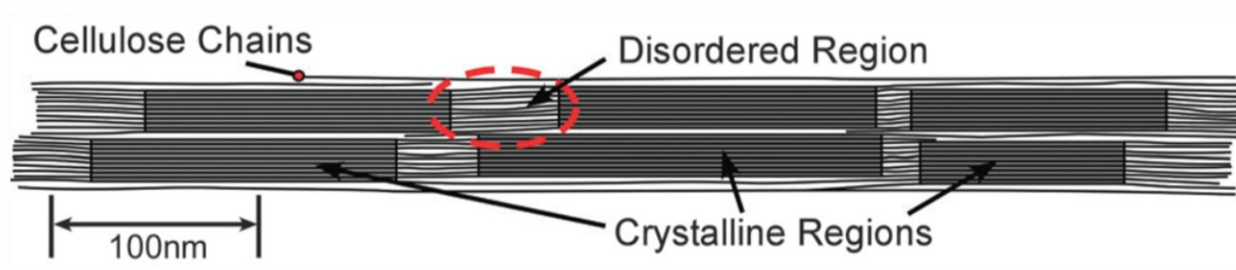


Figure 7: Schematics of a cellulose microfibril with regions of crystallinity and amorphous structure [14]

1.1.4 Hemicellulose

Besides cellulose, hemicelluloses are the most important and common polysaccharides in woody biomass, they make up about 25-35 % of dry matter [12].

In contrast to cellulose, hemicelluloses consist of several different monomer units. Predominant hexoses are glucose, mannose, and xylose which are most often found in the β -D-pyranose form in hemicelluloses. Furthermore, α -D-arabinofuranose, α -D-galactose and 4-O-methylglucopyranosyluronic acid are common monosaccharides. The location of interconnecting glycosidic bonds varies, the most common types are (1 \rightarrow 2), (1 \rightarrow 4) and (1 \rightarrow 6). The number of monomers per hemicellulose molecule is about 100-200, which is significantly less than in cellulose. The naming of many hemicelluloses is connected to their monosaccharide composition. For instance, a hemicellulose composed of galactose, glucose, and mannose is called galactoglucomannan. Proportions of the monosaccharides involved are not random, for example the molar ratios of the most common galactoglucomannan type hemicelluloses are either Gal:Glu:Man = 1:1:3 or Gal:Glu:Man = 0.1:1:4. These two types of galactoglucomannan together account for about 20 % of the dry matter of softwoods [12]. The structure of the main hemicellulose form in softwood is illustrated in Figure 8. It should be mentioned that hemicelluloses often carry acetyl and methyl groups. The O-acetyl-galactoglucomannan structure depicted in Figure 8 contains such acetyl groups, whereas the O-acetyl-(4-O-methylglucurono)xylan shown in Figure 9 contains both mentioned groups [20].

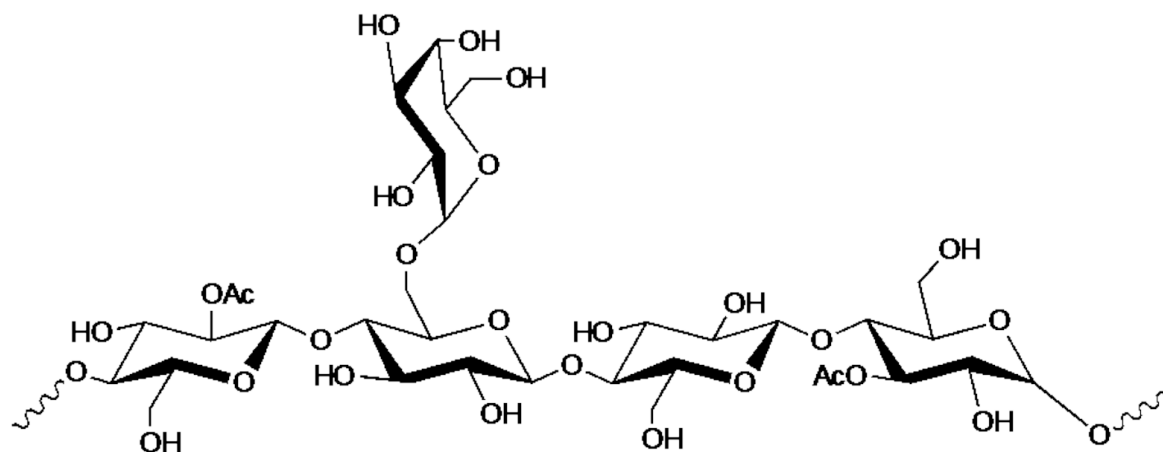


Figure 8: Molecular structure of a O-acetyl-galactoglucomannan type hemicellulose [20]

The most common classes of hemicellulose in hardwood are glucuronoxylans with a share of 15-30 % of the wood and glucomannans with 2-5 % [12]. A common glucuronoxylan variant is presented in Figure 9 [20].

Hemicelluloses have mostly limited solubility in water but can dissolve well in the alkaline range [21]. This aspect can be exploited to separate hemicellulose and lignin from cellulose. In addition to this alkaline extraction, hot water extraction, acid pre-treatment and ionic liquid extraction are among others also used [20].

The importance of hemicellulose for the plant is similar to that of cellulose, it is mainly a structure-giving function. However, the inhomogeneity of hemicellulose allows a more flexible approach to stabilising the plant. In the case of great mechanical stress, plants can respond by storing larger amounts of hemicellulose and lignin in the stressed areas [12].

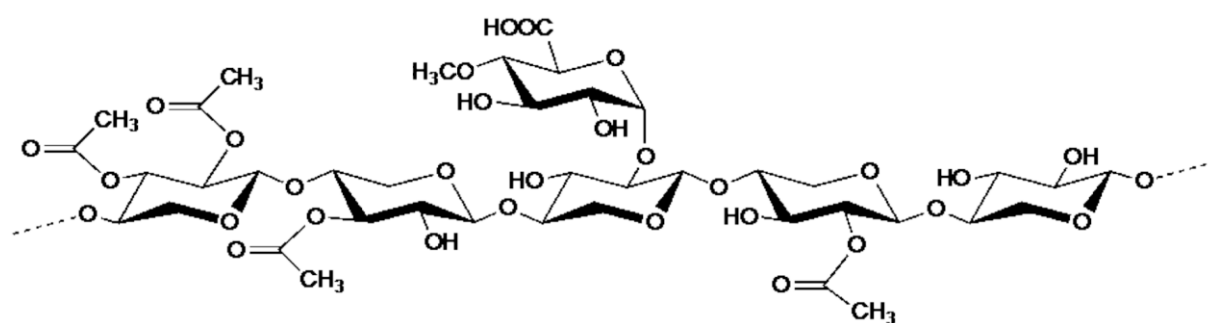


Figure 9: Molecular structure of a O-acetyl-(4-O-methylglucorono)xylan type hemicellulose [20]

1.1.5 Lignin

Besides cellulose with 40-50 % and hemicellulose with 25-35 %, lignin with 18-35 % makes up the third largest proportion of wood dry matter [12].

The word lignin was first used in literature in 1815 by Augustin Pyramus de Candolle for a substance that forms the basis of wood biomass. Candolle described a tasteless, fibrous substance that is insoluble in water and alcohol and soluble in mild bases. Furthermore, a strong coal formation during combustion and treatment with nitric acid was mentioned as well as the fact that lignin precipitates in the acidic range [22]. Chemically, lignin differs fundamentally from the two polymers already described, which are cellulose and hemicellulose. The formal building blocks are not monosaccharides but monolignols. Specifically, these are three phenylpropanoids, namely coumaryl alcohol, coniferyl alcohol and sinapyl alcohol. The structure of these molecules can be seen in Figure 10 [23].

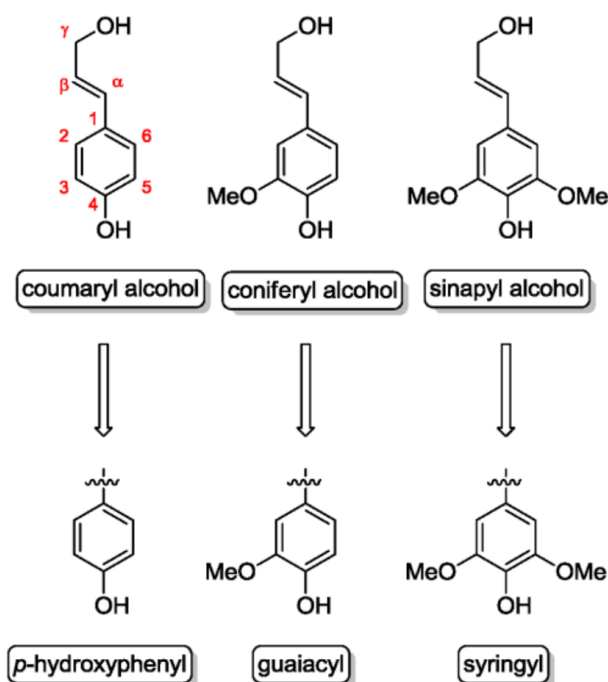


Figure 10: Molecular structure of monolignols and their corresponding fragments in lignin [23]

The numbers and Greek letters in red explain the notation of the positions of coumaryl alcohol. This notation is valid for all structures shown in figure 10 and similar derivatives. A common feature of all monolignols is a conjugated π -electron system extending across the phenol ring to the beta carbon atom. The propenyl group is always in para position to the phenolic hydroxy group. The molecules can be distinguished by the localisation and number of methoxy substituents. In the case of coumaryl alcohol, there is no methoxy group, coniferyl alcohol is substituted once at C3 and in the case of sinapyl alcohol the groups are located at C3 and C5 [23]. The aromatic fragments of the lignin structure formed from interconnections of monolignols are

called p-hydroxyphenyl, guaiacyl unit and syringyl unit. In literature they are usually abbreviated with H, G and S respectively. In plants, radical polymerisation of the three monolignols produces a complex three-dimensional polymer [2]. In lignin, there is no structured order of the monomers, the linkage is random due to its radical nature of polymerisation. This bio polymerisation is still well orchestrated and regulated by numerous processes [24]. It is assumed in the literature that milled wood lignin (MWL) is very similar to native lignin. Native lignin refers to lignin occurring in the living plant and MWL is produced by aqueous dioxane extraction of finely milled wood [25]. The molecular size distribution of MWL from spruce wood has a range of 200 g/mol to 1 million g/mol. This corresponds to an upper limit of about 5500 monolignols. The number average is 4500 g/mol which relates to 25 monolignol units. The molecular weight distribution of MWL of spruce wood is shown in Figure 11, note the logarithmic representation of the abscissa [26].

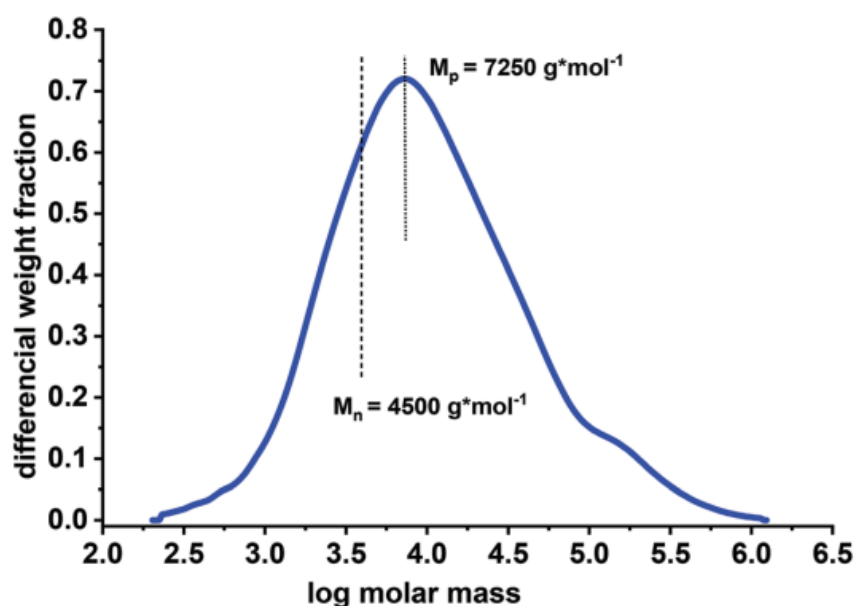


Figure 11: Molecular weight distribution of spruce wood MWL [26]

In addition to a broad distribution of the molecular size, the lignin structure is complicated by a variety of different linkages between the monomer units. Since the structure of native lignin is hardly accessible experimentally and lignin preparations possibly change its structure, the literature does not agree on whether lignin is linear or branched. However, Balakshin et al. were able to make a strong argument for branching in 2020 with the use of several independent test methods and comparison to literature data. Figure 12 shows structural model of a typical lignin molecule proposed by Balakshin et al. that corresponds to a number-based average molecule consisting of 25 monomers [26]. The dotted bonds in Figure 12 describe structural elements that are not clearly defined by this model and may vary. Structures that occur less frequently are surrounded by dotted boxes. Below 4 % of the monomers involved are present in such structures. The most common interunit linkage is the β -O-4 alkyl-O-aryl linkage which connects

50% of all monomers. The β -O-4 linkage can be seen in Figure 12 connecting for example units 1-2, 2-3 and 3-4. Alkyl-O-alkyl linkages, of which there exist many variants, connect 32 % of monolignols in MWL. Some examples for alkyl-O-alkyl interunit linkages in Figure 12 are the connections 2-9, 3-12 and 13-14.

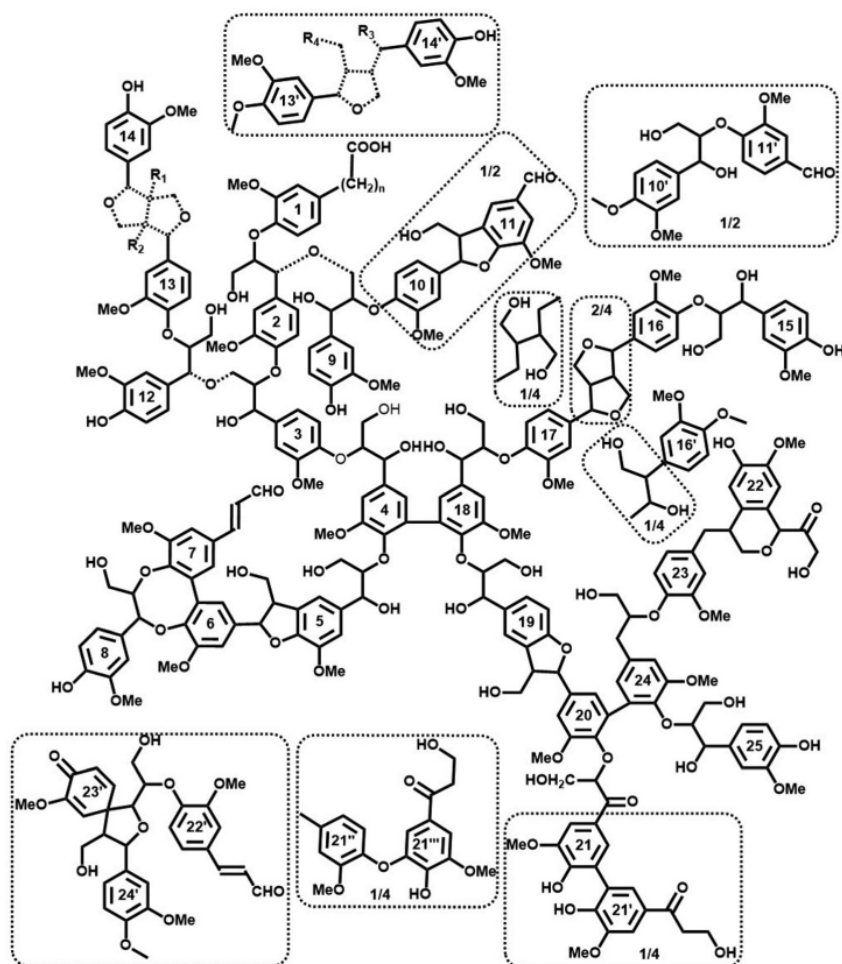


Figure 12: Structural model of spruce MWL [26]

The third most common group which occurs in 27 % of all aryl units are 5-5' linkages like biphenyl and dibenzodioxidine, which can be seen for example in the links between units 4-18, 6-7 and 20-24.

Regarding functional groups, phenolic OH groups, primary and secondary OH groups, carboxylic acids and carbonyls are mentioned [26]. The structural properties described so far refer to MWL. Chapter 2.1 describes technical pulping processes that produce lignins with partly different properties. Such lignins are referred to as technical lignins.

The biological functions of lignin are diverse and still the subject of research. Among the most important are plant growth and development, stability, water transport and protection against

biotic and abiotic stressors. Lignin has importance in drought and insect resistance, and in protection against heavy metals and extreme temperatures [27].

1.2 Motivation and objectives

This thesis results from a collaboration between BioBase GmbH and the Institute of Chemical Engineering and Environmental Technology of the Graz University of Technology. Networking of the project partners and general organisation is carried out by BioBase GmbH, an innovation platform for bioeconomy & circular economy [28].

With advancing scientific and technical development there is increasing interest in profitable and ecological use of organic components such as lignin in the handling of biomass. Lignin is characterised by a non-uniform composition of different chemical building blocks. This inhomogeneity of the underlying chemical bonds results in difficult analysis and highly complex reactions when further processing is attempted.

Lignin is currently, on large industrial scale applications, limited in its use. In industrial areas where large quantities of lignin are produced, it is most often burnt for recycling of chemicals and energy production [29]. The aim of this collaboration and equally of this master's thesis is to address the issue of lignin pyrolysis, a process for heat-induced liquefaction under oxygen exclusion [30]. In the context of this project a literature review with the topic of lignin pyrolysis is conducted. The main questions are the current state of research, possible applications, product distributions and an identification of possible chemical product groups. Further on, an industrial process model is designed based on the knowledge obtained. The constructed model serves as a starting point for the calculation of relevant mass flows and energy balances of the unit operations and the overall process. As a final step a cost estimation for the proposed process is conducted. In summary, this thesis serves to highlight the current state of knowledge on lignin pyrolysis and possible benefits for a biomass-based circular economy.

2 Fundamentals

Chapter 2 describes technically relevant pulping processes of woody biomass and process options for the subsequent isolation of lignin. Lignins that originate from the application of large-scale technical processes are called technical lignins. Different pulping processes produce technical lignins with varying properties. In technical lignins, properties such as molecular size distributions, chemical nature, toxicity, purity, yield, and sulfur content are diverse. These differences, which are elaborated in this chapter, affect the products and applicability of lignin pyrolysis as described in depth in chapter 3. Furthermore, an insight into the topic of pyrolysis of biomass in general is given.

2.1 Pulping processes

Pulping processes are processes in which the macromolecules hemicellulose and lignin are separated from cellulose fibres to produce pulp. Besides mechanical pulping processes, there are also biological and chemical methods.

In mechanical processes, mainly mechanical energy is used to produce wood fibres. In contrast to pulp from chemical or biological pulping processes, high proportions of lignin is present after mechanical treatment. Examples of mechanical pulping processes are the stone-ground wood pulp process or the refiner-mechanical pulp process. There are also thermo-mechanical pulp processes in which thermal energy is used to support fibre production. In chemo-thermo-mechanical pulp processes, chemicals are added to soften and remove lignin [31].

Biological pulping refers to the pre-treatment of wood biomass with microorganisms such as the white-rot fungus, which can metabolically degrade lignin [32], or with enzymes such as laccase or peroxidase, which have equivalent functions [33]. In biological pulping, the pre-treatment is followed by chemical or mechanical pulping. Biological pre-treatment is hardly used industrially, but it could have ecological advantages and is also said to produce pulp with higher strength [31].

Industrially most widespread are chemical pulping processes. In these processes, lignin and hemicellulose are dissolved using chemicals, increased pressure, and increased temperature. Cellulose fibres should remain as intact as possible to ensure sufficient quality of the paper produced. In exchange for the high cellulose fibre preservation that can be achieved in chemical pulp processes, the yield is lowered considerably. Chemical pulping achieves yields of 40-55 %, whereas mechanical pulping can achieve yields of over 90 % due to high proportions of lignin in the resulting pulp. The most important chemical pulping processes are the sulfate process, also known as the Kraft process, the sulfite process and the organosolv process [31]. In this chapter chemical pulping processes will be discussed in more detail, as the industrial

lignin production of mechanical and biological pulping processes is negligible in comparison [34].

2.1.1 Sulfate process – Kraft process

The history of the Kraft process begins with the soda process patented by Charles Watts and Hugh Burgess in 1854. In this process, biomass is delignified with sodium hydroxide under elevated temperature and pressure. The cellulose which does not dissolve is then used to produce pulp for paper manufacturing [35]. 30 years later, this process was modified. C. F. Dahl, a resident of the city of Danzig, which was part of the Kingdom of Prussia of the German empire at that time, added further chemicals to the process. In his patent of 1884, Dahl describes the cooking of biomass in an aqueous solution of sodium salts in the form of sodium hydroxide, sulfate, carbonate, and sulfide [1]. Today, most industrial paper mills use this process.

In Kraft mills, the active species of the aqueous solution in which wood chips are cooked are NaOH and Na₂S. This cooking solution, with an elevated pH, is called white liquor. The cooking process takes place at temperatures of 155-180 °C [31]. Lower cooking temperatures of about 155 °C are used for hardwood. Softwood is cooked at temperatures ranging from 170 to 180 °C [25]. The process pressure in this process is about 8 bar [31]. An overview of the main process steps of a Kraft plant is given in Figure 13 [36].

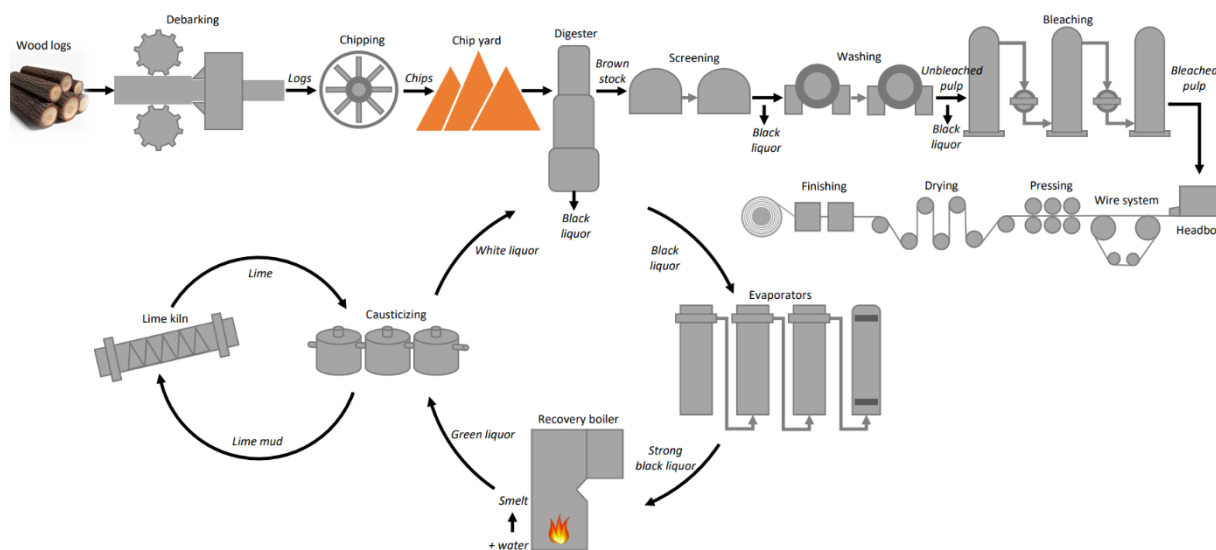


Figure 13: Simplified flow sheet of a Kraft pulp mill [36]

As depicted in Figure 13, wood logs are debarked, chipped, and temporarily stored in a wood chip yard [36]. Wood chips are filled into a digester together with white liquor and are boiled for 1-2 h [25]. The resulting solid material containing mainly cellulose fibres is called brown stock. Separated brown stock is processed into pulp or paper with further treatments including

washing, bleaching, pressing, and drying. Mainly process chemicals, lignin, and hemicellulose are present in the remaining black liquor. As the water content of the black liquor is high, it must be evaporated prior to combustion in the recovery boiler. A range of multi-effect evaporators enables energy-efficient evaporation [36]. Combustion of black liquor in the recovery boiler produces thermal energy and an inorganic salt smelt containing anions such as OH^- , CO_3^{2-} and HS^- . These salts are dissolved in water and the resulting solution is called green liquor. In the lime kiln, lime mud is burnt to lime and this lime is then mixed with green liquor in the causticizer to form white liquor and thus closing the recovery cycle [37]. For energy production and chemical recovery, which is 97 % in typical Kraft plants [36], the black liquor including large amounts of lignin must be combusted [36]. The combustion step is therefore an integral part of the energy balance of the process and the reason that Kraft plants rarely isolate and sell the lignin they produce. Despite the industrial dominance of Kraft mills in terms of pulp volume produced, 90 % of commercially available lignin therefore comes from the sulfite process, which is discussed in chapter 2.1.2 [38].

Chemically, there are two important types of reactions that take place in the digester. Firstly, there are decomposition reactions that lead to fragmentation of lignin and an increase in solubility. The second type of reactions are condensation reactions that counteract the desired fragmentation in forming new bonds. As described in chapter 1.1.5, the most common interconnections in native lignin are so-called β -O-4 linkages. These can be cleaved by the two active species HS^- and OH^- of white liquor. Figure 14 shows an example of an alkaline cleavage of a β -O-4 bond of non-phenolic arylpropane units [39].

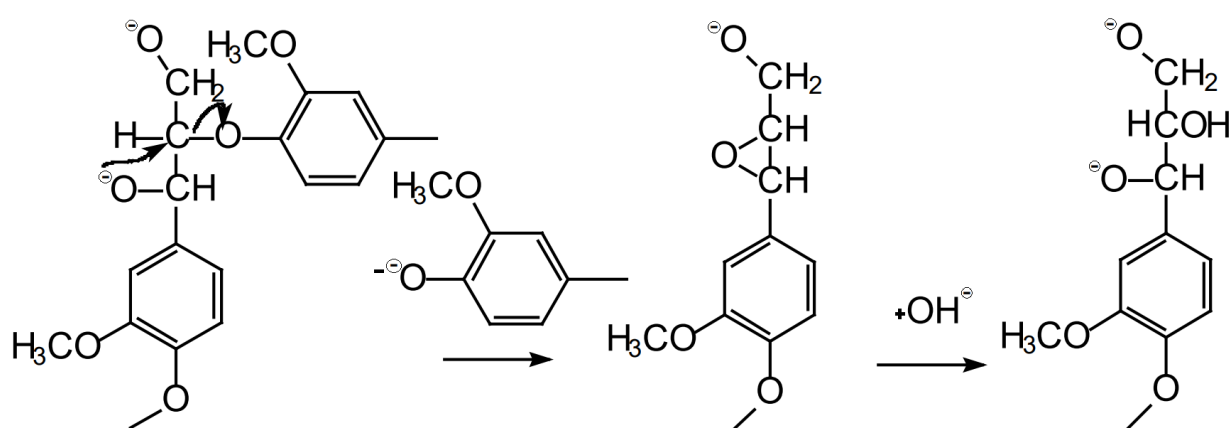


Figure 14: Reaction mechanism of an alkaline β -O-4 bond break in non-phenolic units [39]

Figure 14 shows the nucleophilic attack of a deprotonated OH group in α or γ position. The release of phenolates, as seen in the first step of the reaction scheme, is typical for most decomposition reactions occurring in the Kraft process. With increasing reaction time in the digester, the level of phenolates and thus the hydrophilicity and solubility of lignin fragments increases. The depicted reaction scheme in Figure 14 occurs with non-phenolic (etherified)

arylpropane units. The reaction pathway is different for cleavages of β -O-4 linked compounds in which one or more units have non-etherified phenolic OH groups. Reactions of this type are initiated by hydrogen sulfide anions, as shown in the second reaction step in Figure 15. Starting from the phenolate in Figure 15, a quinone methide is formed in the presence of either an ether bond or an alcohol group in alpha position. In this step, either a phenolate or an OH^- is split off. In the second step, a hydrogen sulfide anion binds to the alpha carbon and leads subsequently to bond cleavage at the beta position [39].

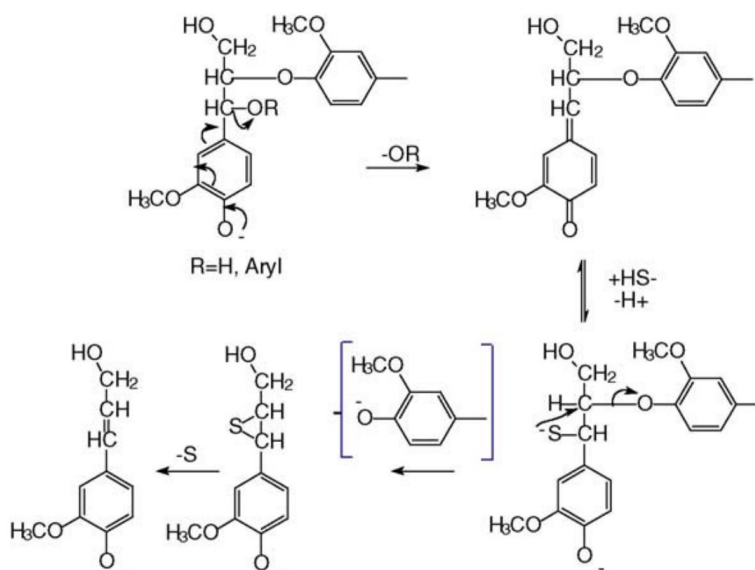


Figure 15: Reaction mechanism of a sulfidolytic β -O-4 bond break in phenolic units [39]

In addition to decomposition reactions, condensation reactions also take place in the Kraft process. The term condensation reactions in this context does not imply a reaction with the split-off of a simple molecule but describes the growth of lignin fragments. Chemically correct, most condensation reactions in Kraft pulping are Michael additions. As shown in Figure 15, quinone methides are reaction partners for nucleophilic molecules. In addition to active OH^- and HS^- species in the white liquor other nucleophilic substrates are also present. One example are carbanions which are formed during Kraft cooking. Figure 16 shows a reaction path in which HS^- competes with a carbanion to react with a quinone methide [39].

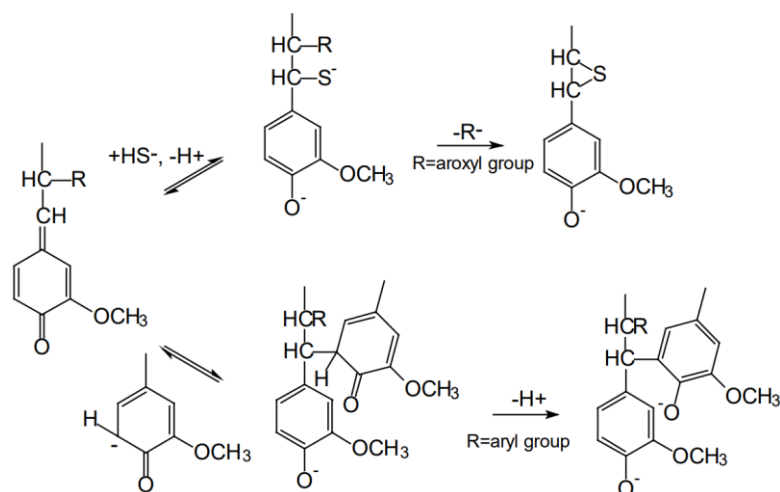


Figure 16: Competing reactions on a quinone methide [39]

In the reaction mixture, decomposition dominates condensation, breaking 90-93% of the β -O-4 bonds. Less common α -O-4 connections are also largely cleaved in the cooking process [40]. The molecular weight of kraft lignin is therefore greatly reduced compared to native Lignin. Typically, the number-based average M_n of a molecular size distribution of kraft lignins is between 1200 and 1820 g/mol [40]. In comparison, M_n in native MWL is at 4500 g/mol [26]. Bonds between two carbon atoms like 5-5' linkages are more stable [40]. Phenylcoumaran as well as diphenylethane subunits partially react in the Kraft process to form diarylethene structures, also called stilbenes, which link up to 4.8 % of all Kraft lignin monomers [41]. Due to the high proportion of sulfur in the reaction mixture of the Kraft process, sulfur-containing structures are also found in the lignin produced, they make up to 1-3 % of Kraft Lignin [40]. Sulfur can occur organically bound in the form of thiols. Further variations of organic sulfur are sulfide and disulfide bonds. Sulfur also occurs in its elemental form and is found inorganically as sulfate in Kraft lignin [42]. Uncleaved residues of cellulose and hemicellulose lead to minor amounts of carbohydrate linkages in Kraft lignin. A hypothetical model of a Kraft lignin molecule summarizing beforementioned structural features is given in Figure 17. This model is purely qualitative and does not provide information about the abundances of the represented structures [43]. In addition to the most common structural features discussed in this chapter, many other structures occur in kraft lignin with lower abundance.

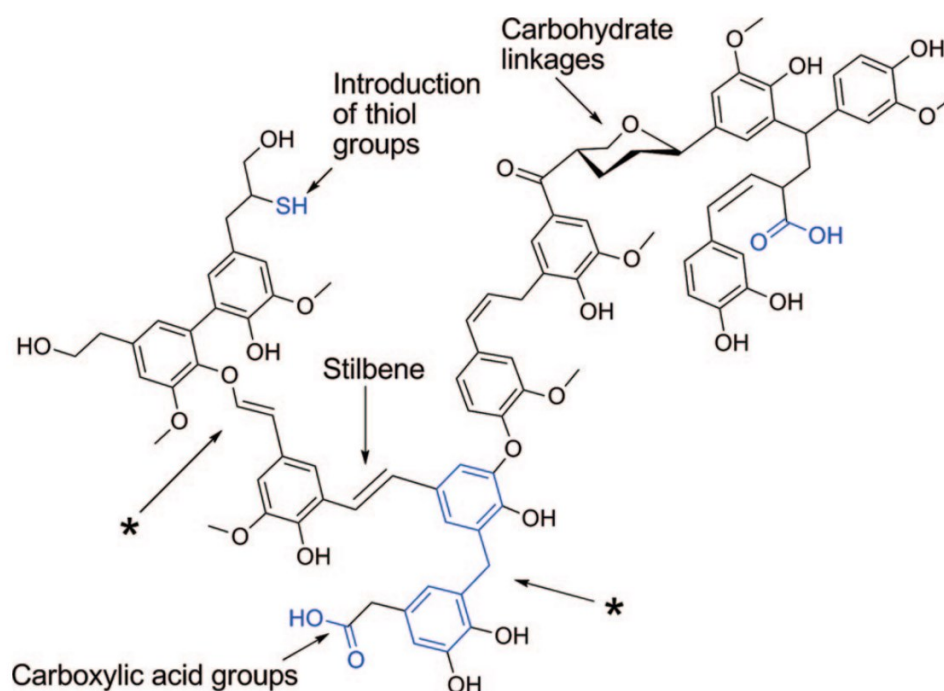


Figure 17: Hypothetical Kraft lignin model structure [43]

Areas marked with asterisks in Figure 17 indicate interunit linkages whose existence is still being discussed in the literature. In particular these are vinyl aryl ether and diphenylmethane linkages [43].

Kraft lignin recovery

This chapter gives a brief introduction about the possibilities of isolation of kraft lignin and the influence of important process parameters. The focus is on industrial applications using acid precipitation, in particular on the “LignoBoost” process.

As mentioned in Chapter 2.1.1, the reaction mixture in the Kraft process from which cellulose has already been removed is called black liquor. There are three main ways to isolate lignin from black liquor. Most commonly, lignin is precipitated by acidification of the black liquor. Various acids can be applied, H_2SO_4 and injected CO_2 are the most common. In addition to acid precipitation, ultrafiltration and electrolysis are also used [44]. Industrially used processes to precipitate Kraft lignin are the West Vaco process, LignoForce and LignoBoost [45].

The most important aspect of acid precipitation of lignin is the pH value. Figure 18 shows an exemplary precipitation result of lignin treatment with H_2SO_4 . The graph in Figure 18 shows two steep increases in lignin recovery, one in the pH range 10-8.5 and second at 4-3. It is assumed that the first increase is related to protonation of phenolic OH groups. The range around pH 3-4 involves protonation of carboxylic acids of hemicellulose degradation products. These hemicelluloses cleaved in the Kraft process are still partially associated with lignin, so their protonation leads to further precipitation of lignin [44].

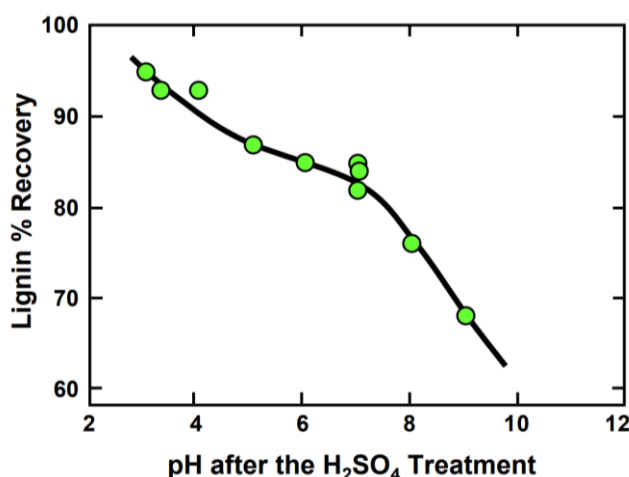


Figure 18: Lignin recovery with H₂SO₄ treatment [44]

Compared to H₂SO₄, acidification with CO₂ cannot be operated to the same extent. With CO₂, pH ranges of 10.5–8.5 are common, although acidification to pH 7 has also been achieved. Acidification to low pH does result in high lignin recovery, but there are negative effects that must be considered industrially. Below pH 7, there is a strong gas evolution, mainly H₂S and CO₂. Besides the foaming during precipitation, the toxicity of H₂S must be mentioned. A suitable gas treatment system must be installed. Furthermore, precipitation in the acidic pH range leads to fine lignin particles which are problematic in the subsequent filtration step [44].

Two other important factors for lignin recovery from black liquor are temperature and ionic strength (IS). Lower temperatures as well as an increase in IS lead to an increase in lignin recovery. The dependence of lignin recovery on temperature and IS is shown in Figure 19. In the depicted experiments, black liquor from a softwood pulp was acidified with CO₂ [46].

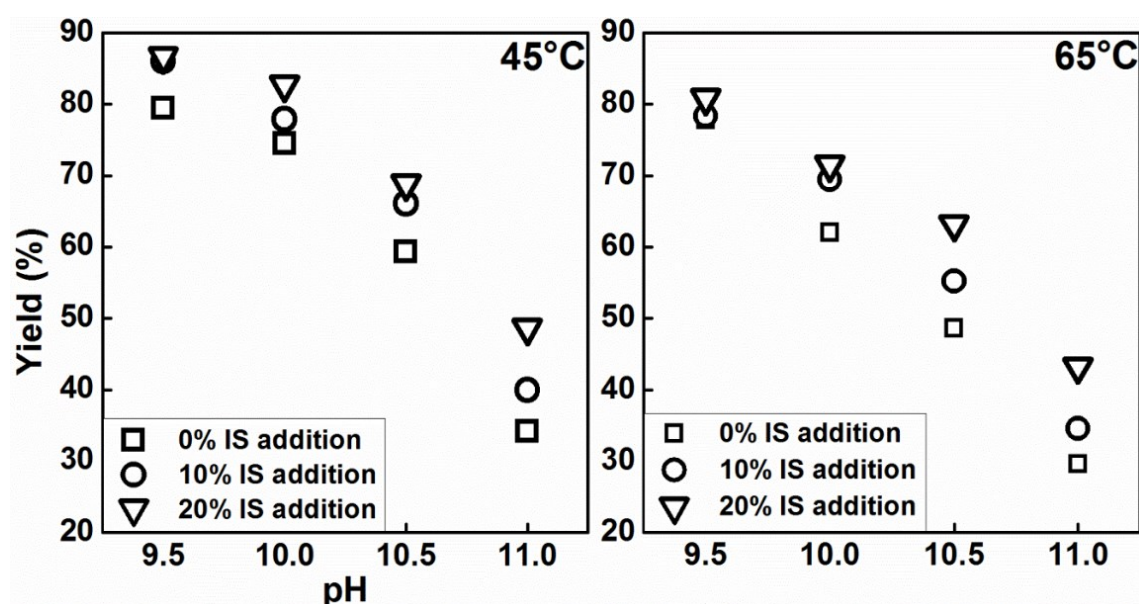


Figure 19: Lignin precipitation with CO₂ from softwood black liquor with varying pH and IS [46]

Figure 19 shows that the lignin precipitation yield is higher at lower temperatures such as 45 °C than at 65 °C [46]. The disadvantage of low temperatures, however, is the reduced filtration performance. Öhman and Theliander conducted experiments to measure specific filter resistances α for the precipitation of lignin from black liquor. In the observed temperature range of 69-80 °C, an exponential increase in filter resistance could be demonstrated. Figure 20 shows this correlation graphically [47].

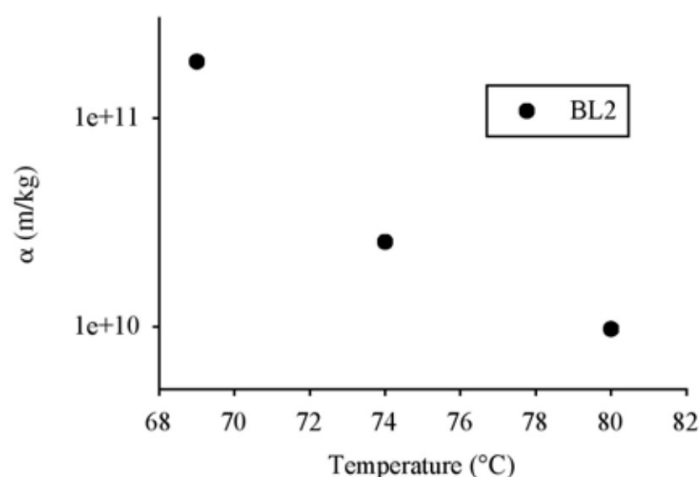


Figure 20: Specific filtration resistance dependence on precipitation temperatures at pH 9.7 [47]

Unlike low pH and temperature, ionic strength does not reduce filtration properties. Öhman and Theliander mentioned in one of their patents on the LignoBoost process that the addition of Na_2SO_4 , despite the increase in yield, also leads to a significant facilitation of the filterability. The specific filter resistance could be reduced from 1.6×10^{10} to 6.9×10^8 [m/kg] by adding 100 g Na_2SO_4 to 2 litres of black liquor at a pH of 9.6 and a temperature of 80 °C [48]. Disadvantages of precipitation with increased ionic strength are the more difficult chemical recovery and the change of the Sodium and Sulfur balance in the chemical recovery cycle of kraft plants [45].

The Na/S balance of the chemical recovery cycle is also disturbed using H_2SO_4 as an acidifying agent [44]. So, from an industrial perspective, in addition to maximising lignin recovery at low cost, it is important to consider the impact of a lignin precipitation step on the existing kraft plant. Välimäki et al. conducted a detailed case study on the effects of lignin recovery from the black liquor of a Kraft plant. Implementing a technology to extract lignin from black liquor can have a positive impact on the plant. The recovery boiler limits the amount of pulp, that can be produced in a Kraft plant. A reduction of the combustible solids in the black liquor therefore leads to a relief of the boiler. Since the isolated lignin does not have to be burnt in the boiler, the plant can produce increased amounts of pulp. This aspect can lead to increased economic profitability [49].

Lignoboost process

The LignoBoost process is a patented method for recovering lignin from the black liquor of a Kraft pulping plant. The two main patents, that form the basis of the technology, are WO2006038863 and WO2006031175 [58,60]. With the LignoBoost process, a total of more than 83,000 tonnes of lignin are isolated per year in four facilities. The plants are located in Finland, Sweden, the USA and Brazil [51].

The inventors Öhman, Theliander, Tomani, Axegard and Norgren, mentioned in the patents cited earlier, have optimized the factors of lignin recovery from black liquor. First, a pH of about 10 is achieved by acidification with CO_2 . In this step, most of the lignin is already precipitated. The precipitate is pressed in a filter press to form the filter cake. The resulting filter cake is then re-dispersed in dilute sulfuric acid at a pH of 2-4 in a second step. Re-dispersion in H_2SO_4 results in a lower gradient of ionic strength during subsequent washing. In single-stage precipitation, the sudden change in ionic strength during washing causes fine lignin particles still in solution to precipitate in the filter or the filter cake. The resulting clogging also leads to impurities in the lignin, as the washing out of unwanted components is hindered. In the double-stage LignoBoost process due to the reduction of the IS gradient, unwanted re-precipitation in the final filtration step is minimized. The LignoBoost process therefore solves the problem of filter clogging with the introduced re-slurry step. As a side effect, the purity of the final lignin is also enhanced [55,62]. A simplified diagram of a LignoBoost process is given Figure 21 [44].

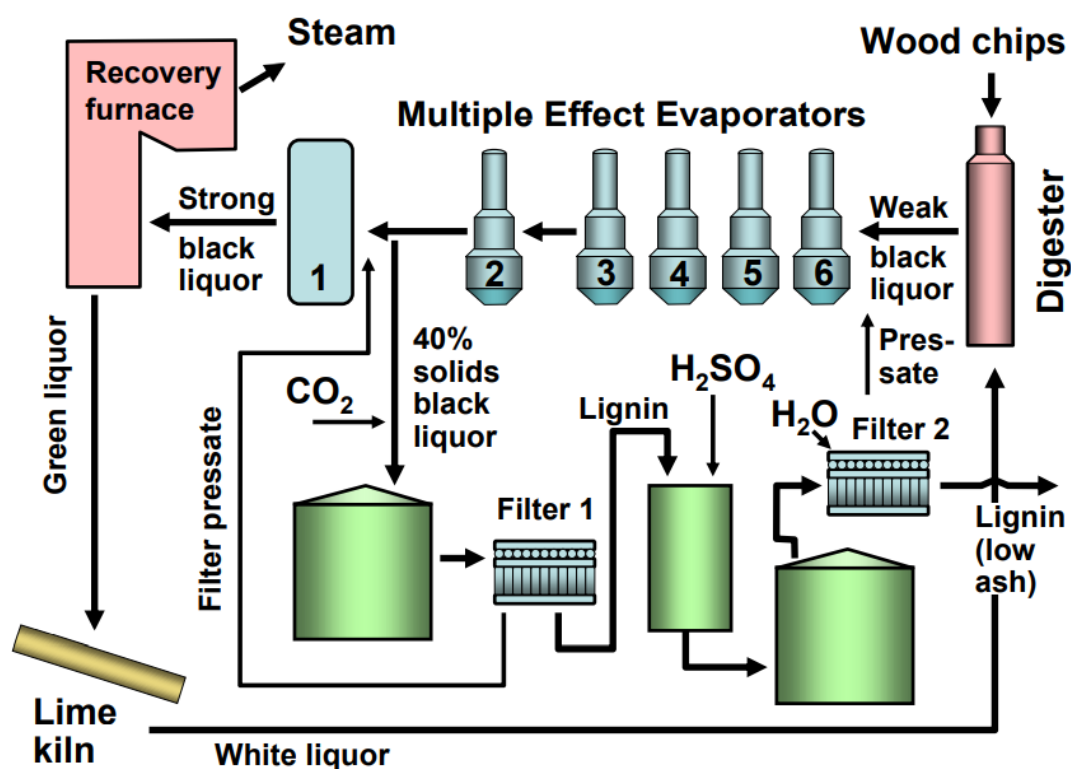


Figure 21: Schematic diagram of a LignoBoost process [44]

As can be seen in Figure 21, thickened black liquor with a dry content of about 40 % is withdrawn from the multi-effect evaporators. This is followed by acidification to pH 9.5-10.5 with CO_2 at 60-80 °C. Precipitation as well as maturation of the lignin takes place in the same reactor vessel. The separation of the liquid proceeds in the first filter press. The dried filter cake is then transferred to the re-slurry tank and redispersed with diluted H_2SO_4 . In the second filter press, the solid is again separated from the liquid and washed with acidified water at pH 2-4. Filtrate flow 1 and 2 are fed to multi-effect evaporators at different positions in the series. The first filtration step produces a filtrate with a relatively high proportion of solids. This high solid stream is introduced at the end of the evaporators, just before the recovery boiler. The low solid filtrate from the second filter press is introduced at the beginning of the multi-effect evaporator row. Finally, the moist filter cake is dried, and the resulting lignin is called LignoBoost lignin. The ash content of LignoBoost lignin varies between 0.2 and 1.4 % [54,55].

2.1.2 Sulfite process

The sulfite process, like the Kraft process, is a chemical pulp process used in paper and pulp production to separate cellulose from the remaining biomass. It was developed in the second half of the 19th century and was until about 1950, the most widely used pulp process. Like the soda process, the sulfite process was gradually displaced by the Kraft process and today accounts for only a marginal share of global pulp production [34,44]. Elevated temperature, increased pressure and the use of process chemicals are employed. Process chemicals are sulfurous acid and a base such as NaOH , $\text{Ca}(\text{OH})_2$, $\text{Mg}(\text{OH})_2$ or NH_4 . Versatility in applicability characterizes the sulfite process, as it can be used over a wide pH range and various bases can be utilized [54].

A process diagram of an exemplary sulfite process with the use of magnesium hydroxide as a base is shown in Figure 22 [54]. The system-specific base, in the example shown $\text{Mg}(\text{OH})_2$, is formed by dissolving MgO in water. By introducing SO_2 gas into this aqueous solution, the sulfurous acid H_2SO_3 is generated, which then dissociates to varying degrees depending on the pH. This cooking acid with a pH of 2-5 is added to the wood chips and reacts in the digester at 130-170 °C for 5-7 hours. The pulp is separated, and the remaining red liquor is thickened in multiple effect evaporators and then burned in the recovery furnace. Magnesium oxide (MgO) produced during combustion can be collected to enable chemical recovery [44,45].

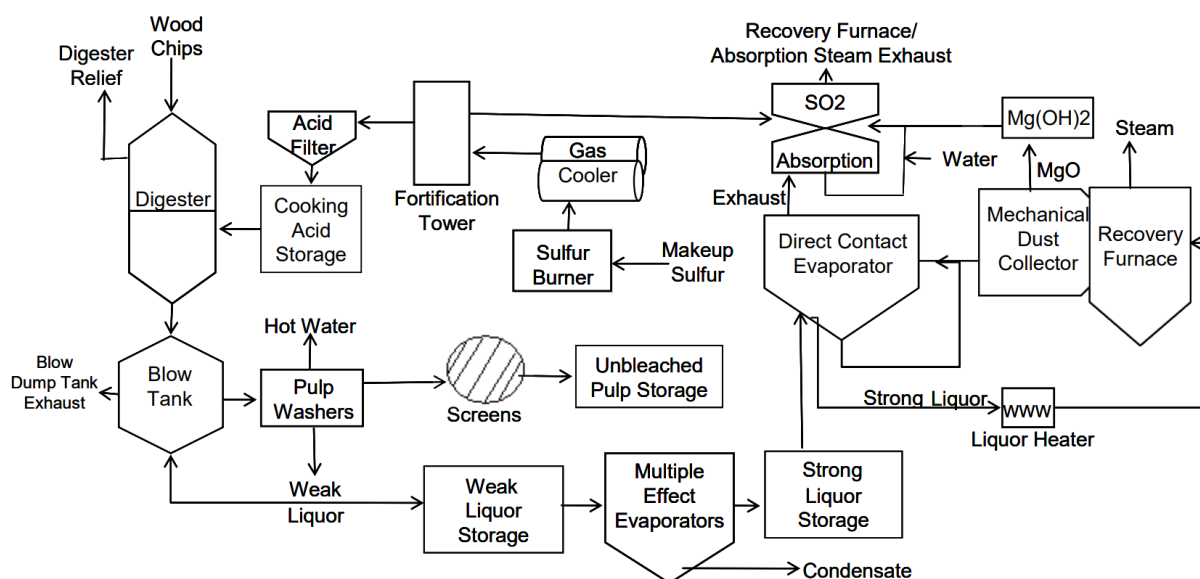


Figure 22: Simplified flow sheet of a magnesium-based bisulfite process [54]

Chemical recovery is possible in the magnesium bisulfite process shown in Figure 22, it is generally more feasible in sulfite processes than in the kraft process [34]. In addition to the bisulfite process, there is also acidic sulfite pulping, alkaline sulfite pulping, and multistage sulfite pulping. These processes are operated at different temperatures and with various counterions of the base [53].

Important chemical reactions in the sulfite process are sulfonation and condensation reactions. In contrast to the reaction mechanisms in kraft pulping, the solubility of lignin is not produced by fragmentation and the associated formation of phenolates. In the sulfite process, the introduction of sulfonate groups is decisive for the solubility of the resulting lignin. Lignins originating from the sulfite process are therefore referred to as lignosulfonates. An example reaction for sulfonation in the pH range of 1-5 is given in Figure 23 [38].

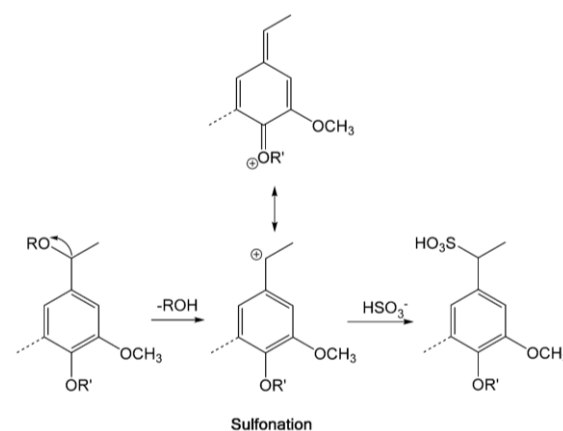


Figure 23: Sulfonation mechanism in acidic sulfite pulping (pH 1-5) [38]

The ether or hydroxyl group in the alpha position is cleaved off by hydrolysis. Benzyl sulfonic acid is then formed by addition of HSO_3^- on the alpha position of the benzyl cation. This reaction

can occur with phenolic as well as etherified aryl units and is central to the polyanionic character of lignosulfonates. In sulfite processes, which take place in the neutral pH range of 5-7, a different reaction mechanism, shown in Figure 24, is involved [38].

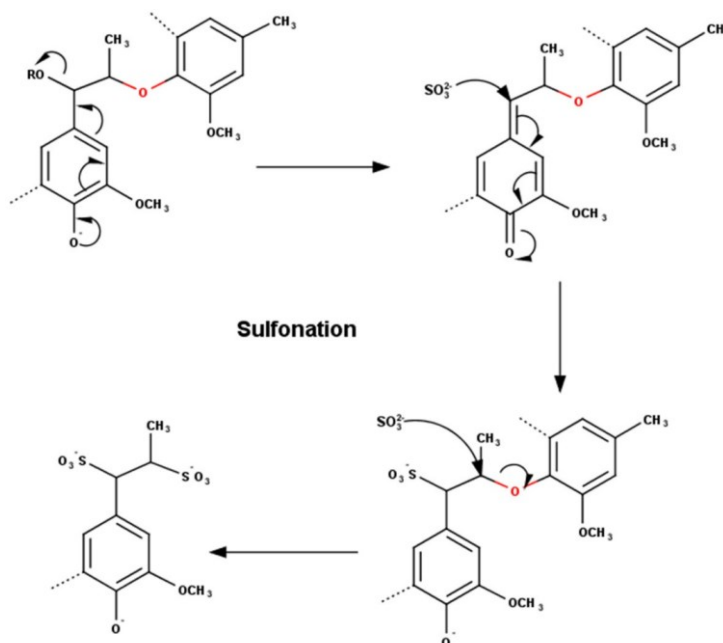


Figure 24: Sulfonation mechanism in neutral sulfite pulping (pH 5-7) [38]

Sulfonation reactions in the neutral pH range require phenolic aryl units and are initiated by hydrolysis of a leaving group in alpha position. The reaction mechanism continues via sulfonation in alpha position followed by further sulfonation in beta position which is facilitated by the former [38].

Since different bases are used in sulfite processes, there are also lignosulfonates whose polyanion skeleton has different counter cations. Thus, there are Na, Ca, Mg or NH_4 lignosulfonates, which show partly different properties. In the case of lignosulfonates, condensation reactions can be of great importance. In the sulfite process, in contrast to kraft pulping, a reduction of molecular sizes does not necessarily occur. Lignosulfonates are often characterized by broad molecular size distributions whose mean value can be strongly shifted towards larger molecules. Number-based average molecular sizes M_n can be similar to Kraft Lignin starting with about 1500 g/mol, but can also reach up to 150 000 g/mol which is significantly higher than that of MWL with 4500 g/mol [26,38,40]. Figure 25 gives an example of a possible lignosulfonate molecular structure, recognizable by sulfonate groups [55].

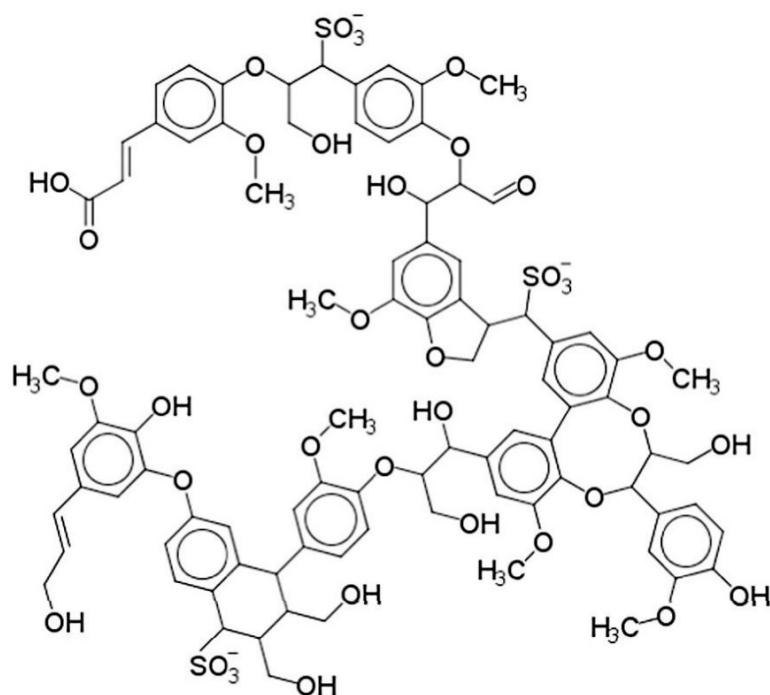


Figure 25: Idealized lignosulfonate structure [55]

2.1.3 Organosolv process

The Organosolv process is a chemical pulping method for separating cellulose, hemicellulose, and lignin. Its operating principles can be inferred from its name. Various organic solvents such as ethanol, methanol, formic acid, diethyl ether amongst many others are used to dissolve hemicellulose and lignin [2]. Elevated temperatures of 100-250 °C and a process duration of 30-60 minutes is common. The organosolv process can be operated with the support of catalysts, but also without them [56]. There are also autocatalytic processes in which the hydrolytic cleavage of acetic acid from hemicelluloses serves as the organic solvent [2]. The first process patenting the separation of lignocellulosic components using ethanol was developed by Kleinert and Tayental in 1932 [57]. Lignin produced with the organosolv process is characterized by a low ash content and the absence of sulfur. Organosolv lignin accounted for 1,3-2 % of commercially available lignin in 2019 [30,49]. However, it is estimated that its Compound Annual Growth Rate (CAGR) is the highest of all technical lignins and will be over 5 % from 2016-2025. The CAGR for the overall available lignin is expected to be 2.2 % in the same time range [29].

Figure 26 shows a simplified schematic of the general steps of an organosolv process, including solvent recovery and precipitation of lignin [56]. Lignocellulosic biomass of any origin can be used for cellulose separation with the aid of organic solvents. Mostly acids like H_2SO_4 and HCl or bases like NaOH and KOH are used as catalysts. After organosolv pre-treatment, the cellulose is separated mechanically in the form of filtration or centrifugation. Lignin can be

separated from the so-called spent liquor, for example by precipitation due to dilution of the solvent [56].

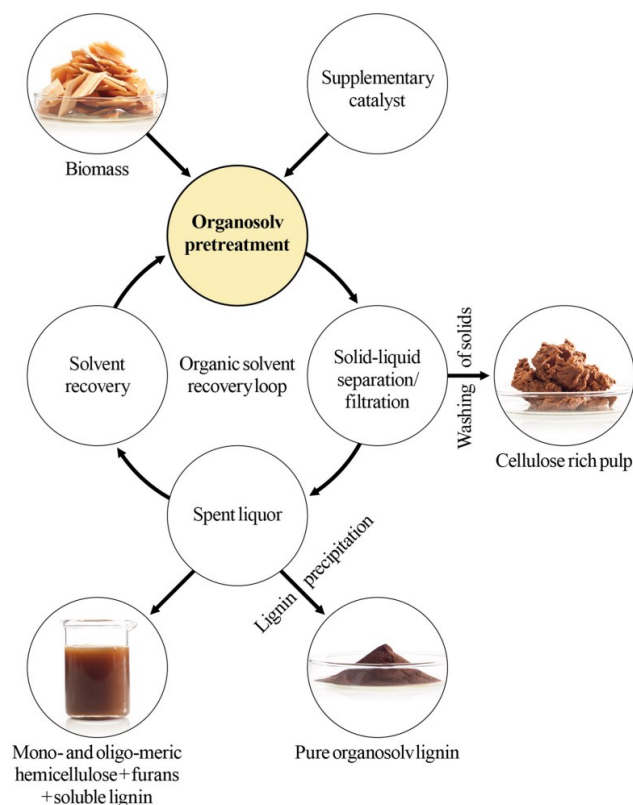


Figure 26: Schematics of an organosolv process with lignin precipitation [56]

The most common solvent in organosolv processes is ethanol. Low cost, feasible solvent recovery, good solubility of lignin, miscibility with water and low toxicity are the main advantages of ethanol in this context. Lignins produced by ethanol organosolv processes are referred to as EOL (ethanol organosolv lignin) [56].

In the example of an acid catalysed process with ethanol as solvent, fragmentation of the lignin molecules is achieved mainly by hydrolytic cleavage of α -O-4 and β -O-4 ether bonds. This results in increased solubility of the lignin fragments in ethanol due to phenolic OH groups formed in the process [56]. Since no sulfur-containing chemicals are used in the organosolv process, except for catalytic amounts of H_2SO_4 , lignin produced by this process is considered sulfur-free. The average lignin molecule sizes, with M_n values of around 1000 g/mol, are smaller than those of other technical lignins [2]. Xiaoyan et al. explored the structure of organosolv lignin from corncob residues. The organosolv pre-treatment was carried out with a solvent mixture of tetrahydrofuran (THF) and water. Findings on the most common structural features in corncob residue organosolv lignin are given in Figure 27 [59].

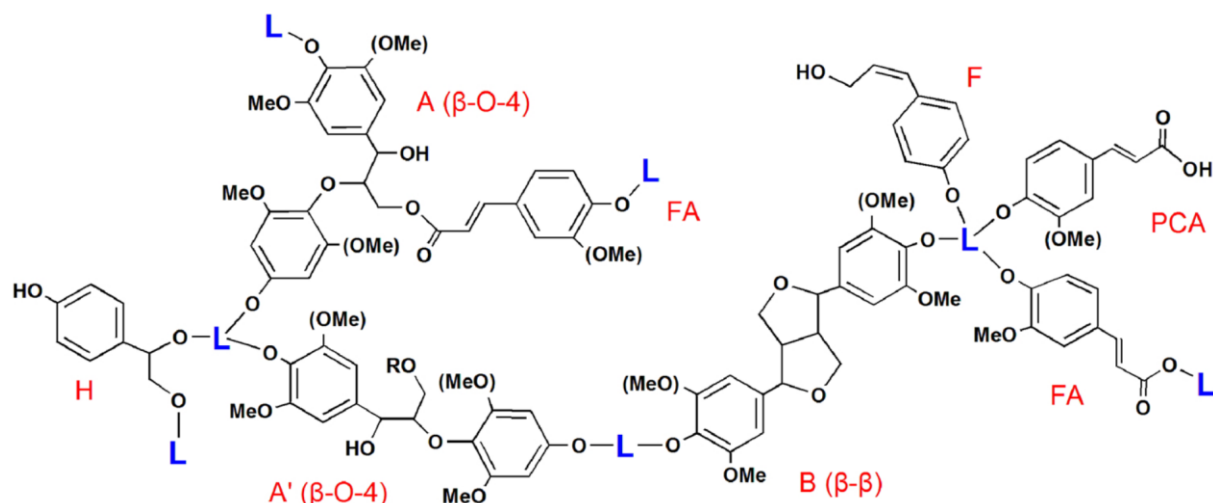


Figure 27: Estimation of the structure of lignin isolated from maize cob residues by THF/H₂O organosolv pre-treatment [59]

In Figure 27, substructures that are not identified are marked with the letter L. The letters A and A' denote β -O-4 interunit linkages with different residues on the gamma carbon, B denotes β - β linkages, FA is used for ferulate subunits, PCA for p-coumarate subunits, F for p-hydroxycinnamyl alcohol end groups and H for phenol end groups [59].

2.1.4 Comparison of technical lignins

This subchapter summarizes important aspects and differences of the technical lignins discussed. Furthermore, an overview of their market sizes is given.

The production of technical lignins can be divided into sulfur processes and sulfur-free processes. Soda pulping briefly mentioned in 2.1.1 and the organosolv process, which can also be referred to as solvent pulping, are sulfur-free processes. Sulfur-containing process chemicals are used in kraft pulping and sulfite pulping. Figure 28 gives an overview of this categorization and examples for possible process parameters [55].

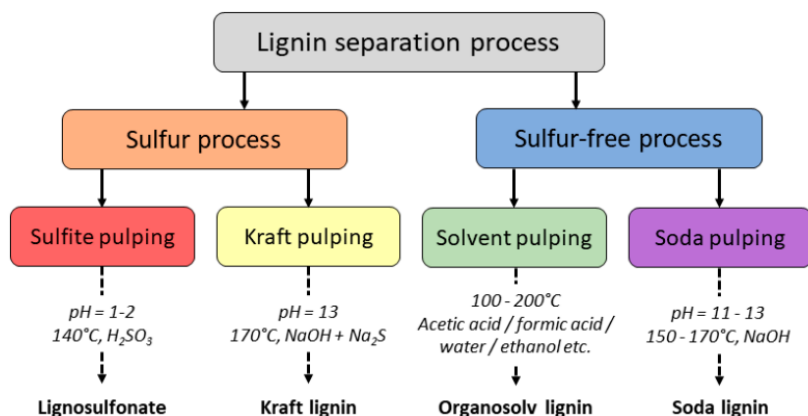


Figure 28: Overview of technically relevant lignin separation methods [55]

Table 1 presents important distinguishing characteristics of kraft lignin (KL), lignosulfonates (LS), and organosolv lignin (OL).

Table 1: Comparison of relevant aspects of technical lignins

	M _n [g/mol]	M _w [g/mol]	S [%]	Pulp prod. ^a [%]	Lignin prod. ^b [%]	Sources
KL	1200-1820	2500-3500	0.2-3.0	93.1	12.8	[38],[40],[58],[60]
LS	1000-14000	4600-400000	3-8	6.0	84.5	[38],[58],[60],[61]
OL	400-1600	1500-5500	0.0	n.d.	1.3	[2],[58],[60]

^aeurope-wide pulp market share from 2018 [60], ^bworld-wide lignin market share from 2018 [58], n.d. ...not determined

The properties shown in Table 1 are not limited to individual wood species and specific pulping process parameters. The data presented is intended to provide an overview of the typical ranges of the properties of the groups of technical lignins listed. Table 1 shows that most of the technical lignin available on the market is derived from the sulfite process. Lignosulfonates are on average less expensive than kraft lignin or organosolv lignin. As an example, market values in 2011 were: 180-500 dollars per metric tonne (\$/MT) for lignosulfonates, 260-500 \$/MT for kraft lignin and 280-520 \$/MT for organosolv lignin [62].

The high availability and low price could make lignosulfonates, regarding economic reasoning, a suitable feedstock for lignin pyrolysis. However, the chemical properties of lignosulfonates, such as their high sulfur content, are a hindrance to efficient pyrolysis. This aspect is explained in more detail in Chapter 3 and is one reason for the selection of kraft lignin as the basis for the calculations and modelling in Chapter 4.

2.2 Pyrolysis

In this subchapter, the basics of pyrolysis, in particular the pyrolysis of lignocellulosic biomass (LCBM), are presented. The general principles and reactors mentioned in this chapter can be transferred to the pyrolysis of lignin, discussed in detail in chapter 3.

The term pyrolysis is not clearly defined, as many variations and feed materials are used industrially and in scientific literature. In this work, pyrolysis is, adapting the definition of Raza et al. [63], defined as follows. Pyrolysis is a thermochemical process that transforms biomass in the absence of oxygen to gaseous products, bio-oil and bio-char. For completeness, it should be mentioned that feed materials can also be used that are not of biogenic origin, such as various synthetic polymers [64].

The most important factors influencing pyrolytic processes are biomass, temperature, heating rate, residence time, particle size, pressure and the type of reactor system used [63]. In addition, there is the potential use of catalysts, the joint pyrolysis of other feedstock materials,

different atmospheres, and the use of multi-stage pyrolytic systems. This variety of influencing factors highlights the complexity of pyrolysis. A classification of different pyrolysis processes can be made based on temperature, residence time and heating rate. Bridgewater et al. show the influence of temperature and residence time on the liquefaction rate of pyrolysis. Figure 29 displays the yield of the liquid phase and chemical aspects of the products [30].

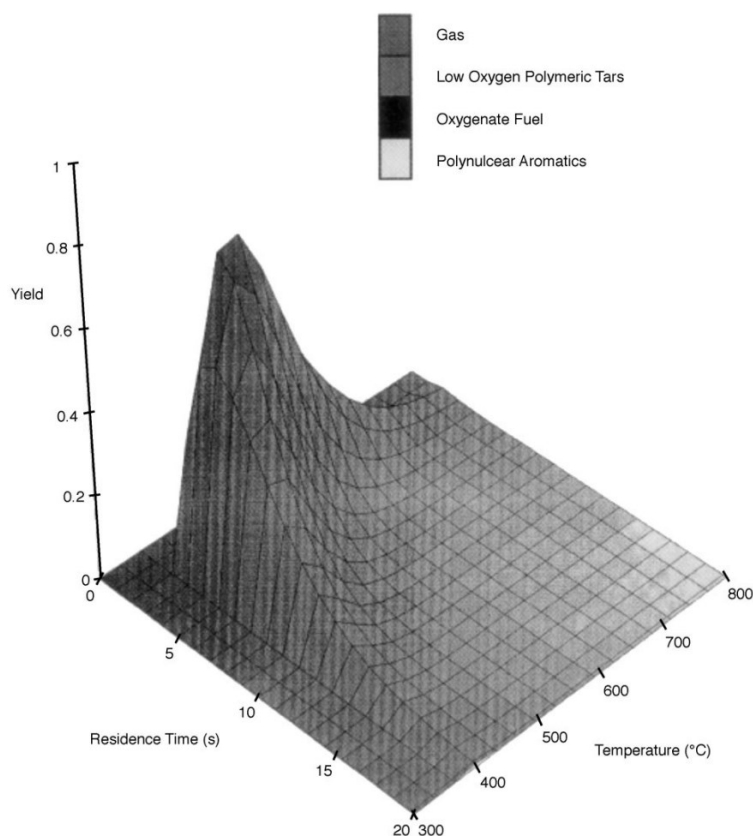


Figure 29: Bio-oil yield and chemical characteristics of pyrolysis products [30]

The graphical representation of the liquefaction rate shows a peak around 500 °C and residence times of less than 2 seconds. In this range, liquefactions of up to 80 % can be achieved. At very long residence times and low temperatures, mainly bio-char is produced. If, the temperatures are very high, gasification is dominant [30]. Huber et al. use these temperature and residence time dependent product differences to classify pyrolysis systems [65]. This classification is listed in Table 2.

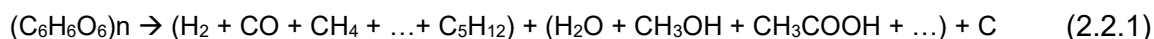
Table 2: Categorization of pyrolytic processes [65]

Name	Residence time	Temperature [°C]	Heating rate	Major products
conventional carbonization	hours-days	300-500	very low	charcoal
pressurized carbonization	15 min – 2 h	450	medium	charcoal
conventional pyrolysis	hours	400-600	low	charcoal, liquids, gases
conventional pyrolysis	5-30 min	700-900	medium	charcoal, gases
flash pyrolysis	0.1-2 s	400-650	high	liquids
flash pyrolysis	<1 s	650-900	high	liquids, gases
flash pyrolysis	<1 s	1000-3000	very high	gases
vacuum pyrolysis	2-30 s	350-450	medium	liquids
pressurized hydrolysis	<10 s	<500	high	liquids

Table 2 classifies different pyrolysis systems according to the parameters temperature, residence time, heating rate and preferentially formed products. As already mentioned, comparatively low temperatures, slower heating rates and medium to long residence times lead increasingly to bio-char formation. These processes are referred to as carbonizations. Conventional pyrolysis can use temperatures of 400-900 °C, residence times of 5 minutes to hours, and slow to medium heating rates. The products of Conventional Pyrolysis vary greatly depending on the process parameters used, but above 600 °C gases are dominant products. Flash or fast pyrolysis is a process with very short residence times, usually less than 2 seconds, and very high heating rates. Bio-oil and gases are usually the major product types of flash pyrolysis. Special applications in pyrolysis technology are for example vacuum pyrolysis and pressurized hydrolysis [65].

2.2.1 Pyrolysis products

As mentioned in chapter 1.1, woody biomass consists largely of varying proportions of cellulose, hemicellulose, and lignin. Since pyrolytic processes are carried out with the exclusion of oxygen, thermal degradation must be considered from a chemical point of view. The macromolecules forming the wood are themselves present in an enormous variety and degradation further increases the variety of compounds in the pyrolysis system. In addition to the almost infinite diversity of reactants formed in the system, there is a multitude of possible chemical reactions that are possible under the respective process conditions. Cellulose is pyrolytically degraded to other degradation products than those of hemicellulose or lignin, and cross reactions of their degradation products are scarcely researched. Raza et al. however give a general and highly simplified reaction equation of pyrolysis in equation 2.2.1 [63].



This reaction equation does not claim to be exact. It is intended to give an insight into possible reaction products. The compounds in the first pair of round brackets on the right-hand side describe the formation of gases that are non-condensable at room temperature. In addition to hydrogen, carbon monoxide and carbon dioxide, also hydrocarbons of various lengths and bonding types are formed. The products summarized by the two following round brackets are to represent the developing liquid phase, the bio-oil. Both, an aqueous phase and a hydrocarbon-rich liquid phase are formed. The hydrocarbon-rich phase, also referred to as the organic phase, contains compounds from most areas of organic chemistry. In addition to alcohols, ketones, carboxylic acids, esters and ethers, many other organic compounds are present. The last part in reaction equation 2.2.1 stands for the formation of bio-char, simplified here as C [63]. However, bio-char is not simply made of carbon atoms alone, chemically it consists of a complex system of linked and partly oxygenated benzene rings [66]. Chemical properties of biochar, in particular biochar from lignin pyrolysis, are explained in more detail in 3.1.1.

Bio-oil

Bio-oil can be produced in large proportions by fast or flash pyrolysis. Temperatures around 500°C, fast heating rates, and short residence times are used to reach liquefaction rates of up to 75 %. This dark liquid has a pH value of 2.5 and contains a large number of oxygenated components [67]. Figure 30 presents bio-oil produced by flash pyrolysis in an ablative reactor [68]. Thermal and storage instability of bio-oil is explained by the high abundance of reactive compounds. The process by which chemical reactions of these compounds subsequent to pyrolysis lead to changes in physiochemical properties is called ageing. In addition to an increase in viscosity, the water production associated with progressive ageing requires mention. Table 3 lists important properties of bio-oil [67].

Table 3: Properties of bio-oil [67]

Properties	Bio-oil
Moisture content [wt%]	15.0-30.0
pH	2.5
specific density	1.2
C [wt%]	54-58
H [wt%]	5.5-7.0
O [wt%]	35-40
N [wt%]	0.0-0.2
S [wt%]	trace
ash [wt%]	0.0-0.2
higher heating value [MJ/kg]	16-19
viscosity [kg/ms]	0.04-0.1
solids [wt%]	0.2-1.0
distillation residue [wt%]	< 50
pour point [°C]	-33

**Figure 30: bio-oil from ablative flash pyrolysis [68]**

Table 3 shows the properties of bio-oil produced by fast pyrolysis of wood. In addition to the high water and oxygen content, the low pH value, which can be explained by the formation of significant amounts of carboxylic acids during pyrolysis, is a very unfavourable property [67]. Acetic acid is the most important representative of carboxylic acids and can make up to 16.5 % of dry bio-oil under controlled pyrolysis conditions and with a hemicellulose rich feedstock [69].

A clear phase separation into an aqueous and an organic phase of bio-oil can occur when the aging of the oil is advanced. Fresh bio-oil is present in a multiphase emulsion system in which drops of the aqueous phase are embedded in the organic matrix. In addition to the droplets of the aqueous phase, there are also larger droplets in which waxy solids or char are present. This multiphase system is temperature dependent. Between 25 and 42 °C, the solubility of the waxy crystals increases gradually. At temperatures above 53 °C, the droplets of the aqueous phase dissolve in the organic matrix. At higher temperatures, there is one liquid phase and char dispersed. Figure 31 shows microscopic images at 25°C of bio-oil produced by pyrolysis of softwood bark residue (SWBR). In the left part of the figure, the phase interfaces are visualized. The droplets of aqueous phase and waxy solids in the organic matrix, which were described previously, can be seen. By using polarized light, the waxy crystals can be seen in more detail in the right part of Figure 31 [70].

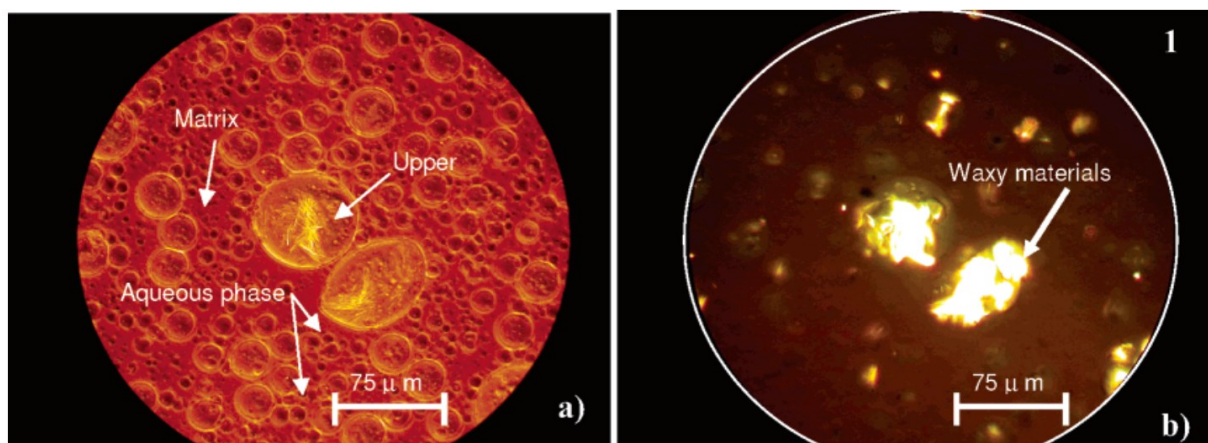


Figure 31: microscopic image of SWBR bio-oil at 25°C. a) phase contrast b) polarized light [70]

The reason for the complex physical properties is the large variety of different molecules in bio-oil. Figure 32 shows a gas chromatographic (GC) analysis of bio-oil produced by fast pyrolysis of corn cobs. The mass spectrometer (MS) downstream of the gas chromatograph identified over 150 molecules in this sample [69]. More sophisticated analytical methods such as comprehensive 2-dimensional gas chromatography coupled with time-of-flight mass spectrometry (GCxGC-TOFMS) can detect over 850 compounds in comparable samples [71]. The downstream processing of bio-oil in terms to fine chemicals is currently still limited due to the diverse product range. Applications of bio-oil are mostly in the fields of: Fuel, resins, adhesives, flavours, and heat recovery through incineration. In these areas, there is no focus on individual chemicals, bio-oil is considered as a bulk product [72].

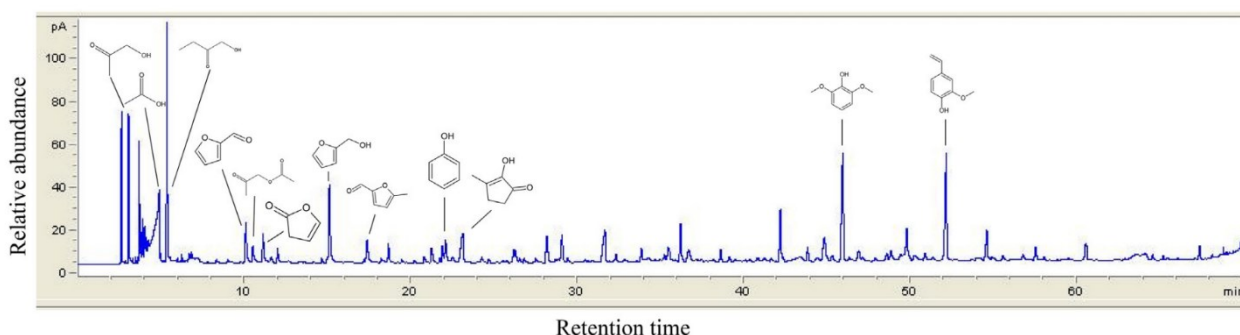


Figure 32: GCMS analysis of corncob pyrolysis bio-oil [69]

2.2.2 Reactor types

In this subchapter, the most important reactor types used in the pyrolysis of biomass are briefly presented. As already mentioned in chapter 2.2, the product distributions in pyrolysis depend, among other parameters, on the heating rate and the residence time of the biomass in the reactor systems. Reactor types differ in heat transfer, biomass feed inlet system, processable biomass size, biomass residence time, reactor geometry, capacity, and product separation.

The pyrolysis system is individually adapted to the feed, in order to achieve desired results, such as solid, liquid or gaseous main products. In addition to fluidized bed reactors with stationary or circulating fluidized beds, ablative reactors, rotating cone reactors, screw reactors, fixed bed reactors or vacuumized reactor systems are used for the pyrolysis of biomass [73].

Fixed bed reactors

Fixed-bed reactors are used in pyrolysis mainly for research purposes on a laboratory scale. The reasons for this is the simple and inexpensive applicability, which facilitates the experi-

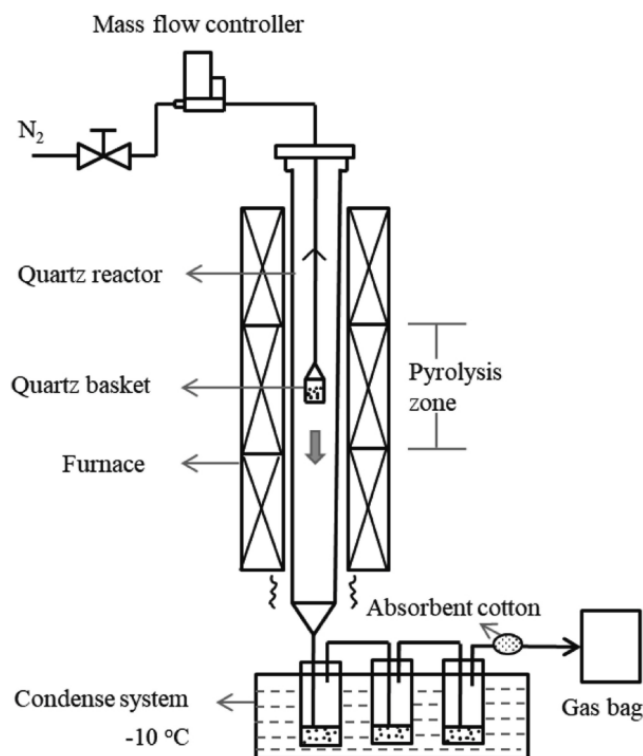


Figure 33: Laboratory scale fixed bed reactor [74]

mental variation of process parameters and allows for a simple implementation of catalysts [67]. Furthermore, defined biomass amounts of a few milligrams can be used and their reaction products can be quantitatively analyzed. In feasibility studies concerning the use of new catalysts or reaction conditions, the fixed-bed reactor is frequently the method of choice in the scientific literature.

For subsequent scale up experiments, other reactor types such as fluidized bed reactors are usually chosen. Process parameters determined by fixed bed reactor experiments are frequently used as starting points for subsequent scale up investigations. A schematic diagram of a fixed-bed reactor used for catalytic pyrolysis in laboratory scale is shown in Figure 33 [74]. The biomass to be pyrolyzed as well as the added catalysts are placed in a quartz basket. The quartz basket is lowered into the reactor when the set temperature is reached. Control of the residence time of pyrolysis vapors is determined by the carrier gas feed rate. Downstream of

the reactor, a condensation system and a collecting bag for non-condensable gases are installed [74]. Despite the excellent suitability of fixed-bed reactors for research, they are rarely used for pyrolysis on an industrial scale. Due to the low mixing of the feedstocks, the quality of the heat transfer is compromised. Longer residence times are the result, which in turn lead to reduced liquefaction rates. Since predominantly the liquid products are of utmost interest and a tedious separation of the resulting solids is necessary for the operation of fixed bed reactors, other reactors are commercially used [63].

Fluidized bed reactors

Rapid heat transfer and good biomass mixing can be achieved by fluidising the solid reactor bed. Fluidisation is the term used to describe the shift in rheological properties achieved by injection of carrier gas, so that the bed takes on the properties of a liquid during operation. Fluidised bed reactors are very popular for biomass pyrolysis in the industrial environment. One reason for this is a liquefaction rate of up to 75 %. Furthermore, it is possible to operate these reactor systems with a large biomass throughput. Thus, up to 4000 kg/h can be pyrolyzed [75]. The disadvantages of fluidised bed reactors are the complex process design, the use of a carrier gas, and the necessity of separating solid particles from the liquid products. A solid-free liquid phase is desirable, besides trivial reasons, because of the catalytic activity of char particles [67]. Biochar is considered as an active catalyst in cracking reactions in the vapour phase. The reason for this is the high specific surface area and the presence of active metals such as potassium, calcium, or sodium [76].

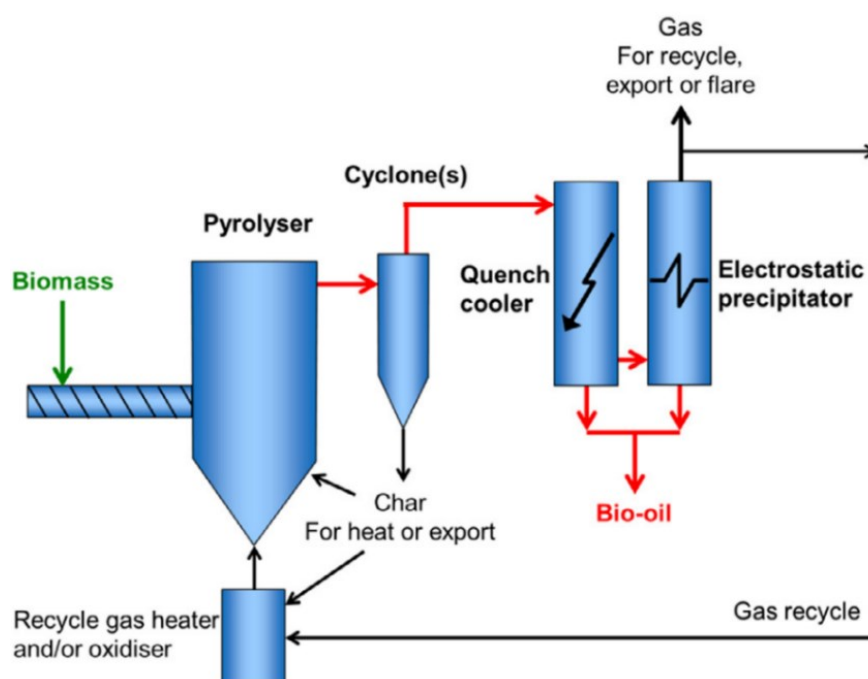


Figure 34: Bubbling fluidised bed reactor [67]

The diagram illustrates a biomass gasification system with the following components and flow paths:

- Biomass** (green arrow) enters the **Pyrolyser**.
- Pyrolyser** (blue vertical cylinder) produces **Flue gas** (black arrow) and **Sand & char** (black arrow).
- Flue gas** is sent to a **Cyclone(s)** (blue vertical cylinder).
- Cyclone(s)** sends **Hot sand** (black arrow) back to the **Pyrolyser** and **Gas** (red arrow) to the **Quench cooler**.
- Quench cooler** (blue vertical cylinder with a lightning bolt) produces **Bio-oil** (red arrow) and **Gas For recycle, export or flare** (black arrow).
- Gas For recycle, export or flare** is sent to an **Electrostatic precipitator** (blue vertical cylinder with a lightning bolt).
- Electrostatic precipitator** sends **Gas recycle** (black arrow) to a **Gas recycle heater and/or oxidiser** (blue vertical cylinder).
- Gas recycle heater and/or oxidiser** sends **Gas** (black arrow) back to the **Pyrolyser**.
- Electrostatic precipitator** also sends **Gas** (black arrow) to a **Combustor** (blue vertical cylinder).
- Combustor** receives **Air** (black arrow) and produces **Ash** (black arrow) and **Hot sand** (black arrow) back to the **Pyrolyser**.

Figure 35: Circulating fluidised bed reactor [67]

The purification of pyrolysis vapours is the same for both stationary and circulating modes of operation. First, pyrolysis vapours pass through one or more cyclones. After separation of the largest amount of solids, the vapours are being cleaned by an electrostatic precipitator and quenched by cooling [67].

Rotating cone reactors

In rotary cone reactors, biomass mixing is achieved by mechanical rotation of conically shaped reactor components. In contrast to fluidized bed reactors, the heat supply in rotary cone systems takes place without a carrier gas. Heat is transferred exclusively via inert heat transfer materials such as sand and is thus more efficient than when carrier gas is used. Disadvantages of this technology include abrasion of mechanical components, the need for biomass particle sizes smaller than 0.2 mm [73], the use of air to burn the biochar, and the more complex design. Figure 36 shows a schematic of a modern rotary cone reactor along with common downstream processes [67]. The rotating cone reactor shown in Figure 36, uses the principle of a transporting bed. The inert carrier material is transported out of the rotating reactor vessel together with the biochar.

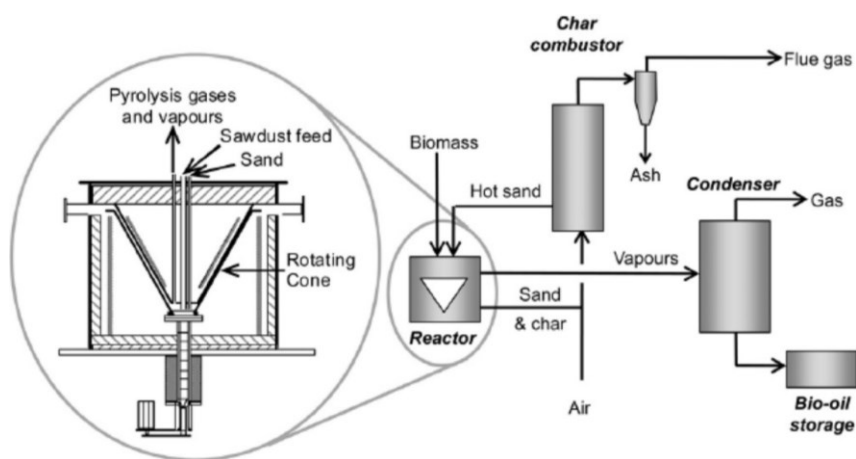


Figure 36: Rotating cone reactor [67]

The combustion of the biochar can technically take place both in the pyrolysis reactor and outside of it in a separate combustor [77]. In the example shown, incineration takes place in the external combustor where the resulting gases are extracted. The hot heat transfer material is returned to the rotating cone reactor. In the left part of the figure, it can be seen that the vapors produced during pyrolysis are withdrawn separately. After potential purification of the pyrolysis vapors, they are condensed and the resulting bio-oil is collected [67]. Biomass throughput of rotary cone reactors can be equivalent to several tons per hour, an example of which is provided by a BTG plant capable of processing 2000 kg/h [63].

Ablative reactors

Ablative reactors are characterized by a principle of operation that differs from the systems discussed so far. In ablative reactor systems biomass particles are pressed against heated and often rotating surfaces. The prevailing pressure and temperature lead to liquefaction of the biomass at the contact surface. Continuously, the resulting liquid film evaporates, and the pyrolysis vapours are withdrawn. As soon as the biomass layer on the heated contact surface

has been pyrolyzed, new biomass is exposed, which in turn is liquefied again. In ablative systems, the speed of the pyrolysis reaction can be influenced by pressure, contact area, temperature and the relative velocity between biomass and the heated reactor surface. One of the major advantages of this technology is the large particle size of the biomass that can be used [67]. Since neither a carrier gas nor a bed of inert heat transfer material including recirculation is required, the reactor system can be installed compactly in a confined space [77]. Furthermore, high liquefaction rates, similar to those of fluidized bed reactors, are possible. The biggest disadvantage is the high degree of wear due to the high pressures and the mechanical stresses caused by fast-moving parts. The wear of ablative reactors is greater than that of rotating cone reactors. A schematic example of an ablative reactor is shown in Figure 37 [67].

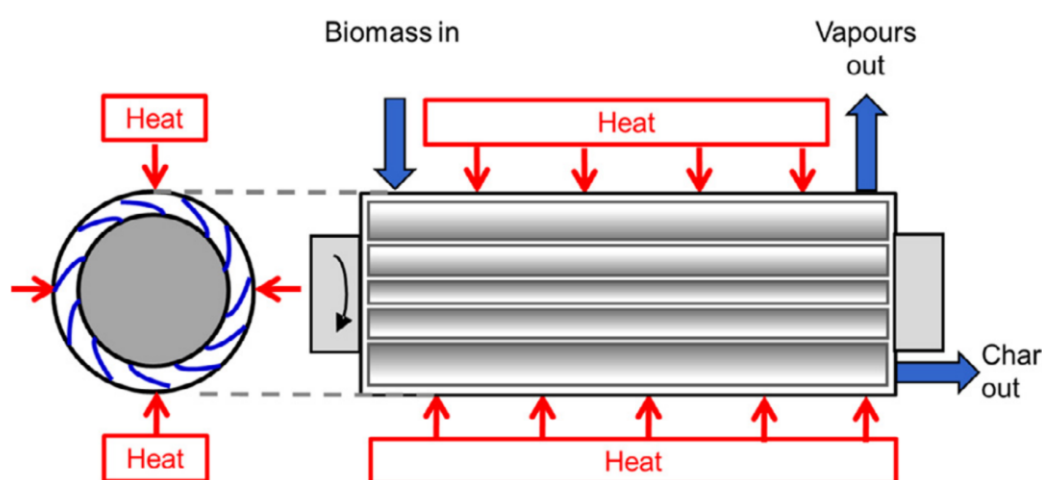


Figure 37: Ablative reactor [67]

An example of large-scale ablative biomass pyrolysis is in California operated by Bioenergy Concept. In the Bioenergy Concept fast pyrolysis reactor, biomass and other organic polymers are processed into bio-oil and fine biochar with a capacity of 500 kg/h [78].

Auger Reactors

In auger reactors, the biomass is conveyed through the reactor vessel together with an inert heat transfer material. Pyrolysis vapor generated in the process are discharged at the upper edge of the static reactor housing and are subsequently cleaned and condensed outside the reactor. The biochar is discharged together with the heat transfer material at the end of the reactor. When a heat transfer material is used in auger reactors, its regeneration and recycling is necessary. Control of the solid material residence time is achieved by means of the rotation speed of the screw conveyor. Figure 38 shows a typical auger reactor using inert heat transfer material [67]. The advantages of screw systems are the simple and inexpensive process design, the absence of carrier gas, and the easy controllability of the residence time [63]. Disadvantages are reduced liquefaction rates of 40-60% and a higher proportion of water in the resulting liquid phase [63,76]. Auger reactors are titled as an emerging technology in the field

of pyrolysis processes. In addition to companies such as BIOGREEN-ETIA, ABRI-TECH Inc. and PYREG GmbH, university institutions such as the Karlsruhe Institute of Technology (KIT) are also conducting research on auger reactor systems. BIOGREEN-ETIA for example, has developed the Spirajoule process, which can process a wide range of raw materials at capacities of up to 2500 kg/h [79].

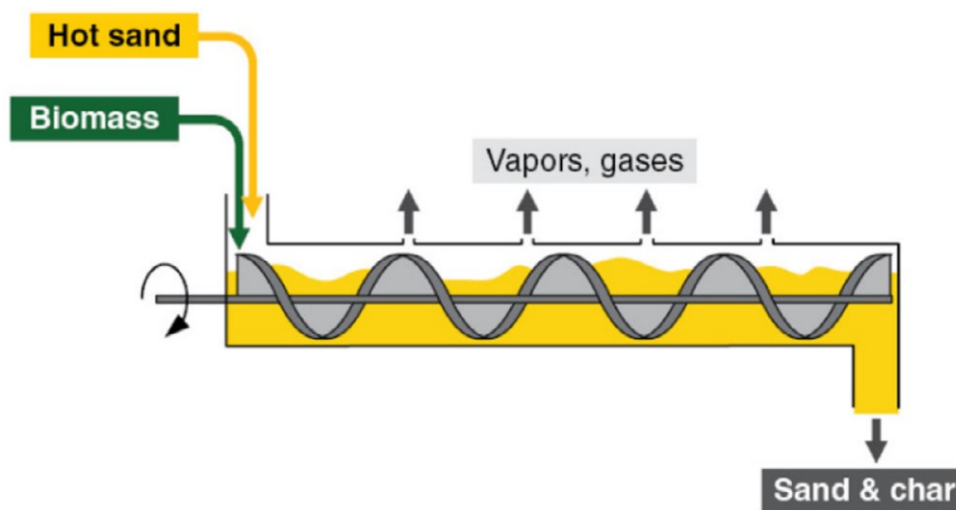


Figure 38: Auger reactor [67]

Vacuum pyrolysis

Reactor systems operated under vacuum are not a separate type of reactor but a mode of operation in which different reactor systems can be used. Figure 39 shows a simple process scheme of a pyrolysis system including vacuum-generating appliances.

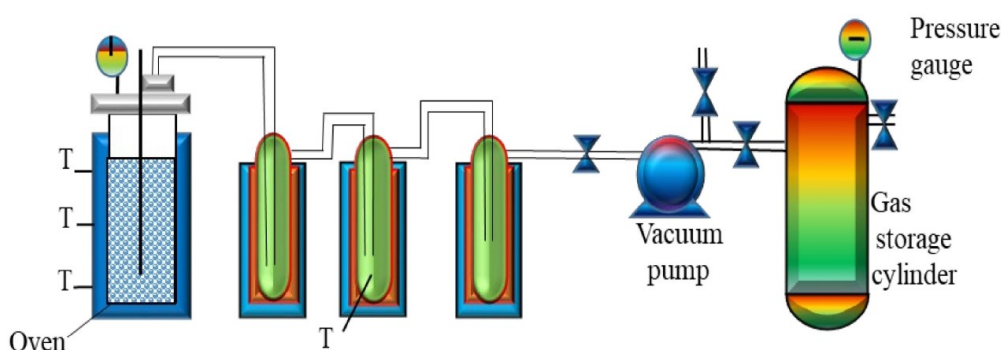


Figure 39: Evacuated pyrolysis system [63]

In research, vacuum pyrolysis systems are often investigated, since in theory advantages over conventional pyrolysis can be expected. Significant advantages are the shortened residence time, due to withdrawal of the resulting pyrolysis gases, high quality biooil and the possibility of using larger biomass particles [63]. Despite these advantages, vacuumized systems have not yet become industrially widespread. In general, complex process design, high costs (investment and maintenance) and reduced liquefaction rates are mentioned as the major drawbacks [67]. One of the few companies dedicated to this technology is Pyrovac from Canada.

Pyrovac developed a system in which the heat transfer takes place through molten salts and the biomass feed as well as pyrolysis is conducted under vacuum. This so-called Pyrocycling process is designed to pyrolyze up to 3500 kg/h of biomass [80].

3 State of the art of lignin pyrolysis

This chapter describes the methodology and findings of the literature review regarding the state of the art for lignin pyrolysis. This guiding question will be broken down in a structured manner and the following sub-questions can be formulated. How developed is the technology for pyrolysis of lignin? What is the scientific activity in this research field and on which sub-areas is the science focused on? The aim and purpose of this research is a summarized overview of the currently most relevant application forms and research directions.

The database "Engineering Village" is used as a basis for the search of scientific publications. For areas with less technical content, "Google Scholar" is sporadically applied. A search in the non-indexed section of Engineering Village yields 4686 hits for the query term "lignin pyrolysis" (as of 08.06.2023). In the course of the search, this area was confined by the targeted use of other technically relevant terms such as: reactor, fixed bed, fluidized bed, industrial scale, or fast pyrolysis. From a chemical analytical point of view, terms such as: GC-MS, MALDI-TOF, GPC, or thermogravimetry were used to effectively limit the area to be screened. By using Boolean operators (and, not, or) in combination with appropriate terms from the subject areas of technology, natural science and analytics, targeted corresponding sectors of the basic set of publications were analysed. After sorting out non-relevant publications by evaluating the titles or abstracts, about 150 sources were declared relevant. Through the references of this publications, new papers can be accessed, and often primary literature is reached. In the course of the research, a total of 269 literature sources were collected from which the overview presented below was compiled. The publications cited in this summary are individual representatives of the respective research fields and not complete collections. The present literature review attempts to provide an overview that is broad enough to narrow down the research field of lignin pyrolysis well, but not too broad to lose clarity.

In the course of the research, it turned out that research in the field of lignin pyrolysis is widely spread. In addition to pyrolysis and its process parameters, research is being conducted into the admixture of additives, the influence of biomass, metal contamination and its effects, catalysts, fundamental research of chemical reactions in this process, purification methods and much more.

First, general information on lignin pyrolysis is explained in chapter 3.1. Then, the state of the art is discussed in chapter 3.2. In the course of this, differences, and challenges to the pyrolysis of woody biomass become more apparent. Finally, in chapter 3.3, the research fields of lignin pyrolysis are presented in a structured way in order to be able to assess the potential for optimizing the process.

3.1 Basic information

In this chapter, introductory information about the pyrolysis of lignin is presented in comparison to the pyrolysis of biomass already described in chapter 2.2. The basic principle of the process is unchanged compared to the pyrolysis of lignocellulosic biomass. Figure 40 shows an exemplary schematic of a process for the pyrolysis of lignin.

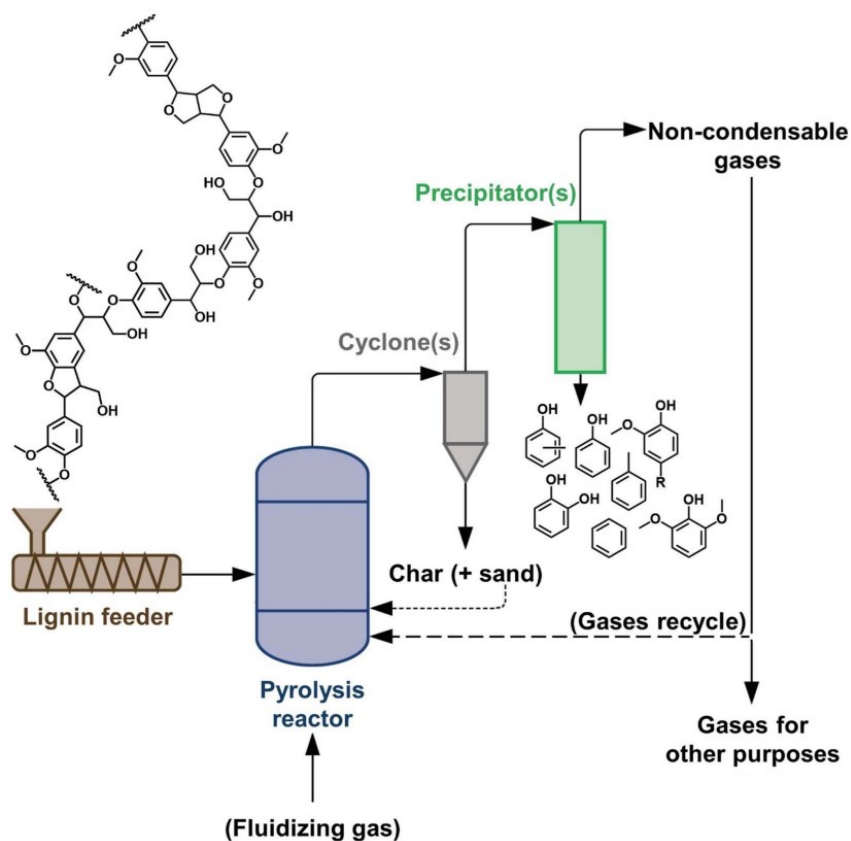


Figure 40: Lignin pyrolysis process scheme [81]

Analogous to the pyrolysis of woody biomass, the feedstock is converted to pyrolysis vapours, char, and non-condensable gases. As shown in Figure 40, the raw material is fed into the reactor via a feeder system. In the pyrolysis reactor, lignin is pyrolyzed at elevated temperatures of about 500 °C and in the absence of oxygen. The reactor shown, is a fluidised bed reactor, but similar to pyrolysis in general, many different reactors are used in lignin pyrolysis. Solid products are separated from the pyrolysis vapours and gases in one or more cyclones and optional filters or ESPs. Pyrolysis vapours are condensed and separated as a liquid phase, the biooil. Gases that cannot be condensed are recycled to the system and serve as a fluidising agent or are otherwise processed, for example for thermal energy generation. From a process engineering point of view, the process does not differ significantly from the pyrolysis of LCBM [81].

Differences become apparent, when considering chemical properties of the feedstock, reactions, and products. If the most important macromolecules are considered, it is clear that both

poly sugars cellulose and hemicellulose, which are present in large quantities in woody biomass, do not play a major role in the pyrolysis of pure lignin. However, if lignin is pyrolyzed together with portions of them, the chemical reactions and products change. The effects of the two macromolecules on the pyrolysis of pure lignin are stated in chapter 3.3.4. As already explained in detail in Chapter 1.1.5, lignin is a strongly cross-linked macromolecule whose basic building blocks are: coumaryl alcohol, sinapyl alcohol and coniferyl alcohol [81]. These phenylpropanoids are shown in Figure 10.

Pyrolysis of lignin can initially be simplified as a fragmentation process; more detailed descriptions of the predominant reactions follow in Chapter 3.1.2. The large lignin macromolecules are broken down by high temperatures. Besides char, water, and non-condensable gases, products chemically related to the monolignols shown in Figure 41 are formed. These monophenols are divided into three groups. Molecules formally derived from coumaryl alcohol are phenols. Guaiacols are formed from coniferyl alcohol, and syringols are structurally related to sinapyl alcohol. Analogous to the nomenclature of structural subunits in lignin, these group types are usually abbreviated with the letters H (phenols), G (guaiacols) and S (syringols). Furthermore, catechols (Ca-type) should also be mentioned, which have two or three phenolic OH-groups and are structurally similar to G-types and S-types. Figure 41 shows examples of important representatives of pyrolysis product groups, present in the oil phase. The high degree of diversity in the products of pyrolysis reflects the structural diversity of lignin molecules [82].

The simplified implementation of lignin pyrolysis from a process engineering point of view and a short insight into the specific products has been given. In the following chapters, this overview will be consolidated by more in-depth details.

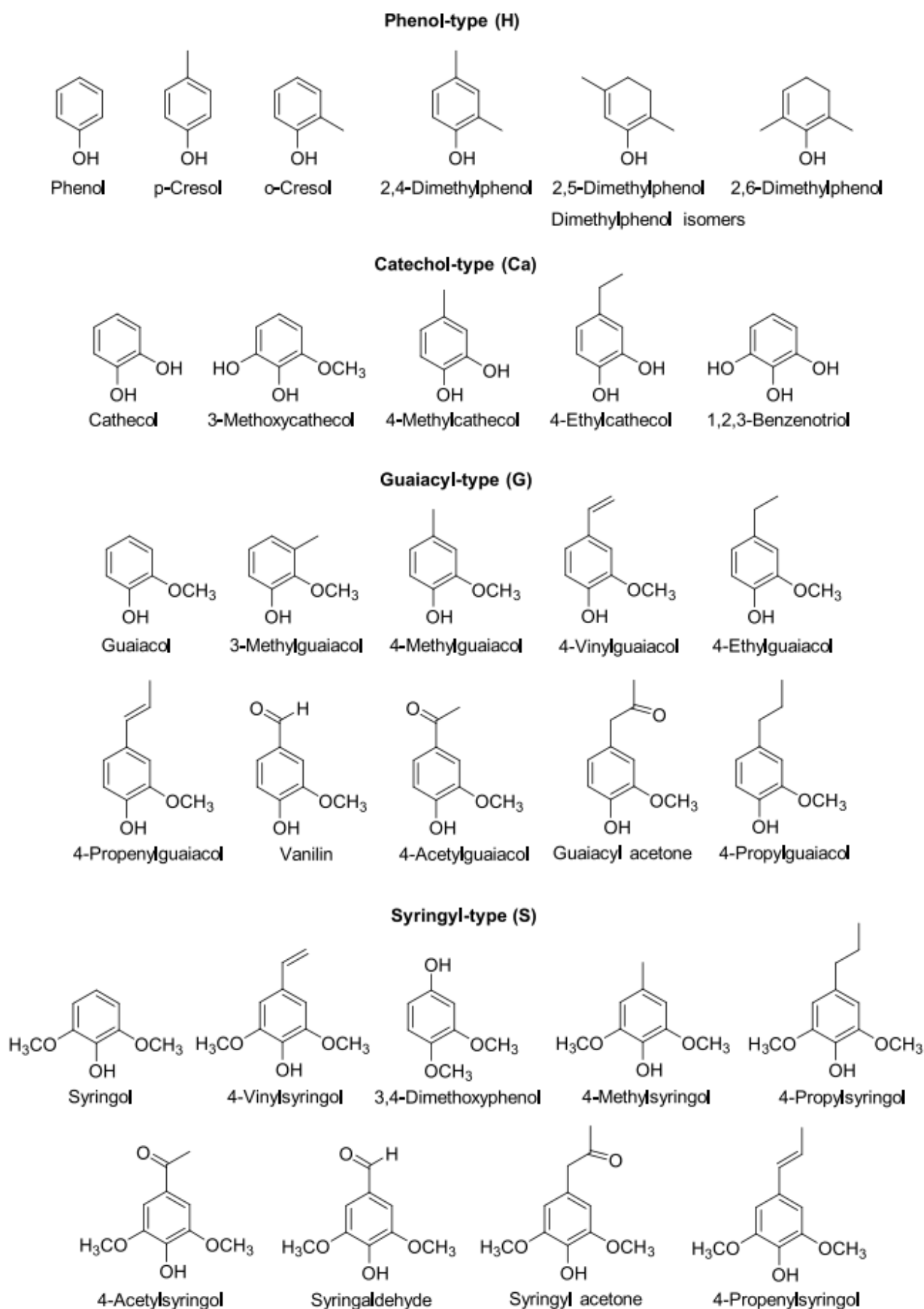


Figure 41: Representatives of monomeric product groups of lignin pyrolysis [82]

3.1.1 Products

The products formed during lignin pyrolysis can be classified on the basis of their states of aggregation at room temperature. The liquid products usually consist of two phases. In addition to the organic phase of biooil, a water phase is also formed. The solid product is biochar, and gaseous products are also formed. Table 4 lists examples of product distributions of lignin pyrolysis experiments.

Table 4: Product distributions of lignin pyrolysis

Org. Ph. [%]	Water Ph. [%]	Pyrolytic lignin [%]	Gas [%]	Char [%]	Lignin	Biomass	T [°C]	Reactor	Type of pyrolysis	Feed	Source
33-35	6-9	n.d.	11-14	40-45	EtOH-org.	beech	600	FB	fast/flash	0,5 g	[83]
22	n.d.	n.d.	37	41	kraft	larch	600	FB	fast/flash	5 g	[84]
30	n.d.	n.d.	20	50	kraft	n.d.	470	FB	fast/flash	0,04 g	[85]
38	n.d.	n.d.	15	47	kraft	n.d.	560	FB	fast/flash	0,04 g	[85]
10	1	n.d.	12	77	EtOH-org.	beech	500	BFB	fast/flash	1 g/min	[86]
29	15	22	16	34	EtOH-org.	hardwood mix.	500	BFB	fast/flash	10 g/min	[87]
21	20	12	17	36	HAc-org.	straw	500	BFB	fast/flash	10 g/min	[87]
25	21	18	13	37	kraft	softwood mix	500	BFB	fast/flash	10 g/min	[87]
30.8	23.9	21.4	15.1	35.6	EtOH-org.	wheat straw	500	BFB	fast/flash	8.3 g/min	[88]
32	19.9	24.1	17.4	30.9	EtOH-org.	wheat straw	500	BFB	fast/flash	8.3 g/min	[88]
30.5	17.1	18.0	15.2	39	soda process	straw/grass	500	BFB	fast/flash	8.3 g/min	[88]
24.4	14.5	14.0	20.7	43	kraft	hardwood	500	BFB	fast/flash	8.3 g/min	[88]

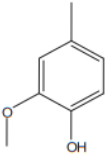
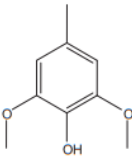
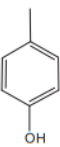
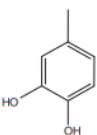
Org.Ph. ... organic phase; Water Ph. ... water phase; EtOH-org. ... ethanol organosolv; HAc-org. ... Acetic Acid organosolv; FB...fixed bed; BFB...bubbling fluidized bed

When looking at Table 4, it should be noted that the sum of oil phase, water phase, gas and coal does not always add up to 100 %. Reasons for this can be, among others, the remaining biomass in the reactor as well as balance inaccuracies. The pyrolytic lignin listed in the table is to be considered part of the oil phase and will be discussed in more detail later in this chapter. Oil phase proportions vary from 10-38 %, although it should be noted that some publications use very small feed quantities and with the resulting little amounts of liquid products a visible phase separation is hindered. The liquefaction rates, i.e. the sum of both liquid phases, vary between 11 and 54.7 %. In comparison, a liquefaction rate of over 75 % can be achieved in the pyrolysis of lignocellulosic biomass. Non-condensable gases range from 11 to 37 % and biochar varies between 30.9 and 50 % in the products of lignin pyrolysis. All publications listed in Table 4 have used short residence times and high heating rates, this form of pyrolysis is

called fast or flash pyrolysis, which generally leads to the highest liquefaction rates as discussed in chapter 2.2.

The data in Table 4 also shows that feed capacities are currently still very limited. In the majority of publications, dealing with pure lignin pyrolysis, feed quantities of a few hundred milligrams to a few grams are used. Experiments with feed quantities in this range must be critically questioned with regard to their quantitative significance. It should be mentioned that most of the studies do not collect a holistic mass balance, insufficiently characterise the feed material and do not consider pyrolytic lignin that is produced in significant quantities. A good overview of the totality of the products formed is provided by de Wild et al. Table 5 shows an example of their results for four different lignins pyrolysis experiments under the same conditions in a bubbling fluidised bed reactor at 500 °C [88].

Table 5: Results of BFB pyrolysis at 500 °C [88]

All yields: %, w/w, dry lignin feedstock	Type of lignin feedstock → Feedstock code → Products ↓	Wheat straw organosolv lignin		Wheat straw/grass soda lignin	Hardwood organosolv lignin
		A	B	Granit	Alcell
Major product fraction	Gas	15.1	17.4	15.2	20.7
	Oil	54.7	51.9	47.6	38.9
	Char	35.6	30.9	39.0	43.0
	Mass balance	105.3	100.2	101.8	102.6
Gases	CO ₂	7.7	9.0	6.2	10.2
	CO	5.8	6.7	6.8	8.1
	CH ₄	1.6	1.7	2.2	2.5
	Total gas	15.1	17.4	15.2	20.7
Water	Water	23.9	19.9	17.1	14.5
Light ends	Acetone	0.30	0.17	BDL	BDL
	Methanol	1.06	0.68	0.99	1.41
	Acetic acid	0.43	0.35	0.31	0.37
	2-Furaldehyde	BDL	BDL	0.10	0.08
	Total light ends	1.8	1.2	1.4	1.9
Guaiacols 	2-Methoxyphenol	0.43	0.37	0.73	0.30
	4-Methylguaiacol	0.44	0.45	0.53	0.48
	4-Ethylguaiacol	0.21	0.21	0.43	0.13
	2-Methoxy-4-propyl-phenol	0.03	0.03	0.03	0.03
	Eugenol	0.04	0.04	0.03	0.03
	Isoeugenol	0.19	0.19	0.17	0.14
	2-Methoxy-4-vinyl-phenol	0.52	0.61	0.87	0.18
	Vanillin	0.06	0.08	0.08	0.15
	Aceto-vanillone	0.05	0.05	0.08	0.06
	Total guaiacols	2.0	2.0	3.0	1.5
Syringols 	2,6-Dimethoxyphenol	0.39	0.27	0.70	0.73
	4-Methylsyringol	0.41	0.34	0.45	1.21
	4-(2-propenyl)syringone	0.07	0.06	0.07	0.11
	Syringaldehyde	0.06	0.05	0.05	0.40
	Acetosyringone	0.12	0.10	0.36	0.13
	Total syringols	1.1	0.8	1.6	2.6
Alkylphenols 	Phenol	0.17	0.13	0.36	0.11
	O-cresol	0.05	0.05	0.10	0.06
	P-cresol	0.16	0.12	0.24	0.10
	M-cresol	0.03	0.03	0.04	0.05
	4-Ethylphenol	0.17	0.10	0.35	0.02
	Total alkylphenols	0.6	0.4	1.1	0.3
Catechols 	3-Methoxypyrocatechol	0.16	0.11	0.50	0.30
	Pyrocatechol	0.41	0.32	0.67	0.25
	Total catechols	0.6	0.4	1.2	0.5
Unidentified	Unknowns	3.5	3.0	4.4	3.6
	Monomers (incl. unknowns)	7.8	6.6	11.2	8.5
Undetected	Oligomers	21.4	24.1	18.0	14.0
Total phenolic material	Monomers + oligomers	29.2	30.7	29.2	22.5

BDL, below detection limit.

Biooil

The main focus of scientific research on the products of lignin pyrolysis is on the organic liquid phase, the biooil. In accordance with the research interest, this diploma thesis will focus on the biooil phase.

Gas chromatography with downstream mass spectrometer can be used to give insights into the chemical diversity of bio-oil. Figure 44 shows a pyrolysis GC-MS of beech wood organosolv lignin at 400 and 600 °C, where the most common molecules are depicted structurally and are assigned to their corresponding peaks [83].

The illustrated GC-MS shows the similarity of the pyrolysis products of lignin to the original macromolecule. At temperatures of 400 - 600 °C, many native substructures can still be retained in the form of variously substituted monophenols. As liquid products of the pyrolysis of lignin, besides phenolic monomers, methoxy benzenes and catechols also small amounts of organic acids, ketones, aldehydes, and other compounds that are not specified more precisely are formed [83]. In terms of quantity, the most important representatives of this light fraction in biooil are methanol and acetic acid. In the scientific literature, however, the interest lies predominantly on monophenols. An overview of the product range of monophenols and catechols,

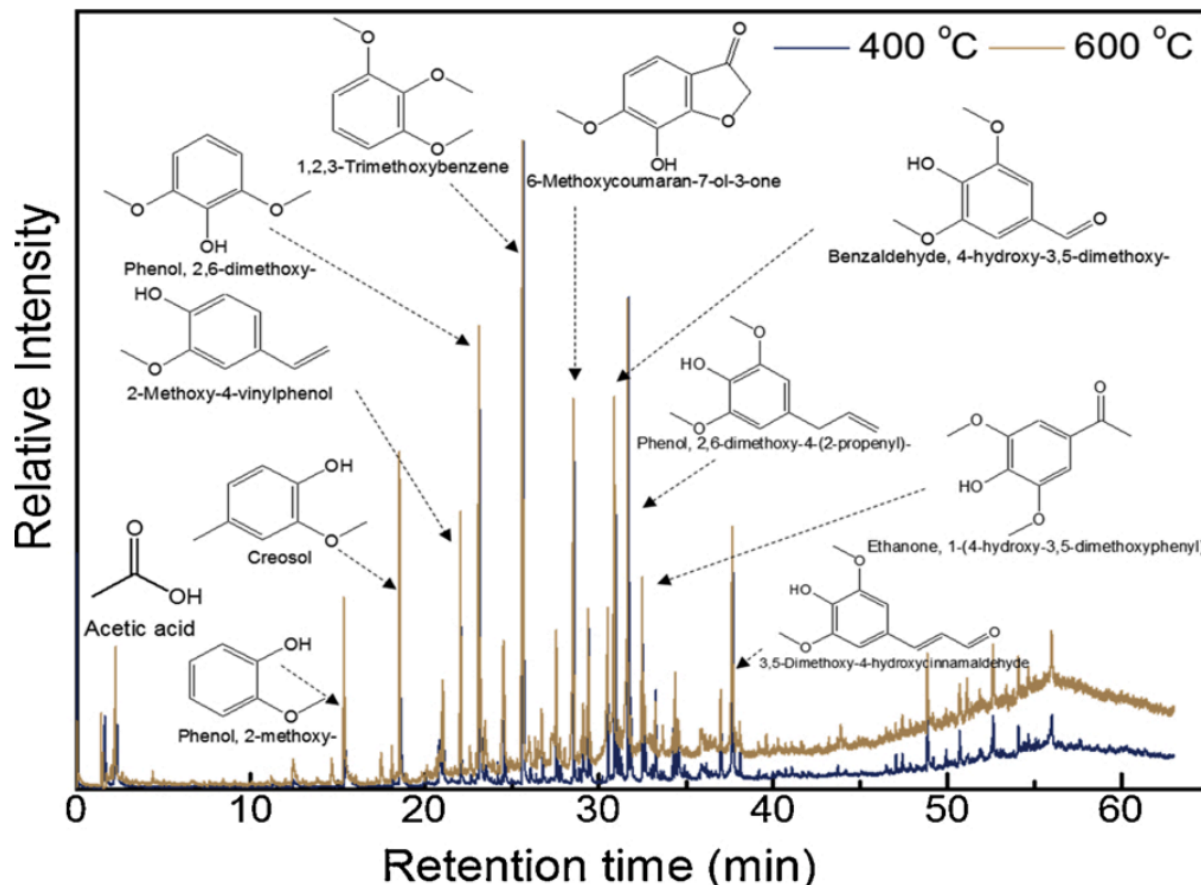


Figure 42: GC-MS of lignin pyrolysis biooil [83]

as well as their nomenclature, has already been given in 3.1. It should be noted that the analytical method of GC-MS cannot reflect all components of the oil phase. In particular, dimers, trimers and other oligomers that have not been broken down by pyrolysis are not detectable. Oligomers formed during the pyrolysis of lignin are referred to as pyrolytic lignin and account on average for about 20% of the total products of pyrolysis [88].

Pyrolytic lignin

Pyrolytic lignin (PL) is already known from the pyrolysis of woody biomass, but there are limited publications on this topic. If no separation of the pyrolytic lignin takes place, it is part of the organic phase of the pyrolysis oil. When looking at studies on lignin pyrolysis, no studies could be found that deal with the chemical structure of pyrolytic lignin produced by pyrolysis of pure lignin. Figure 43 shows a model structure of a molecule of pyrolytic lignin from LCBM [89].

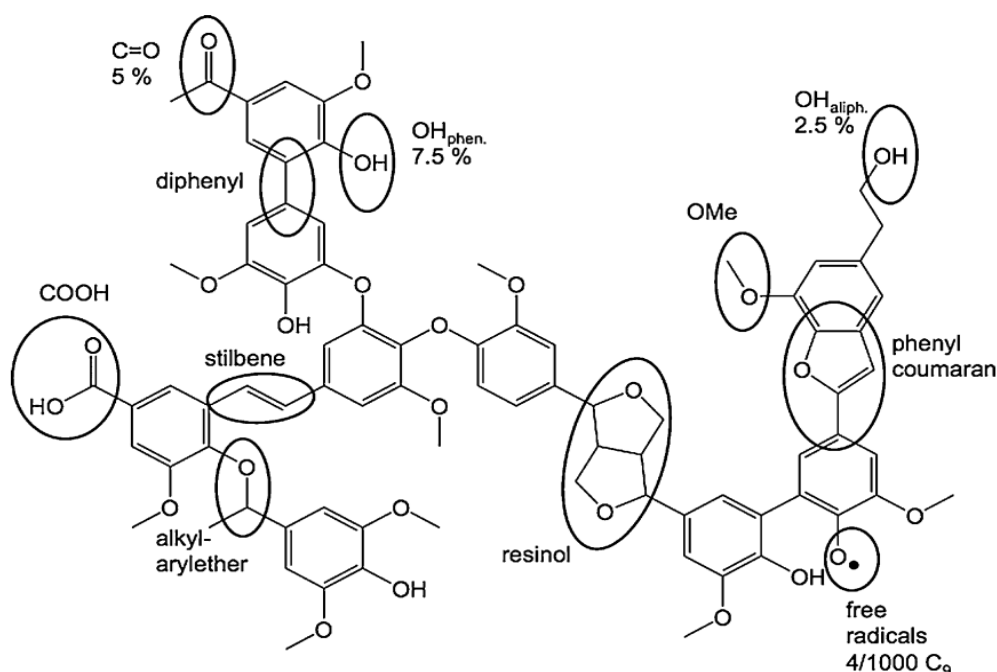


Figure 43: Model of an exemplary PL molecule [89]

Bayerbach et al. have developed this model by statistical comparison of different methods such as wet chemical analysis, elemental analysis, chromatographic methods, and spectroscopic methods [89].

The structure shown is comparable to that of MWL presented in 1.1.5. As a significant difference, it should be noted that β -O-4 bonds, which are very common in native lignin, are hardly present in PL. From a chemical point of view, stilbenes, diphenyl, phenylcoumaran, alkyl-arylether, phenolic OH groups, COOH groups, aldehydes, ketones, and free radicals are the most common characteristics besides the interconnected benzene rings. Pyrolytic lignin exists as a mixture of molecules of different sizes. The molecular size distribution ranges from dimers with a molecular size around 390 g/mol to large oligomers above 4000 g/mol. Figure 44 shows the

molecular size distribution using matrix assisted laser desorption ionisation time of flight mass spectroscopy (MALDI-TOF-MS) and size exclusion chromatography (SEC) of a pyrolytic lignin produced by fast pyrolysis of beech wood [90].

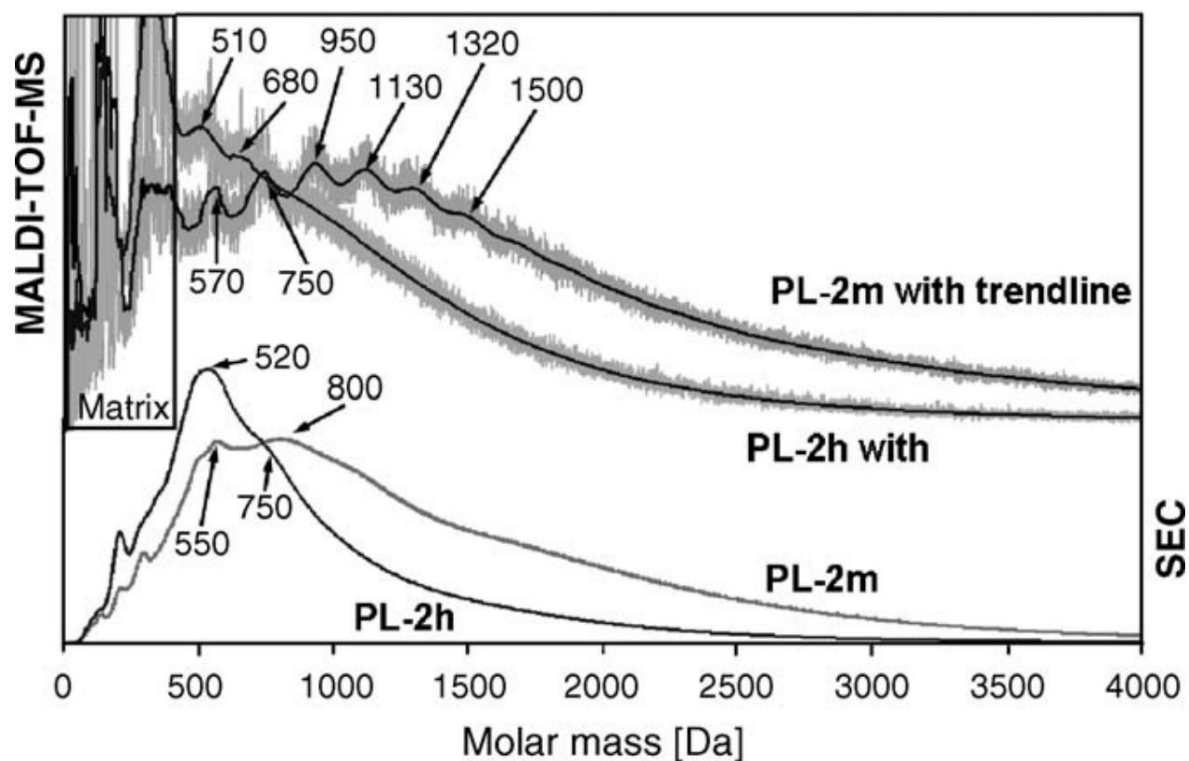


Figure 44: Molecular size distribution of PL measured with MALDI-TOF and SEC [90]

The mean value of the molecular size distribution of PL is much smaller compared to MWL, which, as already shown in chapter 1.1.5, has the mean value of the number-based distribution at about 4500 g/mol. Furthermore, Figure 44 shows that the PL is still reactive. Distributions after different times of pyrolysis are shown. The pyrolytic lignin precipitated and measured two hours after pyrolysis (PL-2h) is characterized by a narrow molecular size distribution with a mean value of about 520 g/mol. When the PL is precipitated and measured two months after pyrolysis (PL-2m), the distribution is broader, and the mean value is 800 g/mol. Precipitation of PL is performed by Bayerbach et al. by uptake in ice-cold deionized water [90].

Applications of pyrolytic lignin

Industrially, PL has no applications besides incineration. To use pyrolysis products in an ecologically and economically reasonable way, more research effort is needed for characterizing and processing PL into profitable chemicals or to significantly reduce PL production. Research is being conducted into new applications for PL on a laboratory scale. An example from literature for the further processing of PL is the catalytic hydrogen treatment of PL at 400 °C in an initial 100 bar H₂ atmosphere and with the use of ruthenium-based catalysts. Kloeckhorst et al.

were thus able to liquefy over 75% of the PL. The main products are alkylphenols and aromatics. This hydrotreatment produces less than 6 % water, 8-12 % gases and only traces of solids. However, the product quantification of this publication is limited, as only 30-50% of the products could be detected and classified by GC [91].

Gas and char

In addition to the liquid products, gases are also produced. The most common in terms of quantity are CO, CO₂ and CH₄. However, small amounts of other light hydrocarbons and H₂ also occur [83]. Currently, the main application of pyrolysis gases is thermal utilization for heat energy production [92].

Due to the high amount produced, biochar is of great importance in lignin pyrolysis. Depending on the process conditions and the lignin used, between 30 and 50 % biochar is produced at temperatures around 500 °C and short residence times, see Table 4. As mentioned in Chapter 2.2, biochar production can be increased by using low temperatures and long residence times. Usually, an attempt is made to keep the amount of gas and biochar produced low in exchange for high liquefaction rates.

Microscopically, biochar of lignin pyrolysis is a porous solid with a small specific surface area (about 5 m²/g) [93]. Activated carbon for comparison can reach specific surface areas of over 1000 g/m² [94]. Figure 45 shows BET surface area measurements of biochar from lignin pyrolysis and charcoal produced from lignin by oxidative conditions [93].

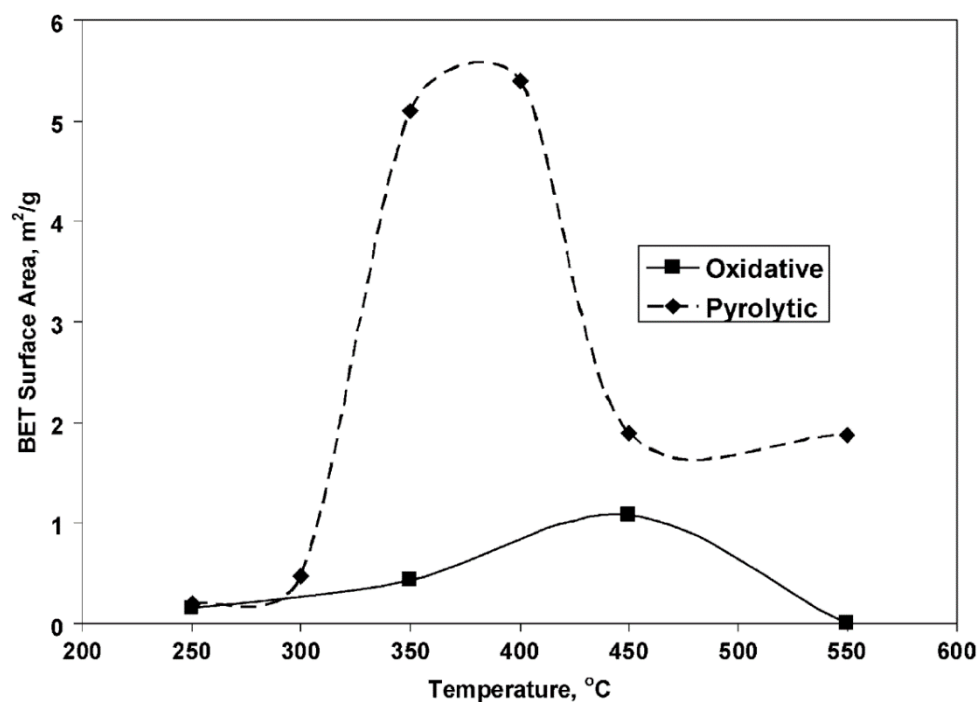


Figure 45: BET surface area of oxidative and pyrolytic lignin chars [93]

Scanning electron microscopy (SEM) can be used to depict the surface properties of lignin and the resulting biochar. Scharma et al. have studied SEM analysis of lignin and its pyrolytic charcoal and have shown that the surface properties are dependent on the pyrolysis temperature. Figure 46 shows the SEM micrographs of pure lignin (a) and the pyrolytic coals at 250 °C (b), 300 °C (c) and 350 °C (d,e). At temperatures around 250 °C, the kraft lignin particles, described by Scharma et al. as polygonal with irregular conchoidal fractures, begin to melt. The first pyrolysis gases are formed which inflate the softened lignin in the form of vesicles. These vesicles remain in shape after cooling. At higher temperatures, the formed vesicles (c) deflate after cooling, resulting in flatter surfaces (e) [93].

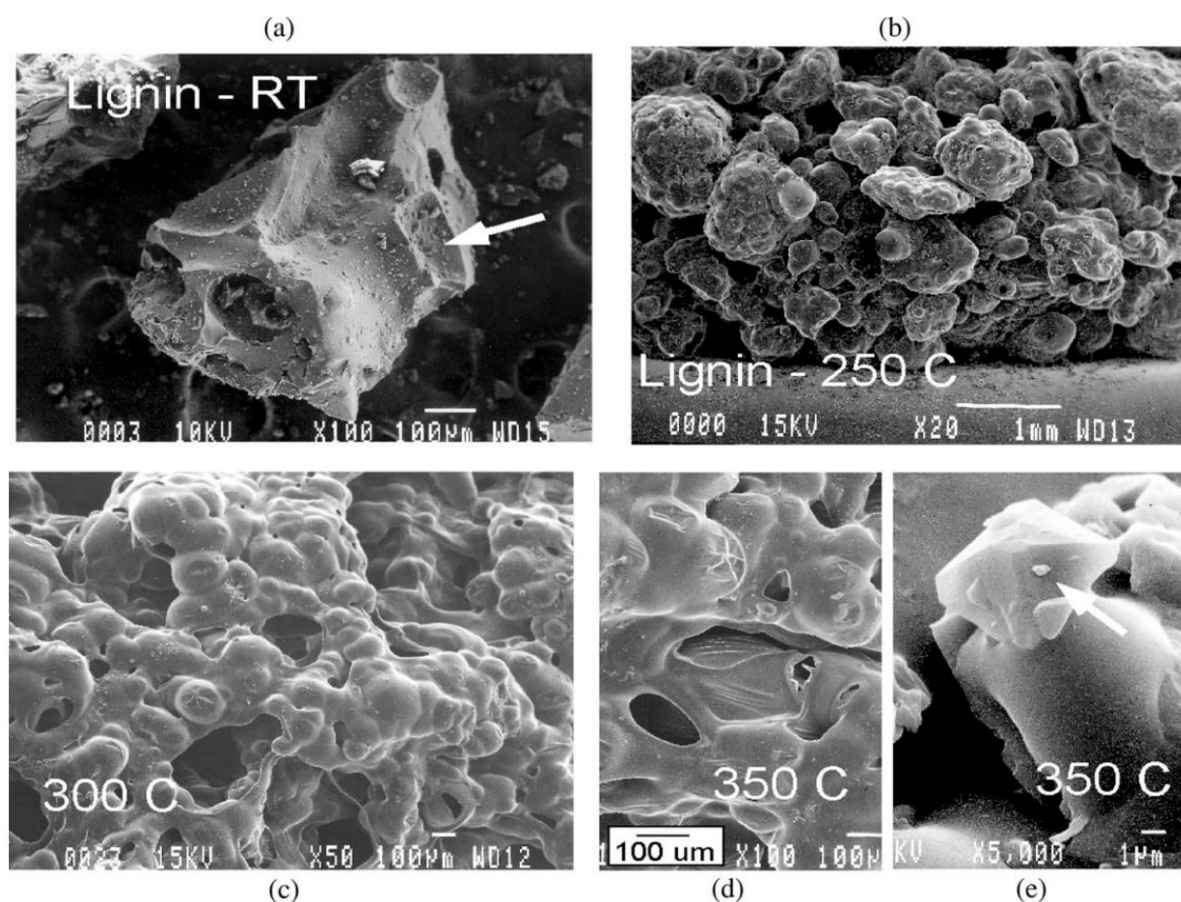


Figure 46: SEM micrographs of kraft lignin and pyrolytic biochar at 250-350 °C [93]

The micrographs at pyrolysis temperatures from 450-750 °C are shown in Figure 47 a-e. The surface structure changes are inhomogeneous at temperatures above 550 °C. On the one hand, molten phases are formed which still form vesicles even at 750 °C (e), on the other hand, very rigid areas are formed in which carbon areas can fracture off (d). It should be noted that the selection of the lignin used has an impact on the surface properties of the biochar. The lignin used by Scharma et al. is a kraft lignin with 5.7 % ash content. This inorganic material

consists mainly of sodium, potassium, and silicon oxides. An inorganic crystal is shown in Figure 46 (e) marked with a white arrow.

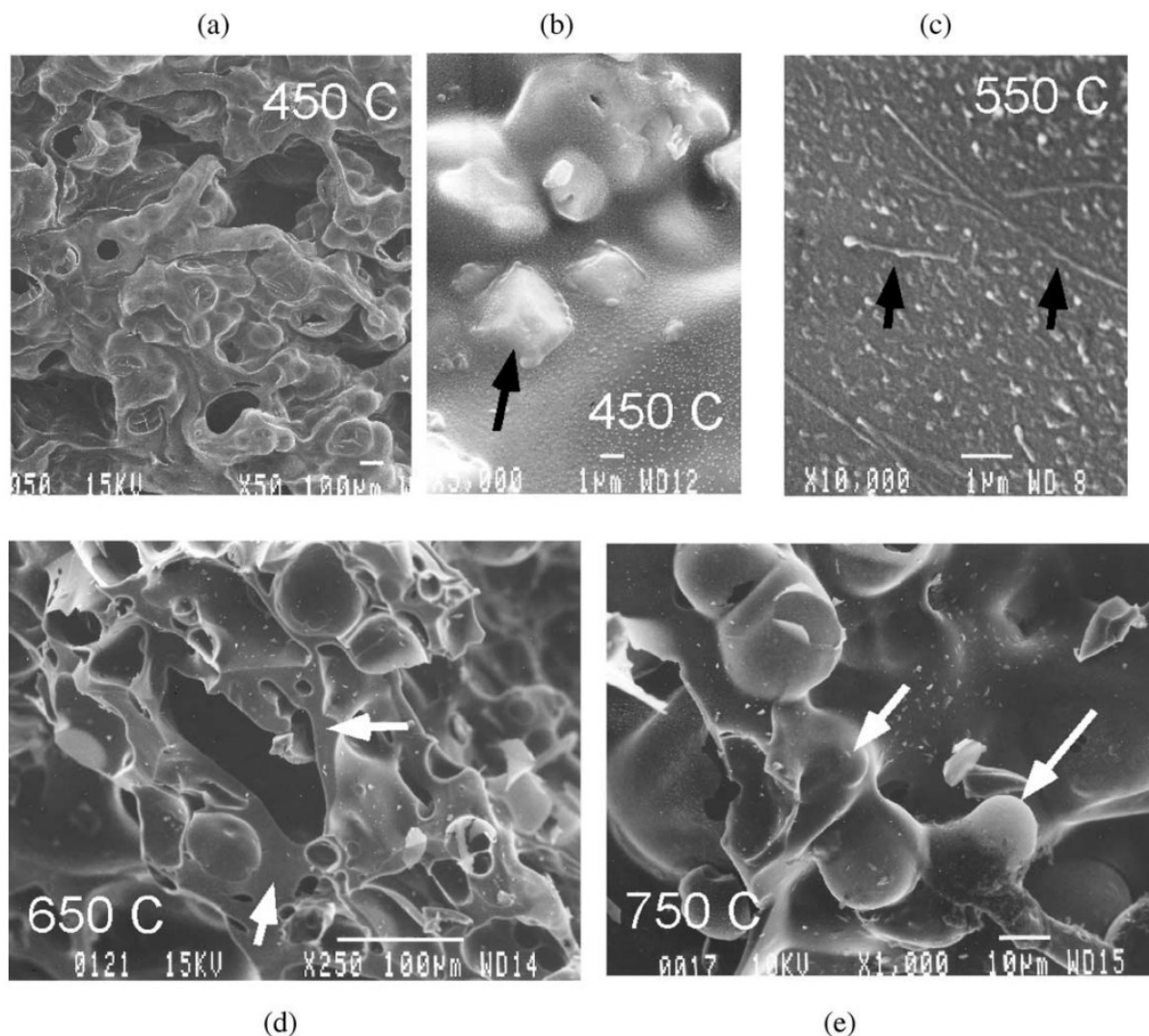


Figure 47: SEM micrographs of kraft lignin and pyrolytic biochar at 450-750 °C [93]

In addition to temperature-dependent surface morphological changes, there is also evidence of changes in chemical properties. Chua et al. show that the carbon content increases steadily with increasing pyrolysis temperature. Hydrogen, oxygen, and nitrogen, on the other hand, decrease with increasing temperature, so that the C/H as well as the C/O ratio increases directly proportional with temperature [95]. The temperature dependence of the bond types of carbon atoms in lignin pyrolysis chars are shown by ^{13}C cross-polarization magic angle spinning nuclear magnetic resonance (^{13}C CP/MAS NMR) by Chua et al. The relative proportions of carbonyl groups decrease with increasing temperature. The same applies to methoxy

groups and aliphatic side chains. The proportion of aromatic C-atoms, on the other hand, increases significantly. Table 6 shows the relative proportions of ^{13}C atoms measured with CP/MAS NMR [95].

Table 6: Relative content of chemical groups in lignin biochars [95]

	raw lignin	pyrolysis temperatures		
		100 °C	200 °C	300 °C
aliphatic (%)	9.66	9.06	8.59	7.01
methoxyl (%)	28.49	28.24	27.60	19.51
aromatic (%)	59.54	59.48	62.40	73.30
carbonyl (%)	2.31	3.22	1.41	0.18
aromaticity (%)	86.04	86.78	87.90	91.27

Zhang et al. extend the range of investigation to temperatures up to 800 °C. The increased proportion of aromatic C atoms with rising temperature results in different chemical structures of the biochar. When the C/H ratios and the ^{13}C CP/MAS NMR results are considered together, it is possible to draw conclusions about the increasing fusion of the benzene rings. At 200 °C, there are on average two benzene rings adjacent to each other. With increasing temperature, the number of adjacent benzene rings increases. At pyrolysis temperatures of 300 °C, an average of three benzene rings are fused. At 350 °C there are four and at 550 °C already 20 benzene rings [96]. Figure 48 shows an example of a possible biochar molecule resulting from lignin pyrolysis at temperatures between 400 and 600 °C [97].

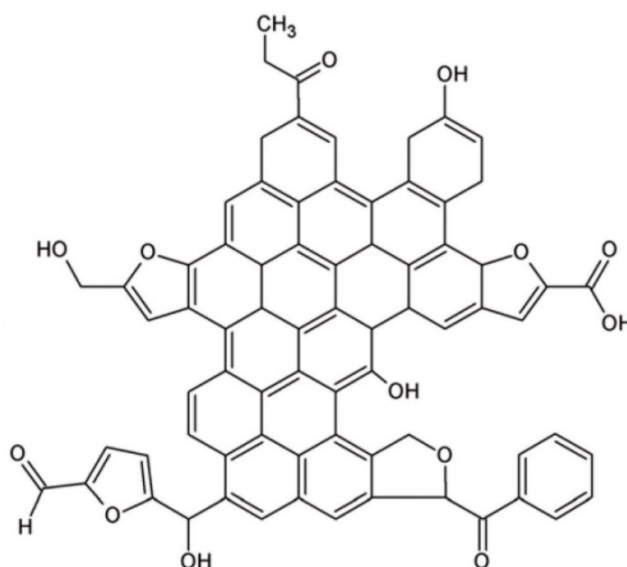


Figure 48: Biochar structure [97]

Besides incineration, burial into soil as an effective carbon sink is mostly the application for biochar [98]. However, intensive research is being carried out into other possible uses for biochar. In a publication in the *Ithaca Journal*, Hans Schmidt has outlined over 50 possible uses for biochar. These range from adsorptive and decontamination applications to agricultural land enhancement, electromagnetic radiation shielding and textile applications [99]. However, most of these applications are not technically elaborated. Chen et al. for example, state that activation and modification of biochar is necessary to improve the low specific surface area as well as the low number of functional groups, for effective adsorption [66].

3.1.2 Reactions

Chapter 3.1.2 deals with the chemical reactions that occur during lignin pyrolysis and yield the products discussed in chapter 3.1.1. As already stated, lignin pyrolysis can be described in simplified terms as a fragmentation process in which large macromolecules break down into smaller molecules. Since different bond types, that occur in lignins, have different bond strengths and therefore break with varying tendency, Figure 49 shows the most common bond variants in lignin including the associated bond dissociation energies in kcal/mol [100].

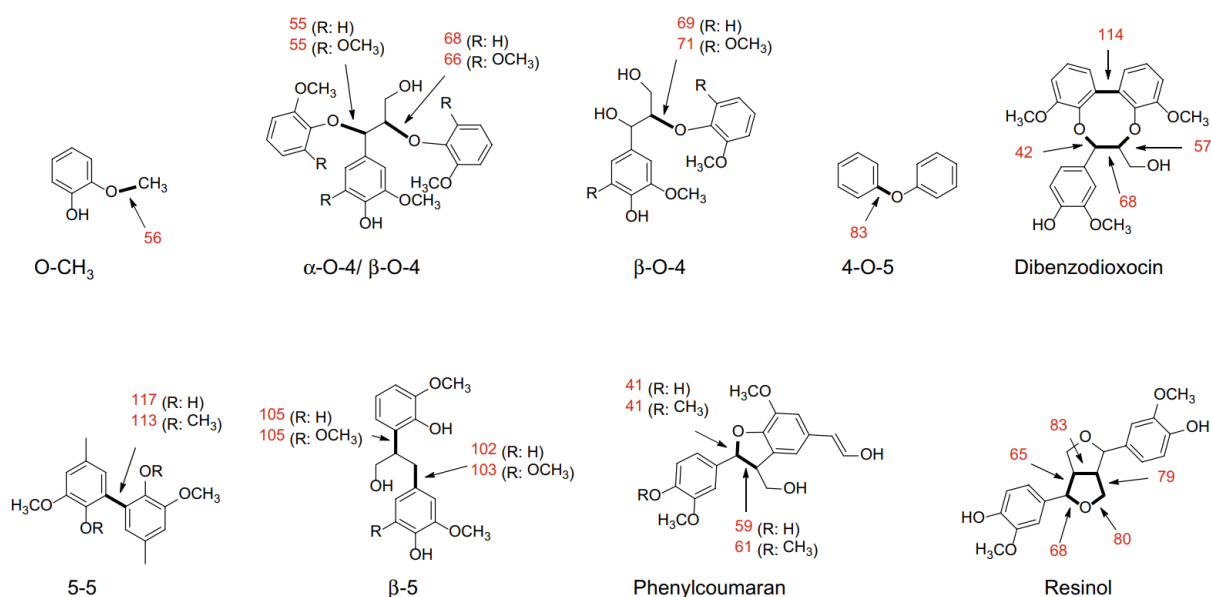


Figure 49: Dissociation energies of frequent substructures in lignin molecules in kcal/mol [100]

The bond dissociation energies shown in Figure 49 provide initial insights into the possible pyrolysis reactions. Thermogravimetric investigations of lignin pyrolysis show that up to about 180 °C the weight-loss rate in mg/s is approximately constant and only little amounts of lignin decompose at these temperatures.

Primary Reactions

Reactions that occur at the beginning of pyrolysis at 200-400 °C are called primary reactions. To be seen in the first peak of the differential thermogravimetry (DTG) curve in Figure 50. Reactions that occur in the primary phase involve bonds with the lowest dissociation energies. In particular, α -O-4 and β -O-4 bond breaks are to be mentioned regarding this aspect [100].

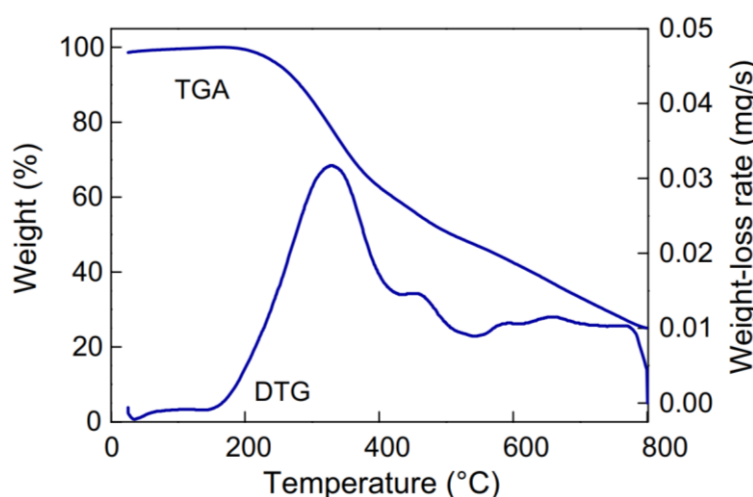


Figure 50: TGA analysis of pyrolysis of Japanese cedar MWL [100]

Methoxy groups have similarly low binding energies as the α -O-4 and β -O-4 bonds but are rarely split off in the primary reactions of pyrolysis. Reasons for the persistence of the methoxy groups in the primary phase are currently not sufficiently clarified. It should be noted that besides the dissociation energies, other aspects such as kinetics, steric effects, inter- and intra-molecular stabilizing bonds, as well as the entropy increase of the reactions are of great importance [100].

At the current stage of research, it is still unclear whether the ether bond breaks take place solely homolytically or also heterolytically. In homolytic breakage reactions, the two binding electrons of a single bond are divided equally between the two reaction products, thus forming radicals. In heterolytic cleavages, one reaction product takes on both bond electrons and thus forms an anion, the second reaction product becomes a cation [100]. Zhao et al. assume that the primary ether breaks proceed mechanistically in a purely homolytic manner [101]. However, Kawamoto explains in his detailed review experimentally supported arguments that support the idea that heterolytic bond breaks also occur. As a general tendency, according to Kawamoto, homolytic bond breaks tend to be more frequent [100].

Figure 51 shows radical chain reactions involving α -O-4 and β -O-4 bond breaks. The starting molecules for pathways A and B can be formed by homolytic hydrogen release of the imaged β -O-4 compound. Thus, either $C\alpha$ radicals (pathway A) or radicals of phenolic origin (pathway B) can be formed, depending on the site of hydrogen release. Furthermore, pathway B can be

started by homolytic α -O-4 cleavage if the phenoxy radical formed contains a β -O-4 bond itself. In both pathway A and B, a guaiacol radical is initially formed, which subsequently reacts further to form guaiacol. In pathway A, a C α -alcohol is formed which reacts subsequently to a C α -ketone. In pathway B, a C α -carbonyl compound is produced via a quinomethide intermediate. Kawamoto considers pathway B to be more efficient because three radicals are formed in the course of it, and with pathway A the number of radicals remains constant throughout the reaction pathway [100].

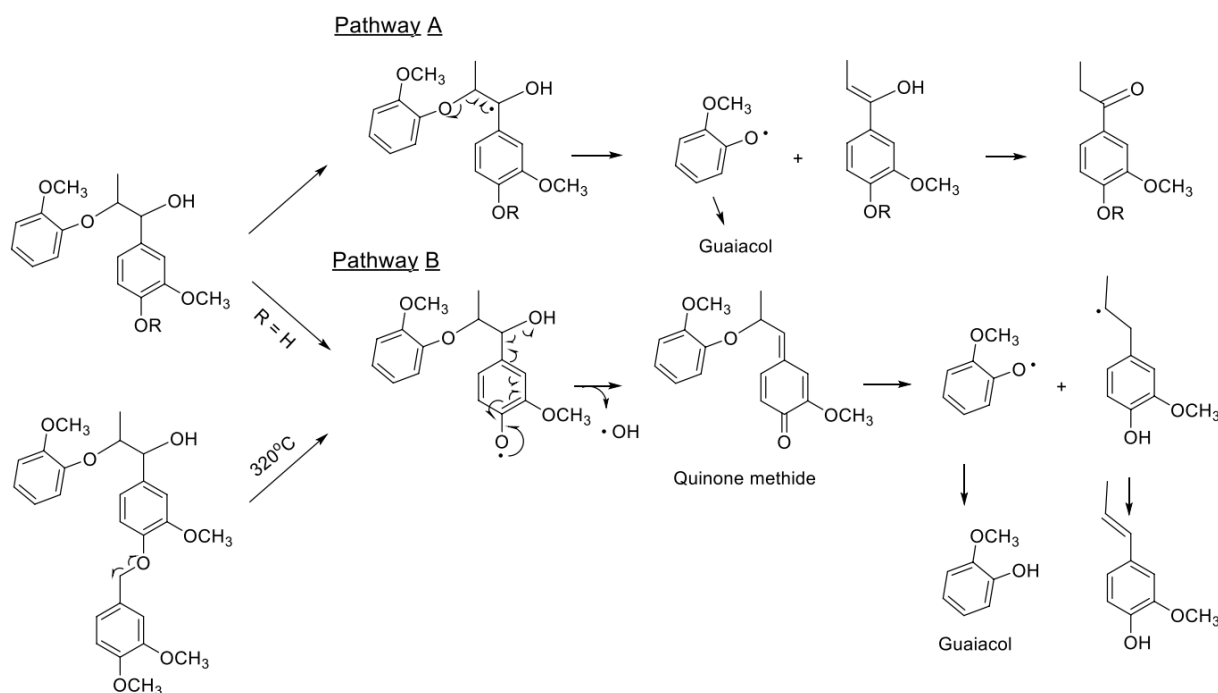


Figure 51: α -O-4 and β -O-4 cleavage related radical chain reaction mechanism [100]

The reaction pathway shown is one example of many possible mechanisms in the primary reactions of lignin pyrolysis. The monomers formed then have various possible subsequent reaction routes. On the one hand, they evaporate and are subsequently liquefied in the condenser. Another possibility is that they react with other reaction products of pyrolysis and thus repolymerize. The repolymerization products subsequently lead to the formation of biochar [100]. Biochar formation takes place at temperatures between 200 °C and 800 °C, formally these reactions do not classify as primary reactions [96].

Figure 52 shows a simplified representation of opposing reaction paths in primary reactions. In Figure 52, a phenoxy radical is split off from a lignin molecule by β -O-4 bond breakage. This molecule is representative for all monomers formed in primary reactions. The left pathway is that of repolymerisation in which a cross-linked macromolecule is formed via various reaction mechanisms (condensation, radical polymerisation, quinone methide mechanism, ...). The resulting crosslinked molecule is biochar whose properties and chemical temperature dependencies have already been described in chapter 2.2.1. The right path leads to the monomer-

containing fraction of the bio-oil. The chemical diversity of the monomers that characterise the bio-oil is not clarified by primary reactions alone. In the secondary reactions, which are explained later in this chapter, there are rearrangements of phenol substituents as well as cleavages. Furthermore, the degradation pathways leading to non-condensable gases are also presented with the secondary reactions, as they take place at higher temperatures as well [102].

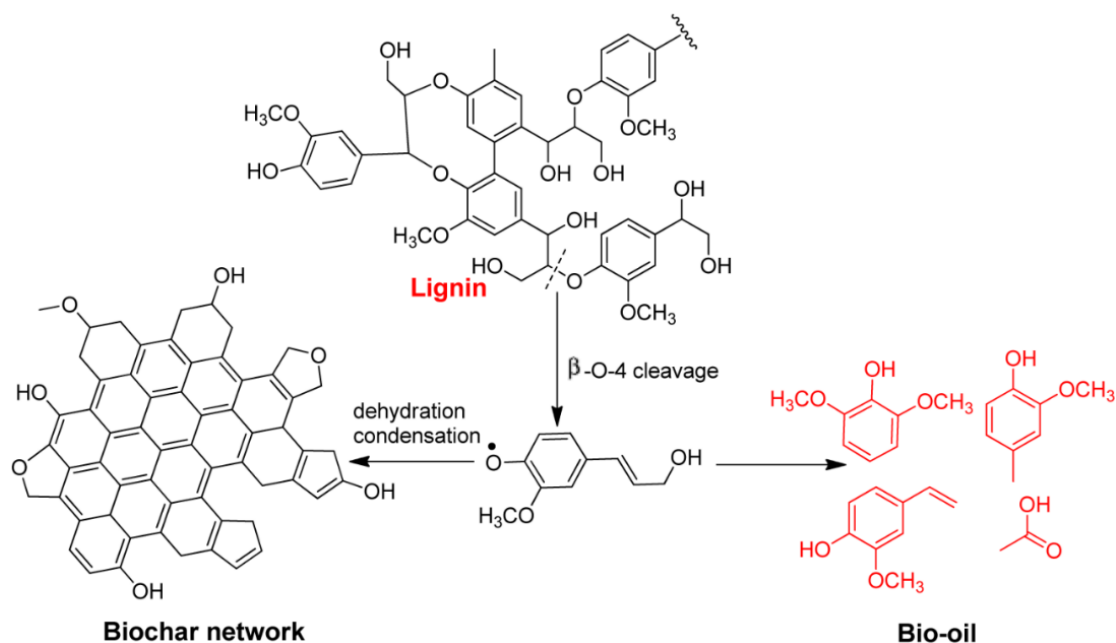


Figure 52: Representation of opposing primary lignin pyrolysis reactions [102]

Secondary Reactions

Recalling Figure 50, the secondary phase in pyrolysis starts with the second peak of the DTG curve, which translates to temperatures above 400 °C. In the secondary phase, in addition to the ether bond breaks, that dominate in the primary phase, C-C bonds also start to cleave. Additionally there are changes in the substituents of the aromatic rings and splitting off of the methoxy and phenolic groups. Furthermore, degradation reactions of monomers to non-condensable gases such as carbon oxides and light olefins can be classified as secondary reactions. The formation of polycyclic aromatic compounds and thus the formation of a biochar network is also classified by some authors as a secondary reaction [100].

Figure 53 shows some examples of reaction mechanisms starting from a guaiacol monomer. In particular, these are reactions leading to catechols, quinone methides, o-cresols and phenols. Starting from the guaiacol monomer, a catechol can be formed under homolytic O-CH₃ bond cleavage (b) with release of CH₃ radicals which in turn can further react to form methane or methanol. Another reaction possibility is the formation of a phenoxy radical (a), which can react further via the formation of the o-quinone methide intermediate (c-g) to form a cresol (h). In the steps f and g that lead to quinone methide, water splits off. This reaction is an example

of a multitude of thermal degradation reactions in which water is formed, which ultimately makes up approx. 20 % of the products, as can be seen in Table 5. Alternatively, instead of the quinone methide formation, the entire methoxy group can be cleaved off in several intermediate steps to form phenols (j-m) [100].

As an example reaction for the generation of non-condensable gases in the course of the secondary phase of lignin pyrolysis, the degradation of a radical catechol monomer to ethine and CO is shown in Figure 54 [100].

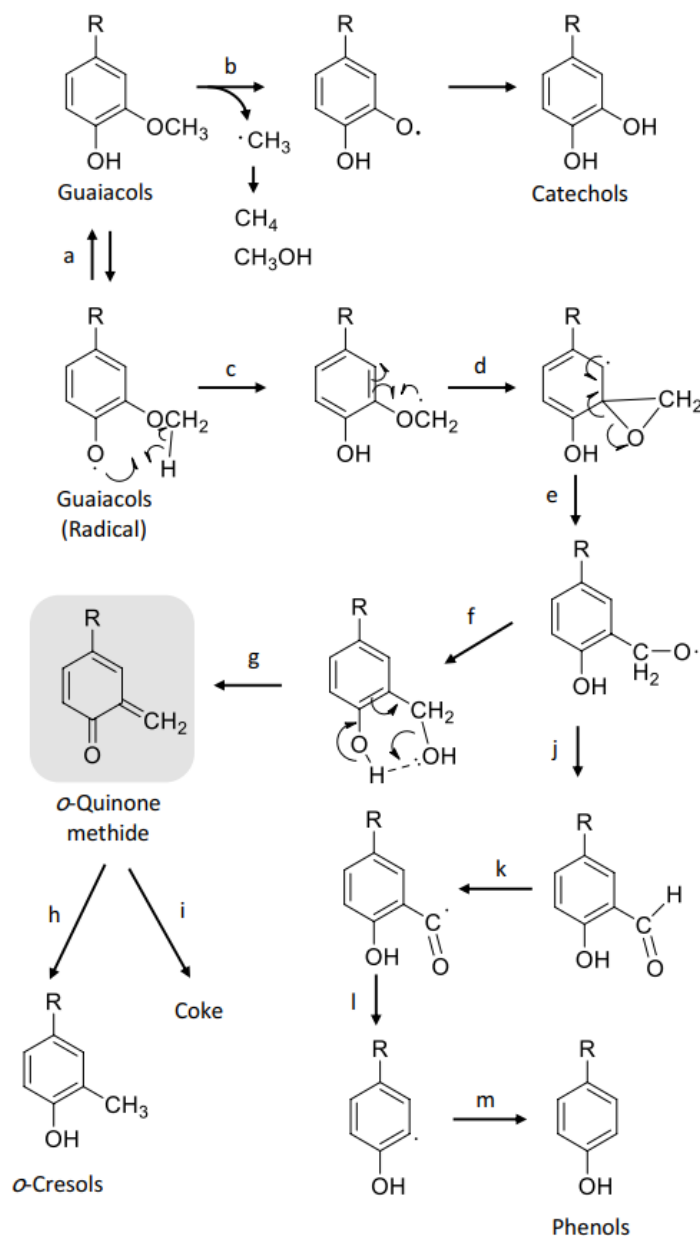


Figure 53: Monomer substitution changes in the secondary phase of lignin pyrolysis [100]

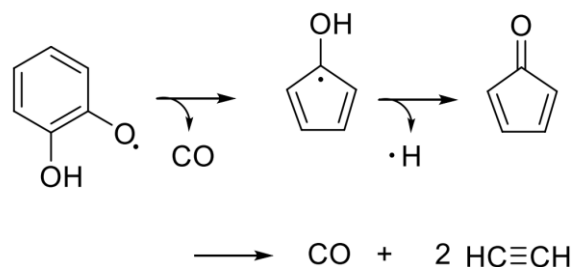


Figure 54: Degradation mechanism of radical catechol monomers [100]

Mechanisms of formation of pyrolytic lignin remain to be elucidated. There is no consensus on this in the scientific literature yet. Most publications dealing with reaction mechanisms of lignin pyrolysis do not consider PL. To understand the formation mechanisms for PL, first of all, it must be clarified whether oligomers are to be classified as primary or secondary reaction products.

Bai et al. have investigated primary reaction products of pyrolysis. The residence time of the vapours in the reactor is reported to be less than 400 ms, and the resulting pyrolysis vapours are condensed as rapidly as possible in a solvent bath cooled with dry ice. These reaction conditions indicate that monophenols and dimers are the primary reaction products of lignin pyrolysis [103]. This publication should be contrasted with the study by Zhou et al. in which residence times of 15-25 ms and cooling temperatures of -100 °C were achieved. The extremely short residence times could be realized by a reduced pressure to 0.3 mbar [104].

Since primary reactions define the first reactions of pyrolysis, the experimental setup of Zhou et al. investigates these initial conditions more accurately. Extremely short reaction times and early and intensive quenching of the reaction products under reduced pressure minimize the influence of secondary reactions. Consequently, it is assumed that oligomers are formed in the first phase of pyrolysis, which subsequently degrade to form monomers.

The GPC results of Zhou et al. also show the influence of thermal ejections of oligomers. In thermal ejection, larger molecules are ejected from the lignin composite by the volume expansion that occurs during the rapid evaporation of components in the lignin. Figure 55 shows molecular size distributions of various biooil phases produced from pyrolysis at different temperatures. In comparison, the molecular size distribution of an organosolv lignin is also shown [104].

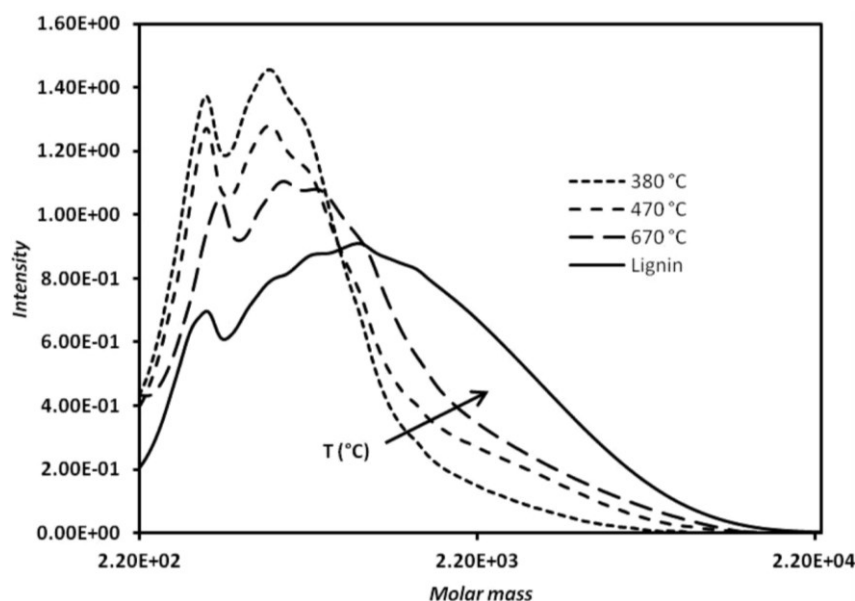


Figure 55: Molecular size distributions of biooils of different pyrolysis temperatures [104]

Figure 55 shows as the temperature of pyrolysis increases from 380-670 °C, larger portions of oligomers are ejected from the lignin. Thus, with extremely short residence times (15-25 ms), very high heating rates (8000 °C/s) and efficient condensation (-100 °C), pyrolysis oils are formed whose molecular size distributions have maxima above 400 g/mol. Those contain mostly oligomers [104]. It should be mentioned that biooil yields of about 90 % can be achieved under the reaction conditions achieved by Zhou et al., as can be seen in Figure 56.

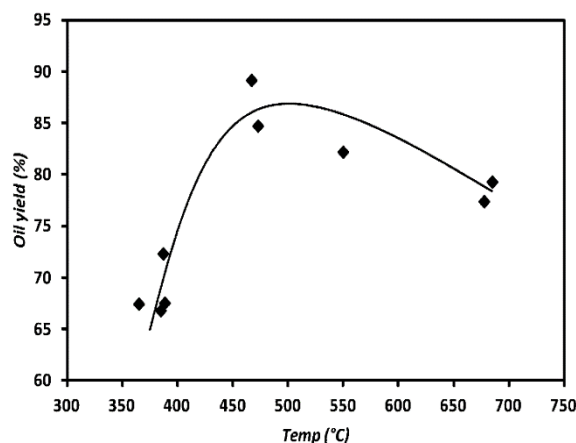


Figure 56: Biooil yield of lignin pyrolysis with heating rate of 8000 °C/s, residence time of 15-25 ms, and cooling of vapours to -100°C [104]

Zhou et al. use a so-called mesh reactor, in which electricity is passed through a fine grid on which the biomass is embedded [104]. This reactor, which is mostly used for research purposes, allows heating rates of over 10,000 °C/s to be achieved. Despite the high temperatures, the temperature variance in the grid can be limited to a maximum of ± 35 °C. More details on the setup used can be found by Hoekstra et al. [105].

Yu et al. note that extreme heating rates and very short residence times lead to a high liquefaction rate of lignin, but the proportion of pyrolytic lignin increases sharply. Lower heating rates and shorter residence times, on the other hand, lead to an increase in the monomer content, but the biooil yield decreases [106]. In order to keep the liquefaction rates high and to form significant amounts of monomers, the optimal reaction conditions still need to be researched intensively.

Summary of reactions

Since existing literature on mechanisms of lignin pyrolysis has so far not considered the aspect of thermal ejection, a proposed schematic is presented below in which current research results are extended to include this phenomenon. It is assumed that degradation reactions take place in the liquefied lignin-rich phase during pyrolysis [100]. Although individual publications illuminate secondary reactions in the vapor phase [107], and radical polycondensations in the gas phase are known [108], they have not yet been sufficiently incorporated into summaries of reaction mechanisms in lignin pyrolysis. Furthermore, no publication is known that summarizes the formation of biochar, pyrolytic lignin, as well as gases and light organic products in addition to the formation of monomers. Besides the thermal ejection, a holistic summary of the current state of knowledge, gathered from sources cited in this chapter, on the possible reaction pathways is presented in the proposed schematic model, depicted in Figure 57.

The lower part of Figure 57, with orange background, shows known reactions that occur during lignin pyrolysis, without taking thermal ejection into account. The upper part, with a blue background, shows reactions that take place after the evaporation of the components or after thermal ejection.

The summarized reaction possibilities in Figure 57 start with lignin in the solid phase. Due to the process conditions during pyrolysis, lignin begins to soften, melt, and decompose. Oligomers as well as monomers split off from the lignin molecule. The resulting oligomers can be gradually degraded to smaller oligomers by further degradation mechanisms. In the primary phase these, are α -O-4 and β -O-4 ether bond breaks. At higher temperatures, C-C bonds also break homolytically. The end of the depolymerization reactions is reached, when two monomers remain after bond cleavage. Reactants and intermediate products of these decomposition reactions can decompose (white arrow), repolymerize (red arrow), or leave the solid/liquid phase via vaporization or thermal ejection (blue arrow). Interactions of involved intermediates to the formed polymers are to be considered as a concerted polymerisation [106]. At temperatures above 400 °C, phenolic substituents start to get chemically modified or are degraded (green arrow). Exemplary reactions with changes in substitution pattern have been shown in Figure 53. Reactions that change the substitution pattern are investigated for monomeric phenols [100].

The diagram illustrates the reaction pathways of lignin during thermal degradation, showing reactions before and after thermal ejection or evaporation.

Legend:

- White arrow: degradation/cleavage
- Red arrow: condensation/growth
- Blue arrow: thermal ejection/vaporisation
- Green arrow: change in substitution pattern

Reactions before thermal ejection or evaporation (Yellow background):

- Lignin** (red box) undergoes degradation/cleavage (white arrow) to form **oligomers** (white box).
- oligomers** undergo condensation/growth (red arrow) to form **oligomers (n-1)** (white box).
- oligomers (n-1)** undergo condensation/growth (red arrow) to form **dimers** (white box).
- dimers** undergo condensation/growth (red arrow) to form **monomers** (white box).
- oligomers** undergo thermal ejection/vaporisation (blue arrow) to form **pyrolytic lignin** (red box) and **biochar** (grey box).
- oligomers (n-1)** undergo thermal ejection/vaporisation (blue arrow) to form **pyrolytic lignin** and **biochar**.
- dimers** undergo thermal ejection/vaporisation (blue arrow) to form **pyrolytic lignin** and **biochar**.
- monomers** undergo thermal ejection/vaporisation (blue arrow) to form **pyrolytic lignin** and **biochar**.
- monomers** undergo change in substitution pattern (green arrow) to form **monomers** (white box).

Reactions after thermal ejection or evaporation (Light blue background):

- oligomers** (white box) undergo degradation/cleavage (white arrow) to form **oligomers (n-1)** (white box).
- oligomers (n-1)** undergo degradation/cleavage (white arrow) to form **dimers** (white box).
- dimers** undergo degradation/cleavage (white arrow) to form **monomers** (white box).
- monomers** undergo degradation/cleavage (white arrow) to form **light organics** (green box) and **non condensable gases** (blue box).
- oligomers** undergo thermal ejection/vaporisation (blue arrow) to form **pyrolytic lignin** and **biochar**.
- oligomers (n-1)** undergo thermal ejection/vaporisation (blue arrow) to form **pyrolytic lignin** and **biochar**.
- dimers** undergo thermal ejection/vaporisation (blue arrow) to form **pyrolytic lignin** and **biochar**.
- monomers** undergo thermal ejection/vaporisation (blue arrow) to form **pyrolytic lignin** and **biochar**.

Decomposition reactions of monomers to form non-condensable gases and light organic molecules only occur effectively at temperatures above 450°C [100]. Since it is assumed that the majority of the monomers are in the vapor phase at temperatures above 300 °C (boiling points of guaiacol and phenol: 205 °C; 182 °C), subsequent reactions also mainly take place in the vapor phase [107,108].

The knowledge about reactions that occur during pyrolysis of lignin is currently still limited. Many topics have not yet been uniformly clarified and the vast number of reactants, intermediates, process-related influencing factors, and reaction mechanisms make it difficult to gain insight. The model presented above is intended to provide a roughly simplified overview of currently known possible reaction pathways.

3.2 State of art of lignin pyrolysis

This chapter shows the current state of art of lignin pyrolysis and presents challenges in lignin pyrolysis in reactors that go beyond the scale of micro-pyrolizers.

In a 2022 review, Singh-Morgan et al summarize the state of the art. The review shows that the most widely used reactor for lignin pyrolysis is the bubbling fluidised bed reactor. Singh-Morgan et al. were able to collect 9 publications with total feed quantities above 40 g in which a BFB reactor was used. For fixed bed reactors and circulating fluidised bed reactors, only 1 publication each is listed with feed amounts in this range. Three papers with corresponding feed quantities deal with lignin pyrolysis in pyrolysis centrifuge reactors (PCR) and one publication with entrained flow (EF) reactors. Critically, however, the majority of these publications are not relevant to the pyrolysis of pure lignin, as mostly feed used with large amounts of cellulose or hemicellulose, or pyrolysis is carried out under a hydrogen atmosphere with the aid of a wide variety of catalysts [81].

In focusing on the use of lignin without the use of catalysts, de Wild et al.'s LIBRA project is the largest project and serves in this chapter as an example for the current state of the art [87,88]. LIBRA (lignin biorefinery approach) is a process in which lignin is processed and pyrolyzed. The project is designed in such a way that, for example, a downstream lignin pyrolysis can be established at existing bioethanol refineries in order to utilize the by-product lignin. Publications on the LIBRA project have been published in 2012 and 2014.. Figure 58 schematically illustrates the process of lignin pyrolysis in the course of the LIBRA project [88].

Pure lignin isolated from wheat straw with an organosolv process using a mix of acetic acid and formic acid was used. This lignin is compressed into extrudates with a diameter of 2 mm and fed into the reactor via a cooled screw conveyor system. A total of 1 kg of pure lignin (>90 % lignin) is thus introduced at a rate of 10 g/min. The reactor is a bubbling fluidized bed reactor with a capacity of 1 kg/h. The pyrolysis tests are carried out at 500 °C. Pyrolysis vapours are cleaned from the resulting biochar with cyclones and particle filters and then condensed. Figure 58 shows an impinger train filled with cooled isopropyl alcohol, but in the continuous sampling experiments condensers, ESPs, and filters connected in series are used. Nitrogen or argon are used as fluidizing gases for the hot sand bed and non-condensable gases are detected continuously. The products are biochar (37%), biooil (44%) and non-condensable gases

(17%). The product distribution is shown in Table 7 [87]. It should be mentioned that due to problems with the handling of lignin, the lignin was pre-treated for pyrolysis and a specially adapted feed system was used. Lignin tends to melt when heated and subsequently blocks feed inlet systems and agglomerates with the heat transfer material of the reactor bed [88]. Details on this challenge regarding lignin handling is explained in more detail in chapter 3.2.1.

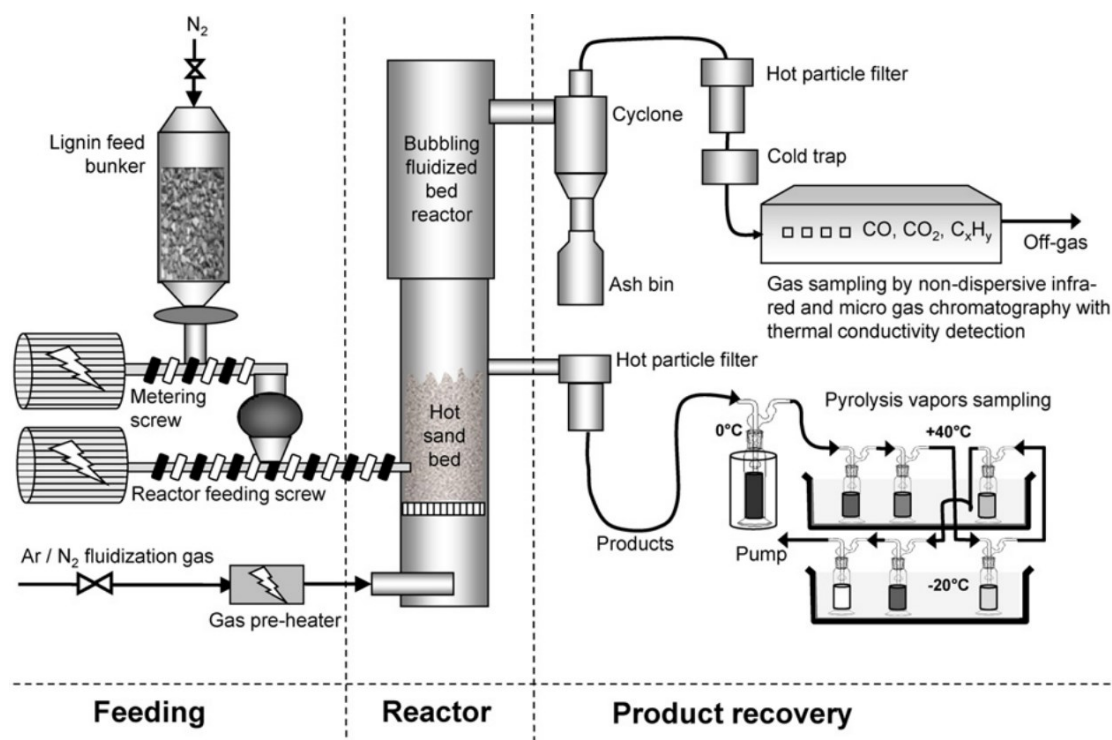


Figure 58: LIBRA Lignin pyrolysis setup [87]

In addition to the continuous sampling tests, batch sampling tests were also carried out in the course of the LIBRA project. In the batch tests, pure lignin is not pyrolyzed alone, but pressed together with natural mineral additives into extrudates with a diameter of 2 mm. The extrudates have a lignin content of >90 %. The additives used are not specified in more detail by the authors, it is simply mentioned that they serve to facilitate the handling of the lignin when the feed is introduced. In the batch trials, 150 g extrudates were pyrolyzed at a feed rate of 10 g/min. Although these are not batch tests in the classical sense due to the continuous feed rate, the influence of the char accumulating in the reactor is reduced. The authors note that continuous operation of the pyrolysis leads on average to slightly increased amounts of biochar and reduced amounts of monophenols. De Wild et al. assume that the catalytic effect of biochar on cracking reactions may be the reason for this deviation [87].

Chen et al. show that biochar can indeed affect the reactions that occur during pyrolysis. It is known from the pyrolysis of LCBM that biochar can catalyse cracking reactions. Chen et al. can classify these reactions more broadly. Pyrolysis products of cellulose are more easily cracked by biochar catalysis, which leads to an increase in the amount of gas and a reduction

of the liquid components. In the case of products formed during lignin pyrolysis, biochar catalyses repolymerisation of monophenols. This leads to a reduction of monophenols and an increase in oligomers [111].

When comparing the results of lignin pyrolysis to those from pyrolysis of lignin with mineral additives, it can be seen that the amount of oligomers has indeed increased by almost 60 %, specifically from 12 to 19 %. It should be noted that the use of catalysts in the form of mineral additives can have an effect on the distribution of the product. The product distributions of the pyrolysis results are compared in Table 7 [87].

Table 7: Product distributions of LIBRA pyrolysis results of wheat straw organosolv lignin [87]

	lignin	lignin + mineral additives
biochar [%]	36	39
gas [%]	17	17
water [%]	20	15
oligomers [%]	12	19
monophenols [%]	6	8
light organics [%]	4	2
sum	95 %	100 %

It should be noted that the state of the art for lignin pyrolysis is currently not very well developed. There is hardly any data in the literature on trials with feed quantities that exceed the order of magnitude of a few grams.

3.2.1 Challenges of lignin pyrolysis

This chapter briefly summarises the challenges encountered in the pyrolysis of lignin.

Broadly speaking, the difficulties can be divided into two areas. One part of the challenges are mechanical problems involving the handling of lignin. The second part includes challenges involving the product distributions of lignin pyrolysis and the chemical composition of the products. Requirements of this kind are referred to in the following as product quality challenges. Table 8 lists the most common difficulties that occur during the pyrolysis of lignin.

Table 8: Challenges of lignin pyrolysis

mechanical challenges	product quality challenges
blockade of feed Inlet system	biooil yield
deposits in condensers and ESPs.	monophenol yield
agglomeration with heat carrier material	abundance of pyrolytic lignin
discharge of unreacted lignin	specificity of individual monophenols

Mechanical challenges

Literature often describes difficulties with the handling of lignin during pyrolysis. In particular, there are blockages of the feed inlet system, deposits of products in condensers and ESPs, agglomerations of lignin with the heat transfer material, and undesired discharge of fine and non-pyrolyzed lignin.

In an international collaboration among renowned researchers from the pyrolysis field, including Bridgewater, de Wild and Nowakowski, problems with the handling of lignin are examined in more detail. They mention that the processing of lignin in conventional fluidised bed reactors is almost impossible [112]. Figure 59 shows feed inlet screws that have become blocked by molten lignin [88,111].



Figure 59: Blocked feed screws caused by molten lignin. left: Bridgewater et al. [112] right: de Wild et al. [88]

Pneumatic conveying methods with a small cross-section can become completely clogged. To overcome this problem, push rods had to be used to manually convey the lignin into the reactor, as shown in Figure 60 [112].



Figure 60: Single valve with funnel (left) and push rod (right) [112]

In addition to feed inlet blockages, product deposits also occur in condensers, filters, or ESPs. On the one hand, these deposits lead to product losses or more difficult product recovery and, on the other hand, to a reduction in the effectiveness of the equipment. Figure 61 shows deposits in supporting equipment of the lignin pyrolysis in the example of an heavily loaded ESP body [112].



Figure 61: Deposits on ESP body [112]

Figure 61 shows the ESP from an experiment where no biooil could be collected, all pyrolysis products stuck to the ESP, the reactor bed, and other parts of the apparatus. Melting and agglomeration are particularly evident in the reactor bed. The principle of fluidized bed reactors is, as explained in chapter 2.2.2, a fluidization of the reactor bed, for an effective heat transfer and a good mixing of the feed material. Agglomerates of molten lignin, formed biochar, and heat transfer material lead to a solidification of the reactor bed. The bed is no longer fluidised, and the reactor is thus massively reduced in its effectiveness of heat transfer and mixing [112].

Furthermore, it can occur that the lignin isolation process results in a very fine powder that has particle sizes of less than 100 μm .

In reactors operating with fluidizing gas, this fine lignin can be suspended by the gas and thus be discharged partially unreacted from the reactor vessel. In order to be able to process very fine lignin it is possible to take up lignin in suitable solvents such as ethanol. The resulting

slurry can be re-solidified by evaporating the ethanol. Subsequent crushing yields particles with an increased particle size, effectively reducing the particle fraction with diameters less than 100 μm . Pyrolysis of this pretreated lignin reduces the amount of unreacted discharge of particles from the reactor [112].

Product quality challenges

In addition to the mechanical challenges, difficulties with product quality also arise in lignin pyrolysis. Product quality refers to product distribution, yield and chemical composition.

It is known from the pyrolysis of woody biomass that the resulting biooil is not a satisfying source of fine chemicals, as there are hundreds of different molecules in the organic oil phase and separation of these is not yet profitable and hardly feasible. This difficulty remains with lignin pyrolysis. At present, research interest lies in the production of monophenols, which usually account for less than 10 % of the products. This monophenol fraction consists of various compounds [88]. To facilitate the use of this fraction for the production of fine chemicals, it is mandatory to increase the product share of monophenols. Furthermore, it is desirable to produce specific molecules with increased preference within this monophenol fraction. If however, fine chemicals are not the target of the use of the biooil phase, application areas of this compound mixture need to be explored and established.

Optimal process conditions for maximizing the monophenol fraction are not currently established. As shown in chapter 3.1.2, increasing the biooil yield in the purpose of obtaining more monophenols is not possible to implement. While it is possible to increase the liquefaction rate under suitable conditions, the resulting biooil then consists mostly of oligomers. A reduction in oligomeric compounds however leads to a decrease in the amount of monophenols produced [106]. Additionally, during the pyrolysis of lignin, biochar acts as a catalyst for repolymerization reactions of monophenols to dimers and oligomers [111].

3.3 Tuning of lignin pyrolysis

There is currently no solution to meet the challenges mentioned in chapter 3.2.1 all at once. However, individual obstacles can be overcome with appropriate adaptations. Chapter 3.3 provides an overview of influencing factors on lignin pyrolysis as well as the research activities addressing the optimization of this process.

In order to present influencing factor and research activities clearly, the concept of the value chain is chosen as the guiding framework. Contributing factors are presented based on the respective stages of the value chain. Subsequently, the segmented examination of possible influences can serve as a basis for optimizing the process.

According to the Cambridge dictionary, the value chain is defined as "the series of stages involved in producing a product or service that is sold to consumers, with each stage adding to the value to the product or service" [113]. In the case of lignin pyrolysis, a simplified value chain can be represented as in Figure 62.

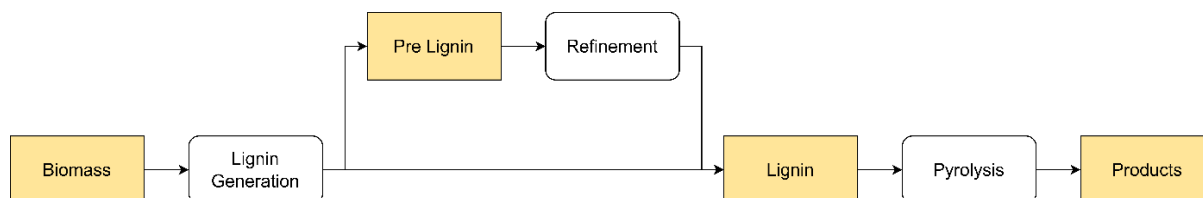


Figure 62: Value chain - Lignin pyrolysis

The value chain of lignin pyrolysis begins with biomass. In the simplest case, lignin is extracted from the biomass by suitable processes and then further pyrolyzed into the corresponding products. This pathway is shown in the lower part of Figure 62. Alternatively, lignin can also be refined before pyrolysis; this path is outlined in the upper part of the figure. For clarity, lignin before refining is referred to as pre lignin. The following chapters discuss the effects of biomass, lignin formation processes, refinement, and adaptations on pyrolytic conditions.

3.3.1 Biomass

In this chapter, the influence of biomass on the pyrolysis of lignin is briefly presented.

Lignin content varies in biomass. Hardwood contains 20-25 % lignin, softwood 25-35 %, and annual plants 15-25 %. Softwoods therefore contain the most lignin on average. To maximize the overall process yield, which is based on the amount of biomass used, the lignin content must be considered [2].

In addition to the lignin content, the proportion of the monomer components contained in the lignin also varies. Softwoods are characterized by a very high proportion of guaiacols (G) followed by low amounts of phenols (H). In hardwoods, guaiacol and syringol amounts (S) are dominant but vary in their proportions depending on the tree species. Herbaceous plants, on the other hand, are characterized by a high variation in all monomer components (G, H and S). Since the first reactions that occur during pyrolysis are degradation reactions that lead to oligomers and monomers, the original substitution patterns of the monomer components are decisive for trends in the chemical profile of the formed biooil. For example, biooils from hardwoods are usually characterized by higher proportions of syringols than those from softwoods [2].

The number and type of bonds linking the monomer units also differs in biomass. On average, hardwood lignin contains more ether bonds than softwood lignin, especially β -O-4 bonds are

more common in hardwood lignin. In softwoods, on the other hand, C-C bonds are more common than in hardwoods. As already shown in chapter 3.1.2, C-C bonds such as the β -5 or the 5-5 bond are characterized by higher bond dissociation energies. This aspect has an effect on the reaction behaviour in the primary reactions, since mostly ether bonds are initially broken in this phase [99, 113].

The biomass used therefore has severe impact on the lignin content, the phenolic substitution pattern of the monomer components, and the types and abundance of bonds between these monomers. This results in effects on the overall yield, the reactive behaviour in the primary phase, and on the contents of the monomeric phenols in the pyrolytic biooil.

3.3.2 Isolation of lignin

In this chapter, the influences of different lignin preparation methods on the pyrolysis of lignin are considered. This master's thesis is limited to organosolv lignin, kraft lignin and lignosulfonates, as these have the greatest global significance in terms of quantity. The processes, as well as the chemical properties of those technical lignins, are already described in detail in chapter 2.1.

Organosolv Lignin

Organosolv lignin (OL) serves as a starting point for the comparisons of the suitability of technical lignins for pyrolysis. OL is characterized by being sulfur-free and having molecular sizes of about 400-1600 g/mol. The number and type of interunit bonds of the monomers of which OL is composed hardly differ from native lignin, since the organosolv process gently retains the structural properties of the lignin used. Since, as shown on the following pages, the specific properties of other technical lignins mainly have a negative effect on pyrolysis, OL is often pyrolyzed for research purposes [2, 47, 50].

The organosolv process is not limited to a particular solvent. Different solvents can change the properties of the resulting lignins. These differences can subsequently affect the pyrolysis and its products. Wang et al choose three common solvent mixtures used in organosolv processes and take willow as biomass to produce three different OLs. The solvent mixtures used are ethyl acetate (EAc) with water, tetrahydrofuran (THF) with water, and γ -butyrolactone (GBL) with water. The resulting lignins are designated EAc-OL, THF-OL, and GBL-OL, respectively [115].

As results of the effects of different solvent mixtures, an increased proportion of lignin molecules with a molecular mass above 6000 g/mol in GBL-OL is mentioned, as well as an increased abundance of oxygen-containing functional groups in EAc-OL. After slow pyrolysis at 500 °C, the molecular size distributions of the biooils are almost identical. Ether bond breaks

that already occur with GBL-OL during the organosolv process are made up for in EAc-OL and THF-OL during pyrolysis. The amounts of monophenols produced are 4.66, 5.81, and 5.83 % for EAc-OL, GBL-OL, and THF-OL, respectively. The lower quantity in EAc-OL is mainly due to a smaller amount of 4-methyl-guaiacol produced [115]. The effects of different solvents in the organosolv process on the pyrolysis properties of the resulting lignins can therefore be neglected.

Lignosulfonates

Publications in which lignosulfonates (LS) are pyrolyzed are hardly found in the scientific literature. Due to the conditions and pulping chemicals in the process, so-called sulfonate groups are incorporated into the lignin structure of LS. As a result, the sulfur content (3-8%) is very high, as shown in Table 1.

Comparative tests show that the pyrolysis of LS produces biooil in very small quantities. Karthäuser et al. compare microwave assisted low temperature (<280 °C) pyrolysis of various technical lignins. Pine wood kraft lignin and spruce wood organosolv lignin reach a proportion of phenolic components in the pyrolysis products of 15.9 and 14.8 %, respectively. In contrast, the amount of phenolic products in the bio oil of pyrolyzed spruce wood calcium organosolv LS is 1.7 percent [116]. When looking at the chemical aspects of the resulting pyrolysis vapours, another challenging aspect of LS pyrolysis becomes apparent. Huang et al. show that between 40 and 60 % of the volatiles in the pyrolysis products of lignosulfonates are sulfur-containing compounds [117].

Low biooil production rates, high ash content, as well as high pyrolytic production of sulfur-containing compounds make lignosulfonates an unattractive feed material for pyrolysis.

Kraft Lignin

The scientific output of KL pyrolysis is comparable to that of OL pyrolysis. The molecular sizes of KL range from 1200-1800 g/mol and are therefore comparable to that of OL. A significant difference is the sulfur content of 0.2-3 % [38, 40], which according to Daniel et al. is disadvantageous for depolymerization reactions during pyrolysis [118]. However, studies in which both KL and OL are pyrolyzed, often show comparable results in product distribution and monomer content. Figure 63 shows the product distributions of pyrolysis of three different lignins at 500°C in a bubbling fluidized bed reactor. Biolignin is a straw-derived OL that uses acetic acid and formic acid as solvents. Kraft lignin is derived from softwood and Alcell lignin is an EtOH-OL derived from hardwood [87].

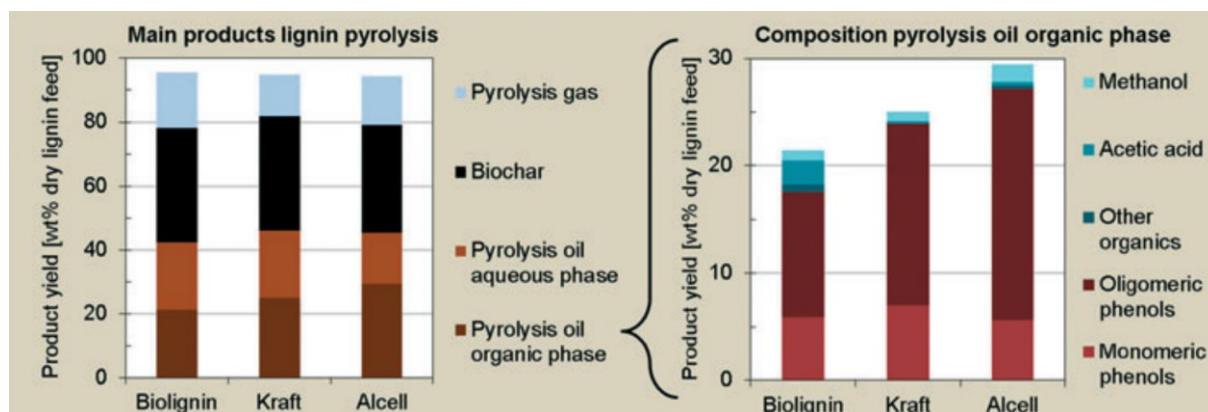


Figure 63: Product distributions of three different lignins, pyrolyzed at 500 °C [87]

As can be seen from Figure 63, KL can be pyrolyzed comparably to OL. Also, in other studies considered, no clear trend for decreased liquefaction rates and monomer yields of KL pyrolysis compared to OL pyrolysis can be observed. Shafaghat et al. for example, performed fast pyrolysis in a fixed bed reactor at 500 °C of different lignins, where the highest liquefaction rates were achieved with KL. Figure 64 shows the product distributions, of the pyrolysis of KL, OL, and two other lignins [119].

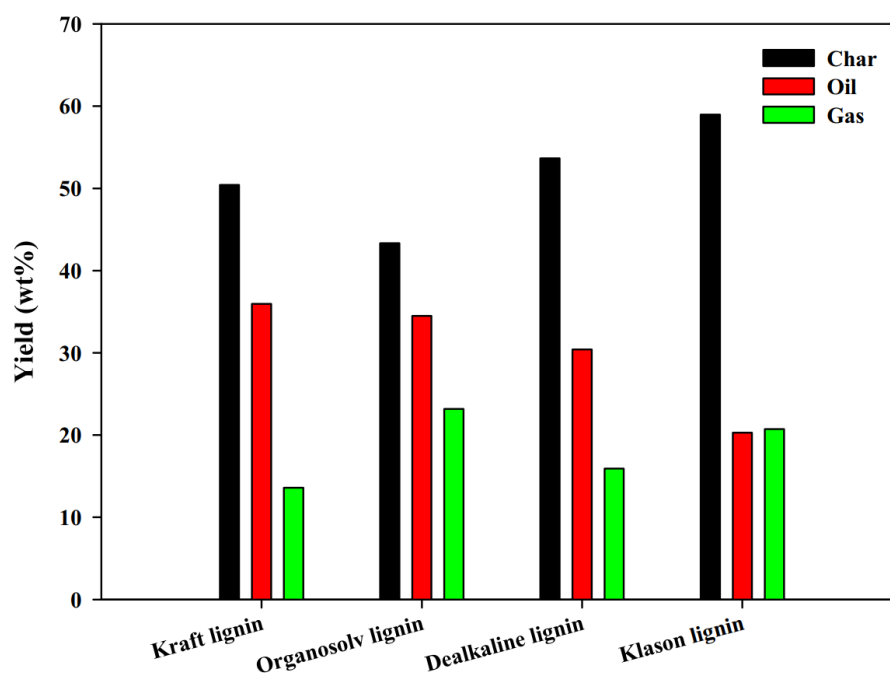


Figure 64: Product distribution of lignins pyrolyzed at 500 °C in a fixed bed reactor [119]

One aspect that puts KL at a disadvantage compared to OL is the production of sulfur-containing compounds during pyrolysis. Borella et al. pyrolyze 5 g KL at temperatures of 350-550 °C and analyse the distribution, amount, and type of sulfuric compounds. Detected sulfur compounds in the gas phase are dihydrogen sulfide (H_2S), methyl mercaptan (CH_3SH), dimethyl sulfide ($\text{CH}_3\text{-S-CH}_3$), carbonyl sulfide (COS), sulfur dioxide (SO_2), and carbonyl disulfide (CS_2). The most common compounds are H_2S and CH_3SH . Dimethyl sulfide, thiols, and thiophenes

are detectable in the liquid phase. In the remaining biochar, which accounts for 42.7 % of the products of the pyrolysis at 550 °C, sulfur accounts for 1.9 % of the mass. Based on a feed amount of 5 KL, which has a sulfur concentration of 1.1 %, this means that 73.8 % of the sulfur remains in the biochar in this study. Borella et al. note that sulfur in the liquid phase has corrosive properties, when used as a biofuel, acts as a catalyst poison, and can lead to the generation of toxic gases such as H₂S and SO₂ [120].

If kraft lignin is to be pyrolyzed on a large scale, measures must be taken to minimise the level of sulfur and its derivatives in the products and appropriate gas treatment is required to minimise toxic product hazards. Apart from the sulfur compounds produced during pyrolysis, KL is a suitable feed material for this process.

3.3.3 Refinement

In this chapter, refinement possibilities of pre lignin are presented. The scientific literature deals with a variety of possibilities to produce lignin whose properties enable improved pyrolysis. These refinement methods include chemical methods such as acetylation, benzyl hydroxyl shielding, oxidative depolymerisation or hydrogenation. In addition, methods are being investigated in which pre lignin or precursors thereof, such as black liquor, are thermally pre-treated. Biological concepts such as degradation by microorganisms or enzymatic depolymerisation are also being investigated. Furthermore, the effects of acid gradient fractionation of prelignin are discussed.

Acetylation

Li et al. use choline chloride/acetic anhydride (ChCl/Aa) to acetylate pine kraft lignin (PKL). The aim of this pre-treatment is the acetylation of the phenolic as well as the aliphatic OH groups. It can be shown that ChCl/Aa is an effective reagent for the acetylation of alcoholic groups. Phenolic OH were acetylated to 94.0 and aliphatic OH to 99.1 %. Subsequent pyrolysis at 550 °C leads to an increased proportion of H-type phenols, with simultaneous reduction of G-type products. This pre-treatment also produces acetylated monomers. In addition to the shift of the phenolic substitution pattern towards the H-type, there is an increase in the biooil yield. Figure 65 shows the product distributions of the pyrolysis of PKL in comparison to acetylated PKL (AL). Acetylation was carried out at 120 °C. Different reaction time was applied ranging from 3-60 min. AL 120-3 thus denotes acetylated PKL that was pre-treated at 120 °C for 3 min ChCl/Aa [121].

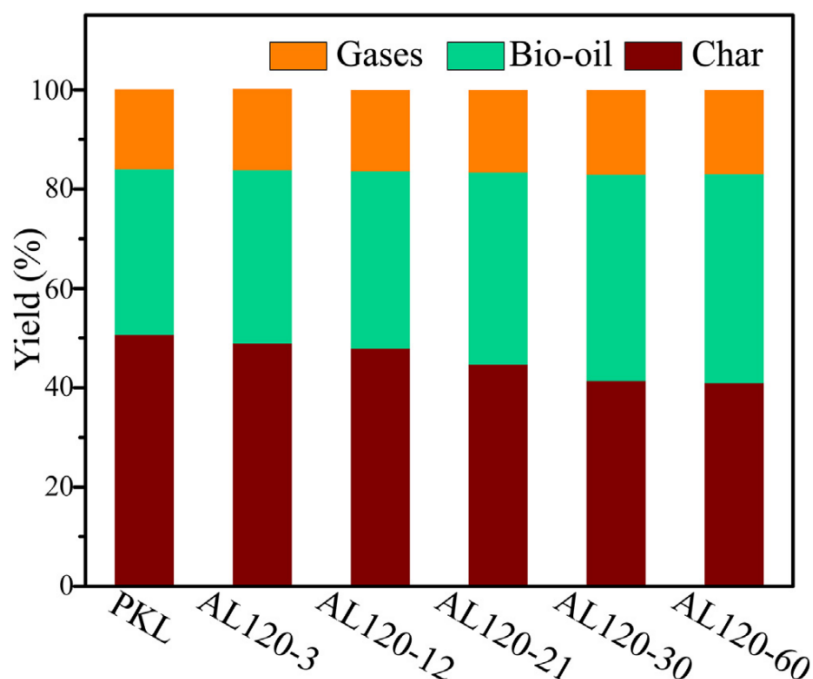


Figure 65: Product distribution of PKL and acetylated PKL [121]

Acetylation can therefore be used with CHCl_3/Aa to increase the amount of biooil and at the same time increase the amount of H-phenols [121].

Benzyl hydroxyl shielding

Fan et al. investigate the effects of benzyl hydroxyl shielding and peroxidation of benzyl hydroxyl on the pyrolysis of lignin. Peroxidation with 2,3-dichloro-5,6-dicyano-1,4-benzoquinone (DDQ) increases the generation of radicals. The shielding of the benzyl hydroxyl groups with propionaldehyde introduces a protecting group that caps two adjacent benzyl hydroxyl groups. With support from this shielding, it will be investigated whether condensation reactions in pyrolysis can be reduced in this way, thereby increasing the yield of bio-oil. Figure 66 shows the experimental concept of Fan et al [122].

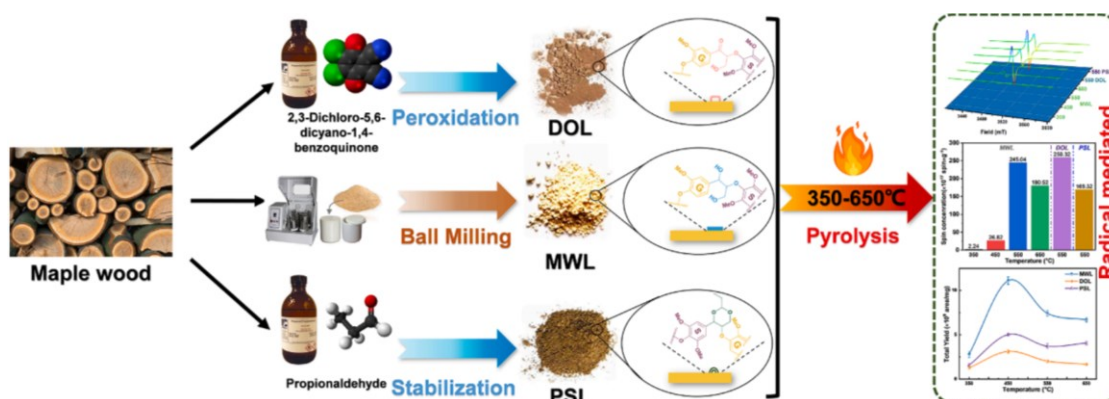


Figure 66: Lignin pyrolysis after benzyl hydroxyl shielding [122]

As pyrolysis is characterised by homolytic ether cleavage reactions in the primary phase, as described in section 3.1.2, effects on the product distributions of pyrolysis are to be expected. Fan et al. show that neither shielding of the benzyl hydroxyl groups nor peroxidation lead to an increase in the biooil yield. Both treatment steps lead to a significant reduction of the liquefaction rate. Figure 67 shows the product distributions of the pyrolysis of different lignins. As a control sample, MWL from maple wood is pyrolyzed at temperatures of 350-550 °C. DOL stands for DDQ oxidised lignin and POL for propionaldehyde stabilised lignin [122].

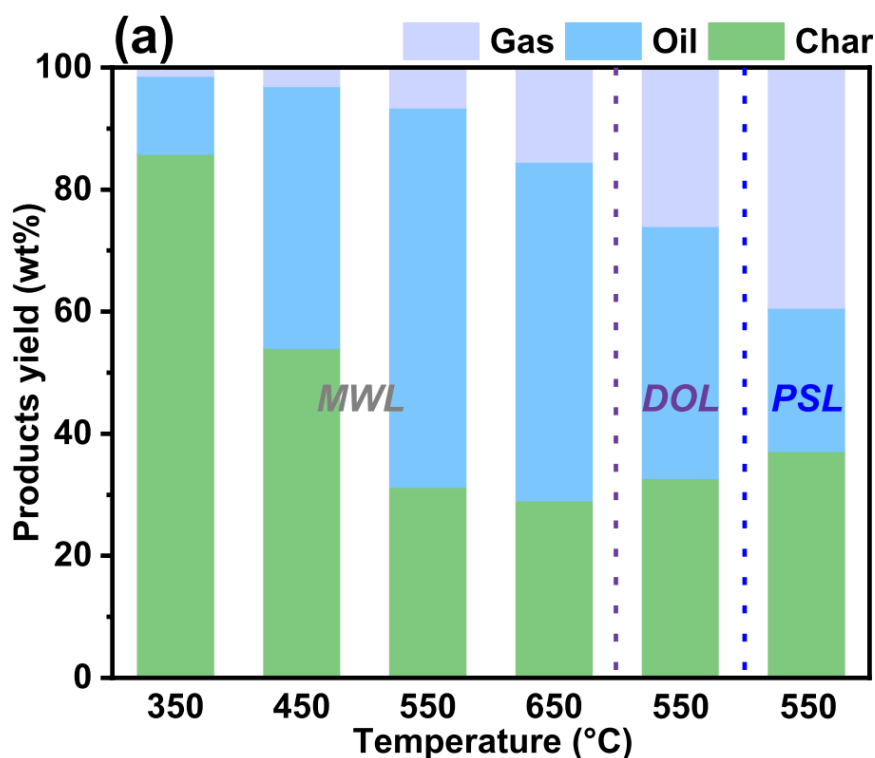


Figure 67: Product distribution of pyrolysis of MWL, DOL and PSL [122]

The study published by Fan et al. indicates that intensive basic research is still needed in the field of reaction mechanisms of lignin pyrolysis in order to make chemical processing methods more effective.

Oxidative depolymerisation

Ahmad et al. investigate the feasibility of oxidative depolymerization of kraft lignin with nitric acid (HNO_3). It can be shown that the molecular sizes (M_w) of Kraft lignin treated with HNO_3 can be effectively reduced. The molecular size distributions of softwood kraft lignin (SKL) before and after treatment with HNO_3 is shown in Figure 68 A and that of that of hardwood kraft lignin (HKL) in Figure 68 B [123]. The effects on product distributions during pyrolysis of HNO_3 treated lignin have not been investigated in this paper.

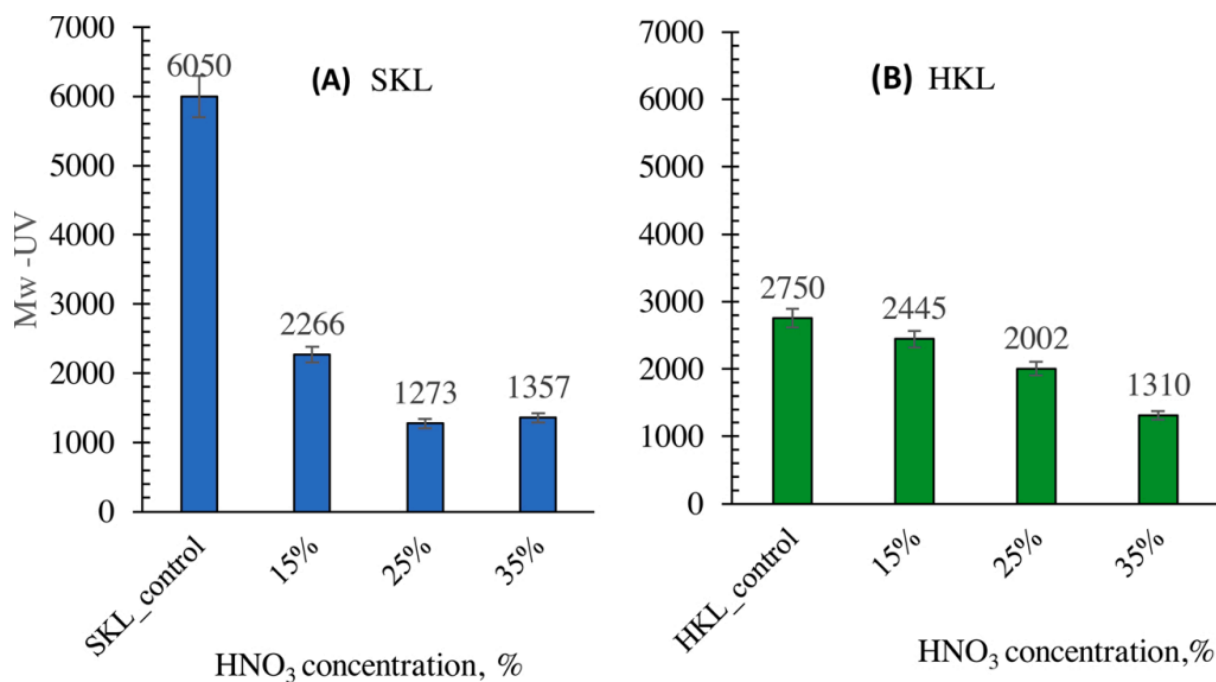


Figure 68: Molecular size distributions of KL before and after oxidative depolymerisation [123]

However, a reduced molecular size is thought to have a positive effect on the liquefaction rate during lignin pyrolysis. Marathe et al. pyrolyze lignins with an average M_n in the range of 350 to 1900 g/mol in a wire mesh reactor at 530 °C. The experimental data of this series of experiments, is shown in Figure 69. The experiments are conducted at 500 Pa and 10^5 Pa, higher biooil yields are obtained at 500 Pa. The numbers 1-14 denote lignin fractions of different molecular sizes. It can be seen that the liquefaction rate positively correlates with decreasing molecular size. [124].

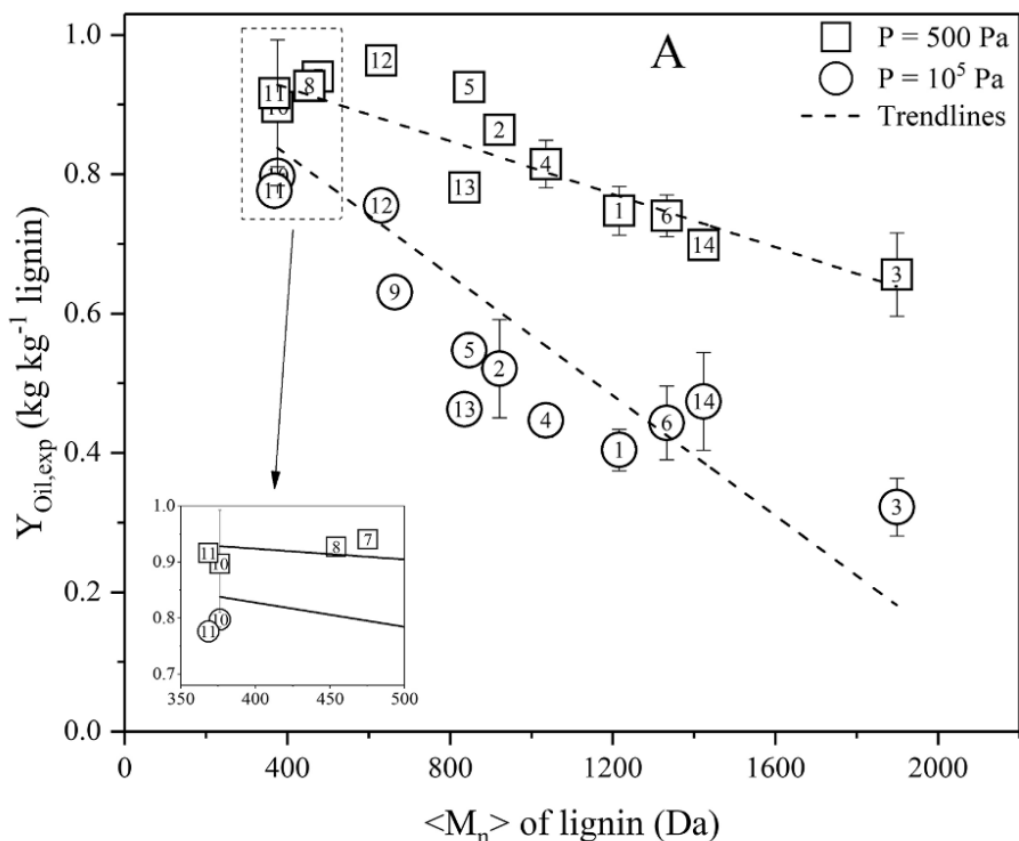


Figure 69: Correlation between molecular weight and biooil yield in lignin pyrolysis [124]

Hydrogenation

Zhang et al. investigate the effects of catalytic hydrogenation on ethanol organosolv lignin (EOL). For hydrogenation, EOL is catalytically treated for 1-7 h at 200-250 °C under 3 bar H₂. THF is used as solvent and ruthenium carbon or rhodium carbon as catalyst. A yield of 48-87 % hydrogenated EOL, so-called HEOL, is achieved. HEOL is then pyrolyzed at 850 °C in an H₂ atmosphere. The resulting products are mainly light olefins. The product range obtained in non-hydrogenating pyrolysis is thus fundamentally different from that obtained under hydrogenating conditions. Figure 70 shows the product distribution of pyrolysis at 850 °C under H₂ atmosphere. Both EOL, referred to as raw lignin in the figure, and HEOL are pyrolyzed [125].

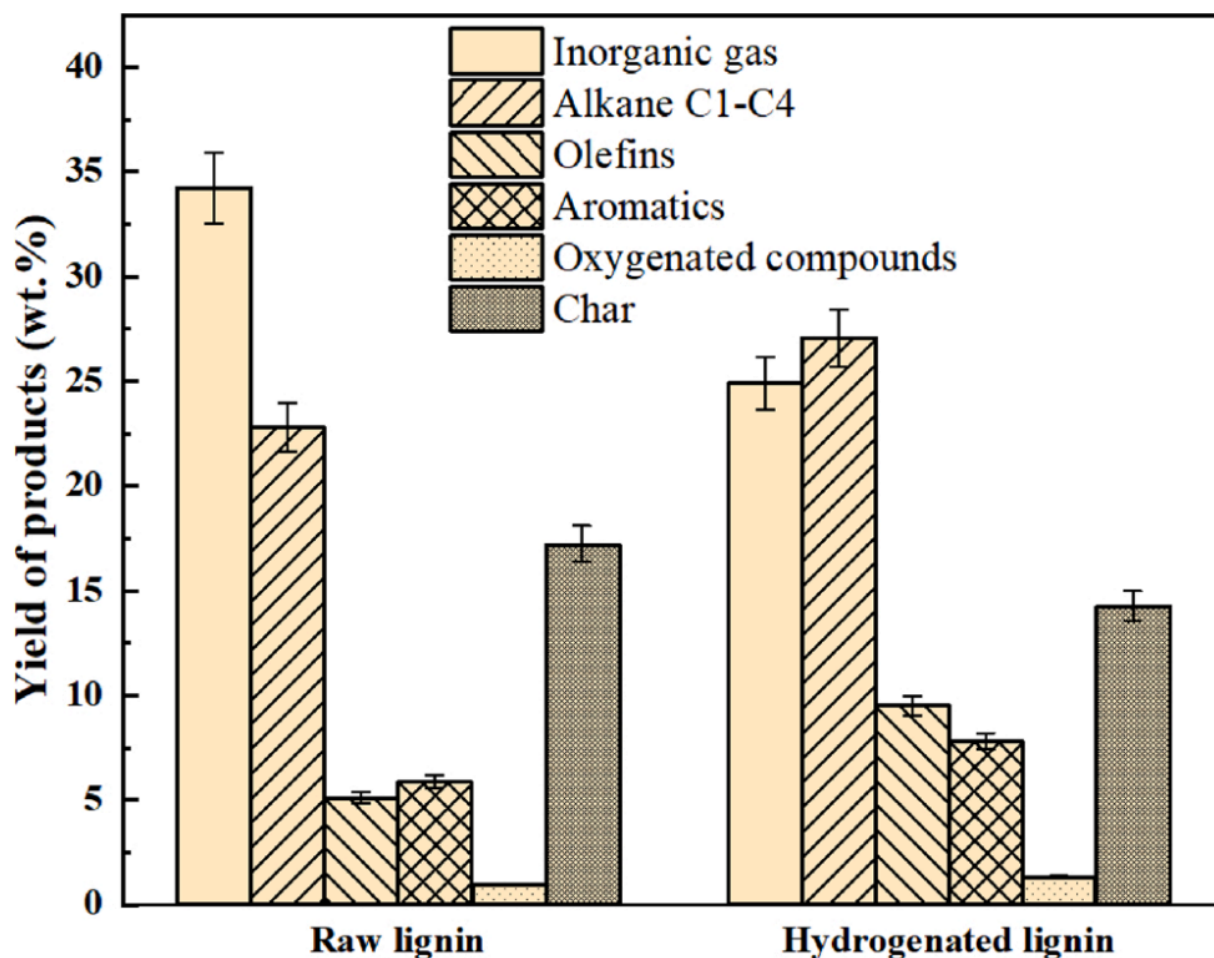


Figure 70: Identified products of EOL and HEOL pyrolysis in H_2 atmosphere at 850 °C [125]

It can be shown that the pyrolysis of HEOL produces less inorganic gas and coal. The proportion of alkanes, olefins, and aromatics, on the other hand, increases. Pyrolysis of lignin with and without hydrogenating pre-treatment can be considered an effective method for the production of light hydrocarbons and aromatics [125].

Heat treatment of kraft black liquor

Demuner et al. investigate the effects of thermal treatment of eucalyptus kraft black liquor on the pyrolytic properties of the lignin precipitated from it. The black liquor is pretreated for 30-150 min at temperatures of 175-225 °C. The lignin is then precipitated by acidification to pH 2 with sulphuric acid. The precipitated KL is filtered and washed several times with hot water. Drying is then carried out at 40 °C. The pyrolysis of the KL is then carried out at 550 °C [82].

The thermal pre-treatment changes the substitution pattern of the monomers of the biooil phase. Demuner et al assume that hydrolysis reactions are responsible for demethylation. The hydrolysis shown in Figure 71 produces phenolates [82].

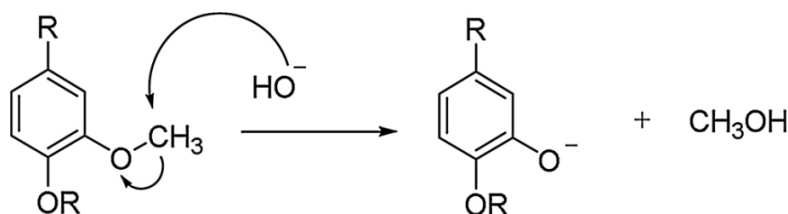


Figure 71: Hydrolytic demethylation [82]

The conversion of methoxy to phenol groups leads to the fact that the products of pyrolysis are increasingly catechols. Figure 72 shows the proportions of phenolic compounds depending on the duration and temperature of the thermal pre-treatment. The proportion of catechols increases with increasing intensity of the pre-treatment. Proportions of syringols with two methoxy groups decrease, and the proportion of guaiacol remains almost constant. Since it is assumed that S-type and G-type monomers hydrolyse similarly readily, the consistency of the G-type phenols is due to the fact that they are formed by hydrolysis of S-types [82].

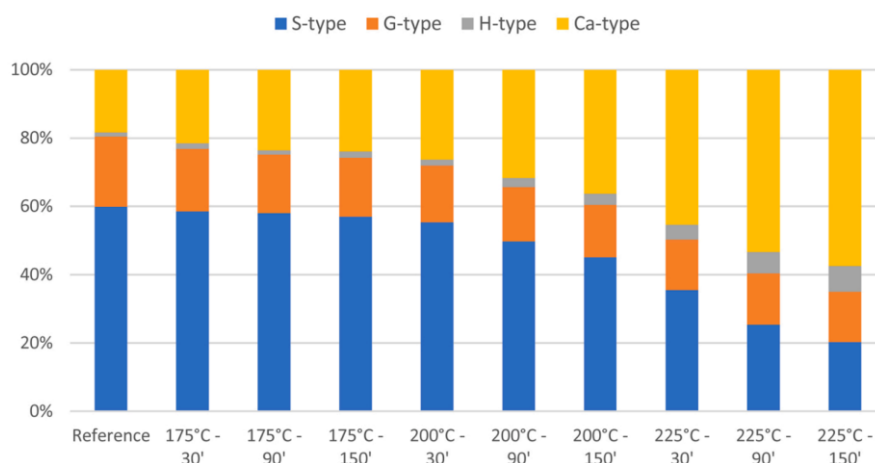


Figure 72: Proportions of phenolic groups in biooil [82]

Thermal pre-treatment of the black liquor can serve to shift the substitution patterns of the monomers of the bio-oil in the direction of catechols.

Drying of Lignin

Gordobil et al. investigate the influence of drying temperature on chemical and physical properties of KL. KL is comparatively dried at room temperature (25 °C) as well as at 55 °C. It can be shown that KL dried at 55 °C (KL 55) is less hygroscopic than KL 25. Furthermore, KL 55 is characterised by a brownish discolouration of the lignin particles. Figure 73 shows the two lignins examined [126].

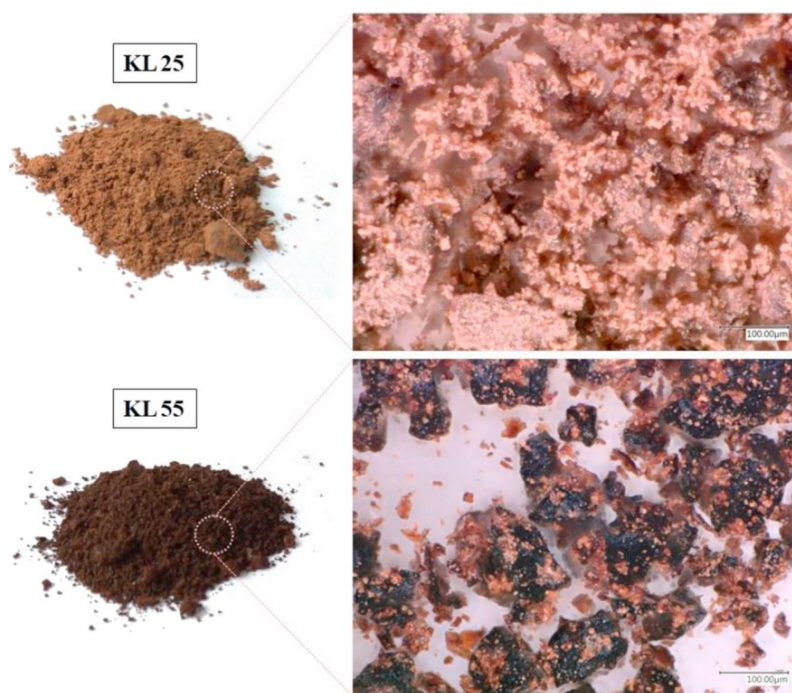


Figure 73: Photographs of KL 25 and KL 55 [126]

Analysis with pyrolysis gas chromatography-mass spectroscopy (Py-GC-MS) shows differences in the substitution pattern of phenolic compounds as well as differences in the side chains. KL 55 has a higher proportion of S-type phenols and a lower proportion of G-type phenols. Further it is mentioned that KL 55 contains more side chains [126].

Gordobil et al. do not examine the impact on pyrolytic biooil yields. However, changing the drying conditions can be used as a simple method to effect changes in the substitution pattern of the phenols.

Enzymatic depolymerisation

Enzymatic depolymerization can be used to effectively reduce the molecular size of lignins. Majeke et al. investigate the effects of enzymatic treatment on the molecular size distributions of four lignins. The lignins studied are soda anthraquinone lignin (SAQ), steam explosion lignin (S-E), and two sodium lignosulfonates (NaE, NaPE). The enzymes lignin peroxidase (LiP) and quinone reductase (QR) are used. The enzymatic treatment was carried out in a tartrate buffer at pH 3. In addition to the enzymes, the buffer solution also contains NADH and H_2O_2 . The enzyme loading is 2 units/mg lignin. After 24 hours, the reaction mixture is heated at 100°C for 15 minutes to deactivate the enzymes. Effective depolymerization can be demonstrated by the molecular size distributions. The mean weight-based molecular size distributions can be reduced by 31%, 41%, 34%, and 52% for SAQ, S-E, NaE, and NaPE, respectively [127].

Results of the pyrolysis of these depolymerized lignins are reported in a second publication by Majeke et al. Pyrolysis takes place at 550 °C in a fixed-bed tubular reactor on a laboratory

scale. It can be shown, that the biooil yield is increased for all enzymatically treated lignins. Pyrolysis product distribution of the untreated as well of the enzymatically depolymerized lignins are shown in Figure 74 [128].

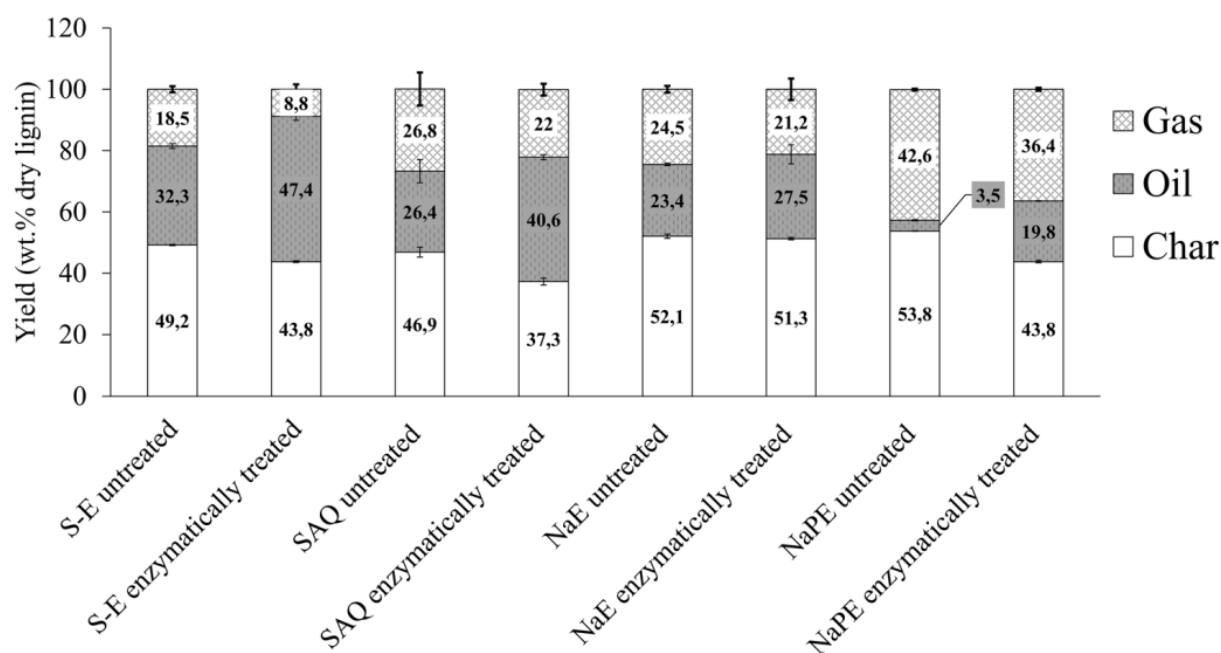


Figure 74: Pyrolysis product distributions of enzymatically treated lignins [128]

Although the proportion of biooil has increased significantly for all lignins, an increase in the phenolic monomers can only be demonstrated for S-E. The proportion of phenolic monomers increases from 5.42 to 7.76% through enzymatic treatment. This proportion refers to the amount of lignin used. With SAQ, the value remains roughly constant at 7.83 and 7.84%. The proportion of monomers in the two liginosulfonates is even declining. For NaP, the proportion drops from 0.88 to 0.70% and for NaPE from 0.78 to 0.49% [128].

Enzymatic depolymerization can be used effectively to reduce the molecular size of technical lignins. Along with this, an increase in the biooil yield can also be expected. However, an increase in bio-oil yield cannot be directly translated into an increase in monomer content for every lignin. This study also shows that liginosulfonates are not particularly suitable for the production of phenolic monomers by pyrolysis.

Acid gradient fractionation

Cao et al. fractionate poplar kraft black liquor by the use of an acid gradient. First, the black liquor is acidified to pH 6 with a 2 molar sulphuric acid. At pH 6, large molecules tend to precipitate. The precipitated lignin is filtered off and this fraction is referred to as LpH6 in the following. The supernatant is further acidified until pH 4 is reached. Precipitated lignin (LpH4) is filtered off again. This process is repeated once more. The last fraction (LpH2) contains lignins with the lowest molecular mass [129].

KL and the fractions LpH6, LpH4 and LpH2 are all pyrolyzed at 500 °C, 650 °C and 800 °C. The product distributions were not collected in this study, but the relative proportions of the phenol types in the pyrolysis products are given. Figure 75 shows the relative proportions of phenol-type (H), guaiacol-type (G), syringol-type (S), catechol-type (C), and aromatic hydrocarbon (AH) products [129].

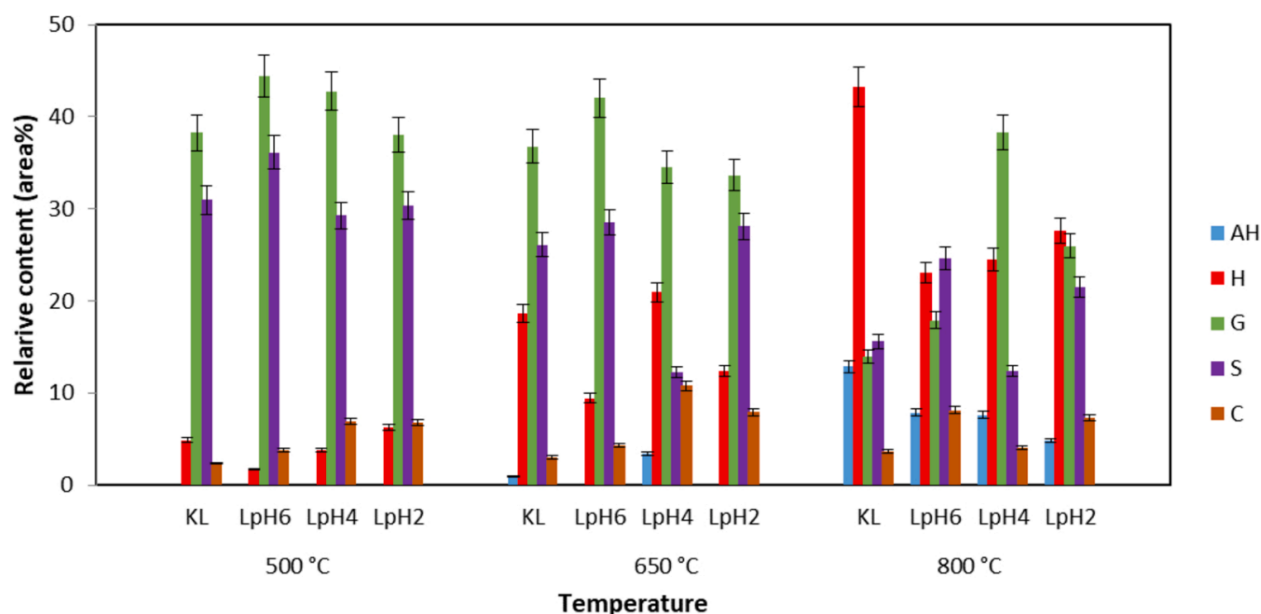


Figure 75: Relative contents of pyrolysis products of KL, LpH6, LpH4 and LpH2 [129]

Figure 75 shows that AH first appear in small quantities at 650 °C. At 850 °C it can be seen that fractions with larger lignin molecules tend to form more AH. Results at pyrolysis temperatures of 500 °C have the highest proportions of G and S types. As the temperature increases, these proportions decrease and more H and C phenols are formed, with the trend being more pronounced for the H type. It can also be seen that fractions with higher molecular weights tend to have a higher (G+S)/(C+H) ratio at 500 °C [129].

Thus, acid gradient-controlled fractionation of KL shows effects on the substitution pattern of phenolic products and could be a suitable means to preferentially produce certain monophenols in pyrolysis.

3.3.4 Process parameters of pyrolysis

In this chapter, influencing factors are described that relate directly to pyrolysis. In deviation from the pyrolysis of pure lignin, substances can be added to the pyrolysis. Here, a distinction can be made between co-pyrolysis and catalysts. Another influencing factors are technical parameters including temperature, residence time, heating rate, and reactor types.

Co-Pyrolysis

Co-pyrolysis refers to the simultaneous pyrolysis of different feed materials. On the one hand co-pyrolysis with cellulose or lignin should be mentioned here, with regard to lignin pyrolysis. The joint pyrolysis of these materials is mainly used to gain insights into mutual effects that are important in the pyrolysis of LCBM. On the other hand co-pyrolysis of proton donors such as low density polyethylene (LDPE) could provide a new application for lignin pyrolysis.

Pienihäkkinen et al. pyrolyzed lignins with differing amounts of carbohydrates (18-38 %). A clear trend is that the liquefaction rate increases with increasing carbohydrate concentration. This aspect is already known from chapter 3.2.1 as a disadvantage of the pyrolysis of pure lignin. It is also known that the handling of lignin becomes more difficult as the carbohydrate content decreases, since the feed inlet system gets blocked due to melting of lignin. Additionally this feature of high purity lignin leads to agglomerate formation in the reactor bed following by a defluidisation of the bed. Figure 76 shows the product distributions of lignin pyrolysis as a function of the carbohydrate content [130]

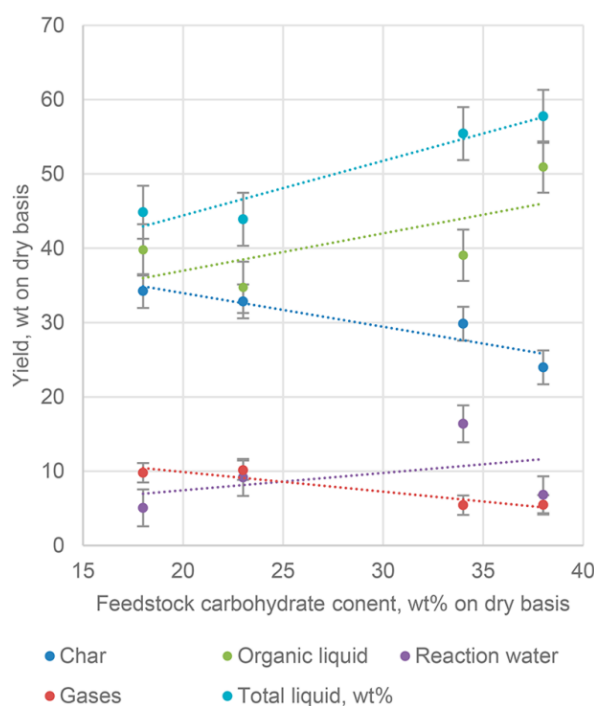


Figure 76: Pyrolytic product yields of lignins with varying carbohydrate content [130]

In co-pyrolysis with LDPE, the plastic serves as a source of hydrogen atoms. Pyrolysis with LDPE can therefore be expected to produce similar products to pyrolysis under a hydrogen atmosphere [131].

Yu et al. investigate the co-pyrolysis of walnut shell (WNS) and LDPE. Since no pure lignin is pyrolyzed in the cited publication, the direct comparison is not suitable. However, investigation

of the interactions of WNS lignin and LDPE guided Yu et al. to the proposed reaction mechanism, depicted in Figure 77 [74].

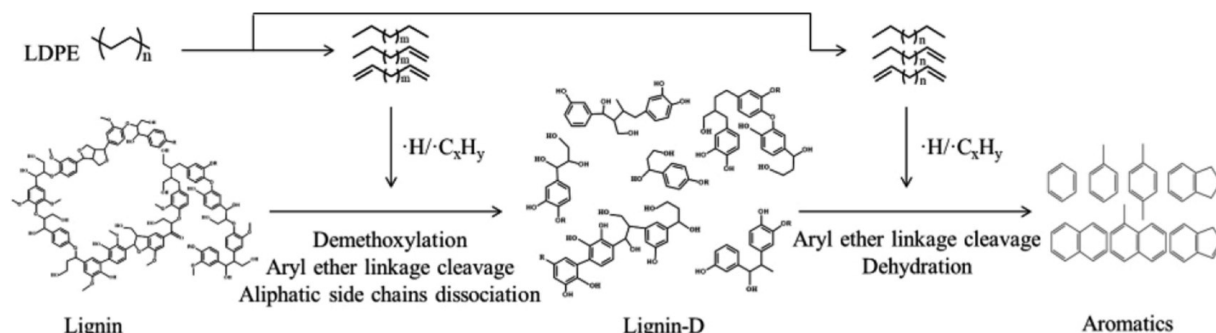


Figure 77: Reaction mechanism for co-pyrolysis (TSCCP) of lignin and LDPE [74]

Two step catalytic co pyrolysis (TSCCP) describes the pyrolysis process used. In the first step, pyrolysis is carried out at 550 °C for 4 min and in the second step at 700 °C for 10 min. In the first step, pyrolytic degradation of the lignin molecule into smaller molecules takes place. Due to α -O-4 and β -O-4 bond breaks as well as attacks of the hydrogen radicals, which get formed during the pyrolysis of LDPE, a degradation of the lignin to the transition product lignin-D takes place. This more easily accessible lignin-D can in the second step be attacked more efficiently by the radicals formed from LDPE. Hydrodeoxygenation reactions, amongst other reactions, then lead to the formation of oxygen-free saturated aromatics [74].

Co-pyrolysis of hydrogen-rich compounds such as PE, PP or LDPE can be used to produce aromatics without the need for a hydrogen gas atmosphere. This co-pyrolysis usually involves the use of catalysts, the one used in the cited study is HZSM-5 (hydrogen form of Zeolite Socony Mobil-5) [74].

Catalysts

There are a variety of catalysts that are used experimentally in the pyrolysis of lignin. These catalysts can have an influence on the products of the biooil or have a positive effect on the introduction of the lignin into the reactor.

Schafaghat et al. studied the effects of different catalysts on the pyrolysis of Kraft lignin. Zeolites such as HZSM-5, hydrogen Beta zeolite (HBeta), spent fluid catalytic cracking (FCC) catalyst, and the hydrogen form of hierarchical Y zeolite (HY) are used as catalysts. Furthermore, aluminum and MgO are examined for their catalytic properties. The catalytic pyrolysis is performed at 500 °C and between 50 and 100 g KL are used. All catalysts lead to a reduced amount of biooil compared to uncatalyzed lignin pyrolysis. The product distributions of the cited pyrolysis experiments are shown in Figure 78 [119].

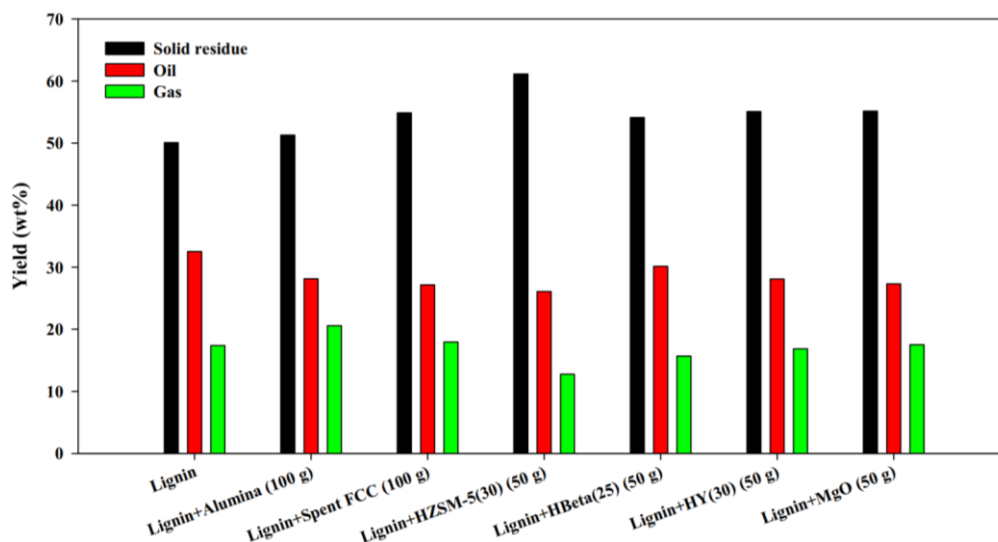


Figure 78: Product distributions of catalytic pyrolysis experiments [119]

It should be noted that although the amount of biooil is reduced through the use of catalysts, the proportion of oligomers is also significantly reduced. Looking at the composition of the organic phase of the biooil, it can be seen that the proportion of H-type phenols in the catalysed pyrolysis has increased, and the proportion of G-type phenols reduced. There is thus a substantial decrease in the number of substituents on the benzene ring. The functional groups are broken down to such an extent that monoaromatics and polyaromatic hydrocarbons (PAH) are formed. Figure 79 shows the proportions of the constituents of the organic phase of the biooils [119].

The yield of monophenols in the study presented cannot be increased by catalytic pyrolysis. However, the catalysts presented can be used to achieve a shift towards H-type phenols as well as monoaromatics (MAHs) and PAHs.

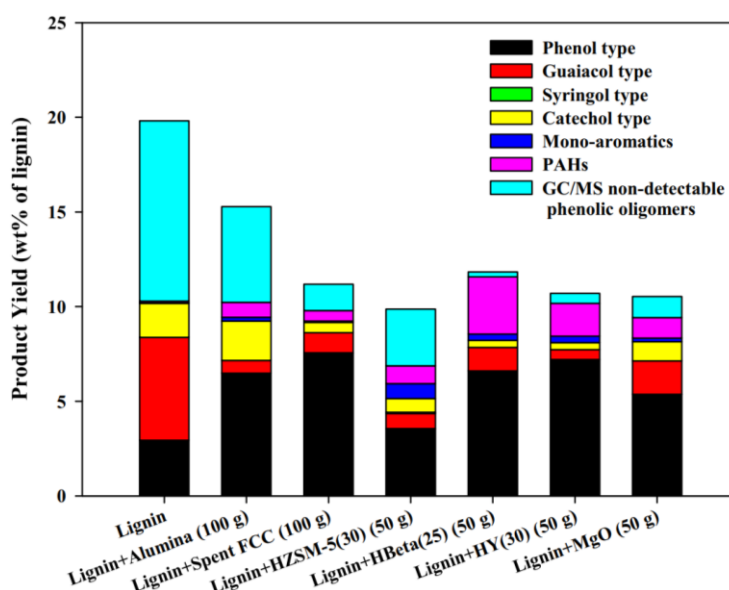


Figure 79: Biooil products from catalytic pyrolysis of lignin [119]

Other tested catalysts and their main impact on lignin pyrolysis are summarized in Table 9.

Table 9: Catalysts in use for lignin pyrolysis

	effects on lignin pyrolysis	source
attapulgit	increased biooil yield, better lignin handling	[86]
Ca(OH) ₂	increased biooil yield, better lignin handling	[86]
Co/CeO ₂	increased S-type production	[132]
Co/TiO ₂	production of MAHs and PAHs	[132]
HZSM-5/Al-SBA-15	decreased biooil yield, production of MAHs and PAHs	[133], [134]
K-salts	Increased rate of demethoxylations	[135]

Reaction engineering

Impact of parameters such as temperature, residence time and heating rate in lignin pyrolysis are comparable to conventional biomass pyrolysis, described in chapter 2.2.

The first important parameter is the pyrolysis temperature. Most of the publications, dealing with lignin, report using pyrolysis temperatures of 500 °C, see Table 4. Fan et al. describe in their review that optimal liquefaction temperatures for lignin are higher than for ordinary biomass, because of the increased relative abundance of C-C bonds. According to Fan et al. this is at 550-650 °C [136]. However, the optimal liquefaction temperature should be questioned critically. The factors influencing biooil yield of lignin are diverse. Different optima can be found due to varying molecular size, chemical composition, type of lignin, reactor type, and heating rate. An example of the deviation from 550-650 °C is the study published by Zhou et al. in which liquefaction rates approaching 90 % are achieved. The results of the cited study show that the optimum biooil yield in the pyrolysis of organosolv lignin is 475-500 °C. In Figure 80, yields of biooil, gas, and biochar from the pyrolysis of organosolv lignin achieved with a wire mesh reactor are shown [104]. Besides liquefaction rates, the influence of temperature also has an effect on the pyrolysis reactions and thus also on the products. Jiang et al. show that H-type and Ca-type fractions increase with temperature. On the contrary, both S-type and G-type phenols decrease with an increase in pyrolysis temperature. There is a temperature dependent shift of substitution patterns in the direction of demethoxylated phenols [137]. Considering phenolic substitution altering reactions, Kawamoto categorizes catechols and H-type phenols as end products of the secondary phase pyrolysis reactions [100].

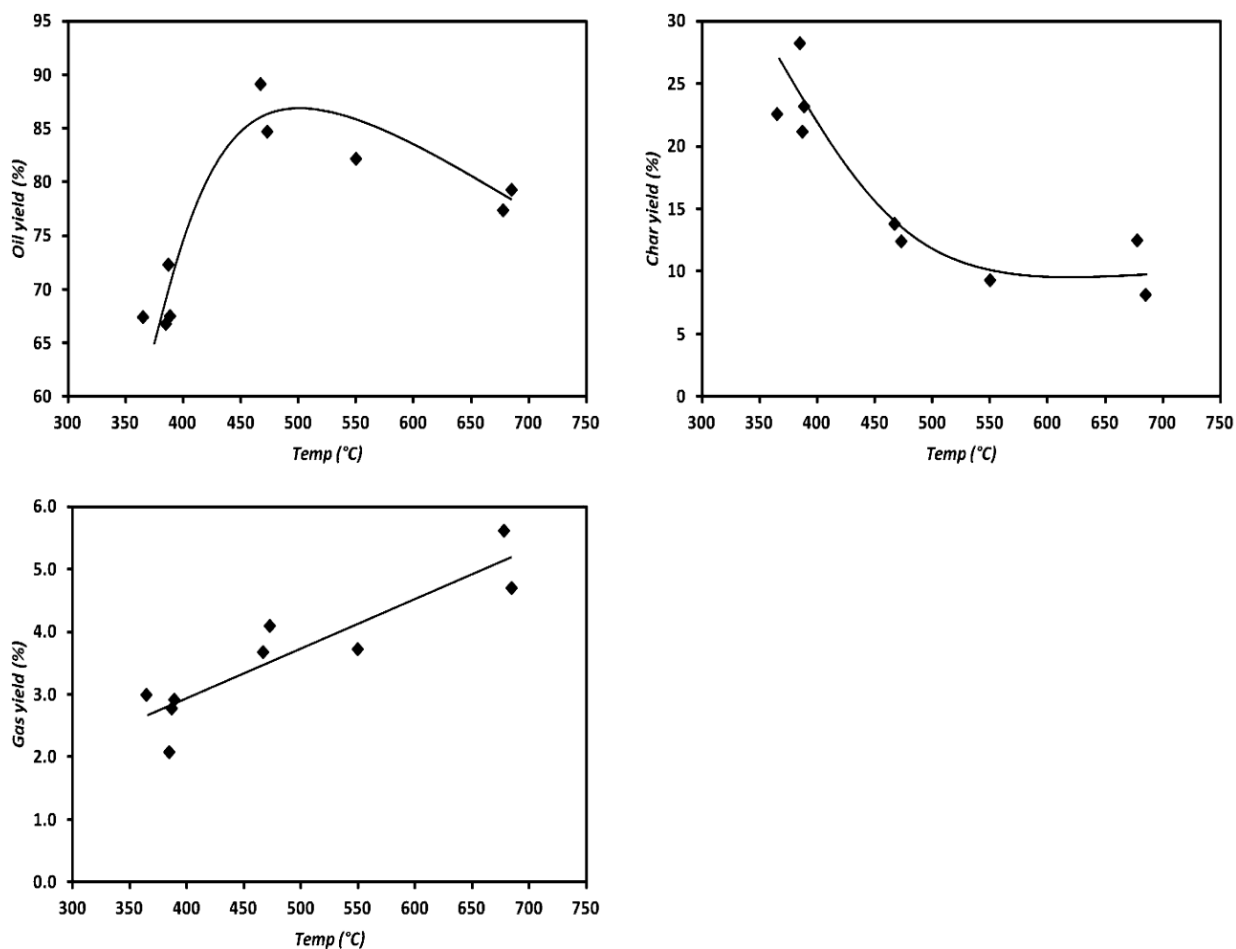


Figure 80: Product yields from organosolv pyrolysis in a wire mesh reactor [104]

The third important aspect, besides liquefaction rate and phenolic substitution pattern is the yield of monomeric phenols. Jiang et al report the highest yield of GC detectable phenols at 600 °C [137].

Besides temperature, the residence time of the pyrolysis vapours is the most significant technical parameter in lignin pyrolysis. In general, it is observed that longer residence times lead to an increased intensity of secondary reactions. As described in detail in chapter 3.1.2, degradation reactions in the form of ring-breaking reactions to light organic molecules and finally to non-condensable gases are part of the secondary reactions. Thus, an increase in residence time leads to a reduction of the organic phase and an increase in the gas phase. Figure 81 shows the dependence of the residence time (0.8 and 4.2 s) on the products of the pyrolysis of wheat straw lignin. Pyrolysis is performed at 550 °C in a pyrolysis centrifuge reactor (PCR) [138].

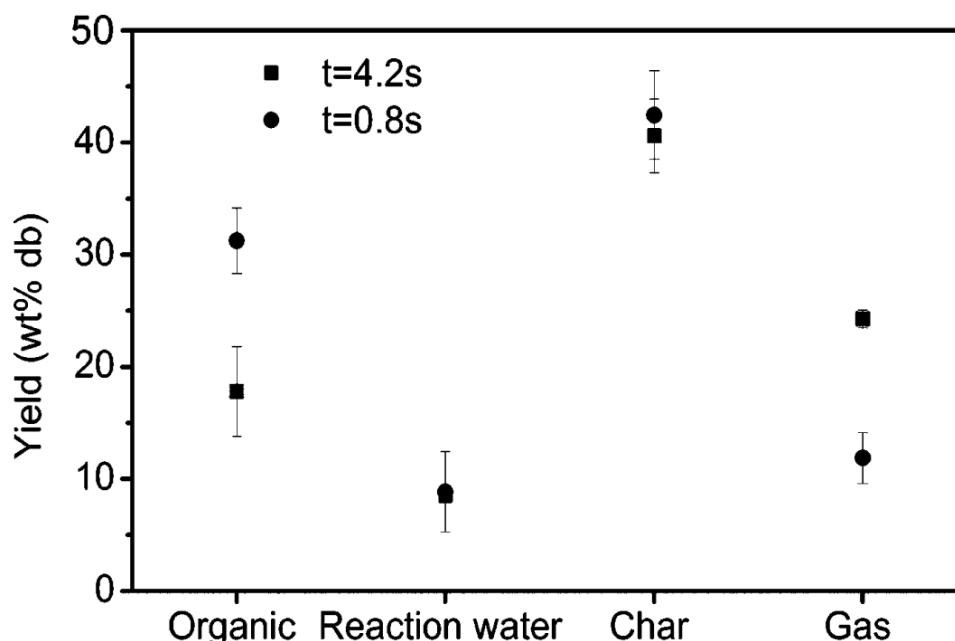


Figure 81: Yield dependencies on residence time in lignin pyrolysis [138]

The yields of the biochar and the aqueous phase shown in Figure 81 are constant in the experiments with varying residence time. Since biochar and reaction water remain constant, there is a shift in the yields of gas and biooil. Significant differences can be seen in the organic phase and gas phase. The organic phase decreases from over 31.2 % to under 17.8 %, while the gas phase increases from 11.8 to 24.3 %. It should be mentioned that the wheat straw lignin used has a lignin content of 78 % and an ash content of 12 %. As already mentioned, Zhou et al. can achieve the highest liquefaction rates of almost 90 %. The residence time used for this is 25-35 ms. However, these experiments almost exclusively produce oligomers [104].

Besides temperature and residence time, reactor types are also important in relation to lignin pyrolysis. The most commonly used reactors are bubbling fluidized bed (BFB) reactors. Occasionally, entrained flow reactors (EFR) or pyrolysis centrifuge reactors (PCR) are also mentioned in the literature. So far, however, neither EFR nor PCR has been able to bring significant improvements to BFB reactors in terms of liquefaction rate and monomer content [81].

3.4 Summary

The literature review presented provides an overview of the state of the art in research as well as technology on the topic of lignin pyrolysis.

Lignin pyrolysis is a process in which lignin is thermochemically processed in the absence of oxygen. The most commonly used reactor systems are BFB reactors [81]. The products are non-condensable gases, biochar and biooil. At 450-600 °C, the liquefaction rate is between 11 and 54.7 % [83]-[88]. The organic phase of the liquid products is called biooil. Biooil contains differently substituted oligomeric phenols and monomeric phenols as well as light organic components [83].

The chemical reactions that occur during lignin pyrolysis are divided into two groups. The dominant reactions of the primary reactions are α -O-4 and β -O-4 bond breaks. These degradation reactions compete with repolymerising reactions. Secondary reactions include the degradation of monomers to light organic components and to non-condensable gases. Furthermore, reactions in which changes in the substitution pattern occur are counted among the secondary reactions [100].

At present, lignin pyrolysis can still be classified as a low-advanced technology. The majority of publications deal with analytical pyrolysis of lignin, which commonly uses feed input quantities in the μg range [81]. The largest known pyrolysis experiment of pure lignin processes a total of 1000 g feed in the course of 100 minutes at 500 °C in a bubbling fluidised bed reactor. Liquefaction rates of 45 % and a yield of phenolic monomers of about 8 % are achieved [87].

Challenges in lignin pyrolysis consist on the one hand of the lower liquefaction rate compared to LCBM pyrolysis and on the other hand of the high proportion of oligomeric phenols in the biooil. In addition to these challenges, there are difficulties with the handling of lignin at elevated temperatures. When handling larger quantities of lignin, authors report severe complications in process control, which can mainly be attributed to the melting of lignin. Blockages occur in the feed inlet system due to melting lignin, and agglomerates formed in the reactor bed inhibit fluidisation [87].

Individual factors influencing lignin pyrolysis are analysed. Based on publications that examine these factors, a foundation is laid for the possibilities of potential process improvements. Figure 82 uses the value chain to show which optimisation options are known from the literature. In addition to the effects of biomass, the effects of different lignin isolation processes are highlighted. With regard to the processing of lignin, there are numerous chemical, physical and biological possibilities to modify lignin before pyrolysis. During pyrolysis itself, temperature,

residence time and reactor type can have significant effects on the products. Furthermore, the influence of co-pyrolysis and catalysts is discussed.

At present, most of the difficulties associated with the pyrolysis of lignin have not yet been clarified. Pre-treatment steps that reduce the molecular size of lignin before pyrolysis in order to increase the biooil yield are promising [124]. Equally interesting is the use of hydrogen-rich substances that are pyrolyzed together with lignin to produce saturated aromatics and alkanes [74]. For a suitable selection of optimisation steps, however, the desired product must be well defined in advance.

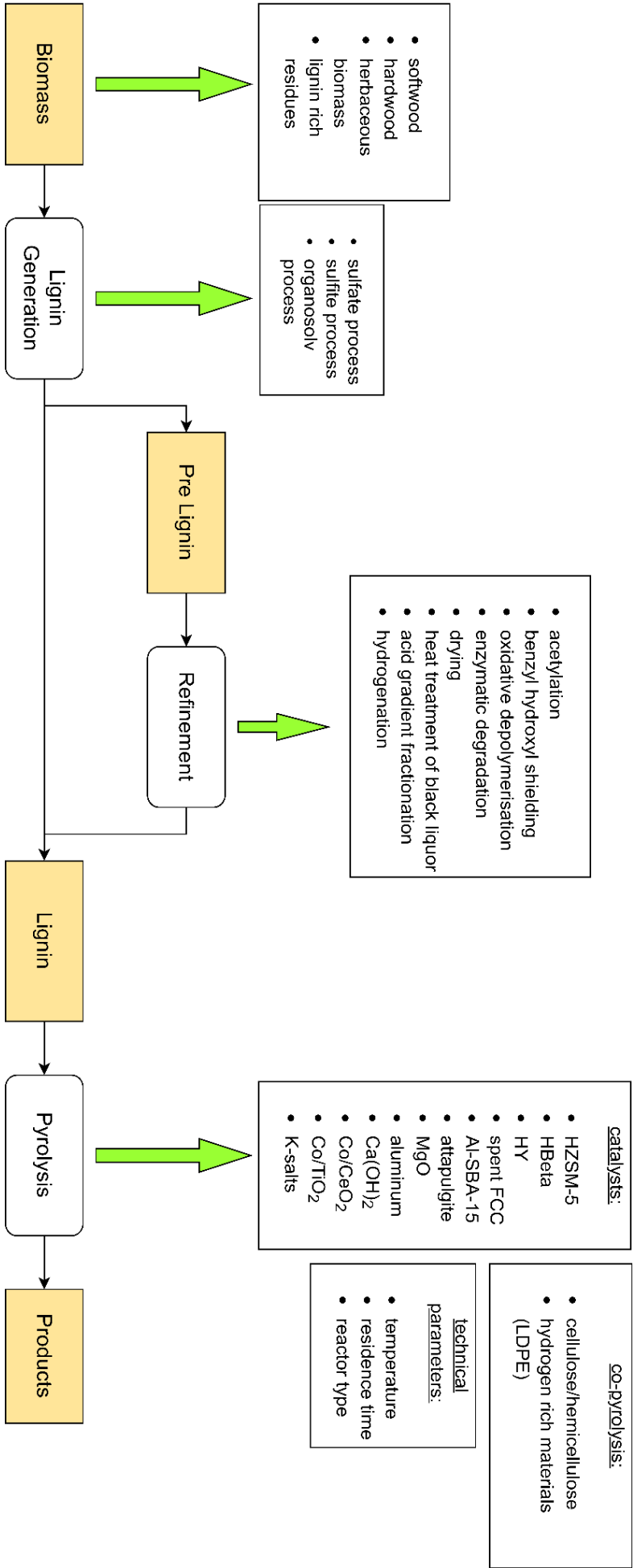


Figure 82: Influencing factors of lignin pyrolysis

4 Process modelling

This chapter presents a process model for the recovery of lignin from the black liquor of a kraft process with subsequent pyrolysis.

For the modelling of the process, a process diagram is first created. The basis of the calculation is the amount of black liquor to be processed, which is 100,000 tonnes per year (t/y). Data from literature on kraft lignin precipitation as well as on the pyrolysis of lignin are used for the quantitative estimation of the mass flows. Based on the mass balance, an energy balance is determined, which is used to estimate the costs of the process. Furthermore, the required process chemicals are included in the cost estimate.

4.1 Process model parameters and boundaries

Chapter 4.1 explains the unit operations and the process flows, followed by the presentation of a simplified process flow diagram in Figure 83. General information about the kraft process as well as details about the effects of process parameters on the lignin recovery from the black liquor are explained in chapter 2.1.1.

The Lignoboost process presented, described in chapter 2.1.1, is used as the basis for the lignin precipitation from the black liquor. In the model presented, it is assumed that the black liquor (BL) with a temperature of 80 °C is taken from a kraft process with a proportion of 30 % dry substance (DS). In the first step of the process, BL is acidified with CO₂ to pH 9.6 to precipitate lignin. Part of the liquid in this mixture is separated from the lignin in the filter press. The liquid stream with reduced lignin content is referred to as lean liquor and is returned to the multi-effect evaporators of the kraft process after the filter press. The resulting filter cake is taken up in diluted sulfuric acid (pH=2.5) and transferred to the slurry tank. During acidification to a pH of 2.5, H₂S is produced. This toxic gas is fed into the kraft process to the recovery boiler. The slurry is conveyed to a second filter press. After pressing and washing with acidified water (pH=2.5), the resulting filter cake with 70 % DS is dried to a moisture content of 0 %. A portion of the wash liquor stream produced during the washing of the second filter cake is recycled back to uptake first filter cake. The remainder of the washing liquor is sent to the early stages of the multi effect evaporation units. Water gained during drying is made available to the evaporator unit as hot steam.

A bubbling fluidised bed (BFB) reactor is chosen for flash pyrolysis at 500 °C. First, the dried lignin is fed into the BFB reactor. The process of pyrolysis produces vapours, gases, and biochar. The gaseous fraction is completely separated from biochar in a cyclone. The collected biochar is incinerated to produce energy. The pyrolysis vapours are liquefied in a condenser

that is operated with water from a nearby river. Remaining non-condensable gases are heated to pyrolysis temperature and fed back to the BFB, serving as fluidising gas for the reactor bed. In steady state, the accumulating excess gas, which is called off gas, is discharged and burnt.

Following process relevant assumptions are made to simplify the modelling. For the precipitation of lignin, it is assumed that BL is continuously drawn from the kraft process, with a constant content of 30 % DS and a temperature of 80 °C. Acidification with CO₂ is done from the off gas of the pyrolysis, it is assumed that other contained gases have no effect on acidification. The effect of sulphuric acid on evaporation in the kraft process is not considered. Losses due to appliance leaks or other causes are not taken into account. It is assumed that lignin melting does not negatively affect the feed inlet and the fluidisation of the reactor bed. Furthermore, complete biochar separation and complete condensation of the pyrolysis vapours are assumed. Water from the nearby river is available in unlimited quantities and at a temperature of 10 °C.

Further assumptions and simplifications, especially concerning the product distributions and the thermodynamic simplifications in the design of the unit operations, are given in chapter 4.2 and 4.3.

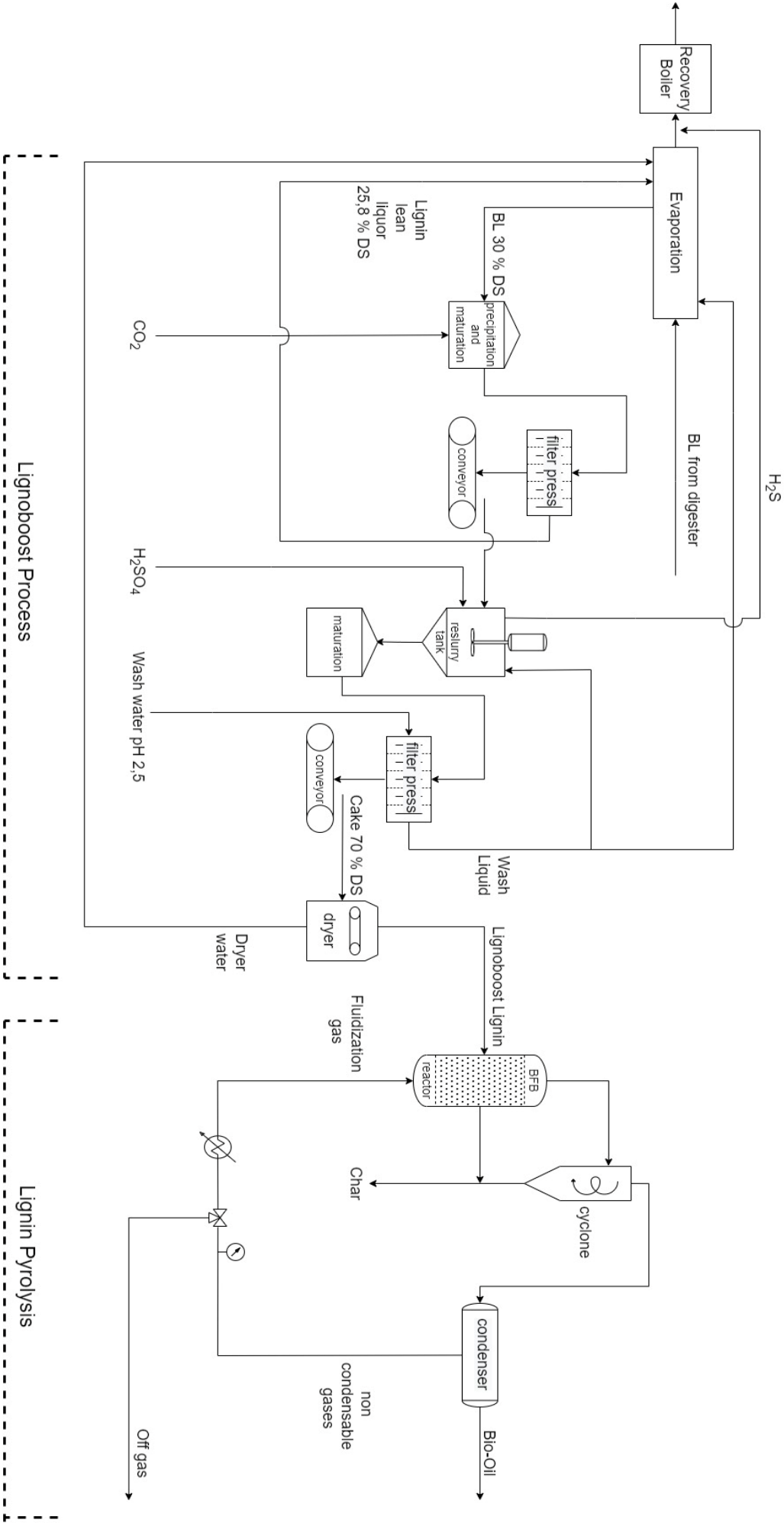


Figure 83: Lignin precipitation from kraft black liquor with subsequent flash pyrolysis

4.2 Mass balance

In this chapter, the mass flows of the process are quantified. The balancing of the lignin precipitation process, the LignoBoost process, is started, followed by the balancing of the pyrolysis. The calculated process flows are shown in Figure 85. In chapter 4.2.3, the demand on chemical supplies is calculated.

4.2.1 Lignin precipitation and drying

In subchapter 4.2.1, the mass balance of lignin precipitation from black liquor (LignoBoost process) with subsequent LignoBoost lignin drying is evaluated. The term LignoBoost lignin is used to emphasise that the precipitated product is not 100% pure lignin. Assumed model parameters are given in Table 10.

Table 10: Model parameters for LignoBoost process

parameter	abbreviation	value	source
BL processed per year	$\dot{m}_{BL/y}$	100,000 t/y	-
operating time	t_{op}	8000 h/y	-
BL DS	DS_{BL}	30 %	[44]
lignin yield	y_L	60.5 %	[4]
filter cake DS	DS_{cake}	70 %	[139]
LignoBoost lignin content in BL with 30 % DS	LBL_{BL_30DS}	10.6 %	[140]
lignin content in LignoBoost lignin	Lig_{LBL}	96.5 %	[141]

Using the model parameters given in Table 10, the calculation of the mass flows is straightforward. From the production quantity of 100,000 t/y and the operation time of 8000 h/y, a hourly mass flow of black liquor ($\dot{m}_{BL/h}$) of 12,500 kg/h results. The mass flow of precipitated LignoBoost lignin is calculated according to formula 4.2.1 a.

$$\dot{m}_{LBL} = \frac{\dot{m}_{BL/h} \cdot \frac{LBL_{BL_30DS} \cdot y_L}{100}}{\frac{Lig_{LBL}}{100}} = \frac{12500 \frac{kg}{h} \cdot 0.1058 \cdot 0.605}{0.965} = 829.13 \frac{kg}{h} \quad (4.2.1 a)$$

This results in a mass flow of pure lignin (\dot{m}_L) of 800.11 kg/h. The mass flow of the filter cakes (\dot{m}_{cake}) is calculated from the ratio of the mass flow of LignoBoost Lignin and the dry mass fraction of the cake. The result is: $\dot{m}_{cake}=1184.47$ kg/h. It is assumed that the total mass of both filter cakes, as well as the lignin content in the cakes, is the same. The proportion of dry matter in the lean liquor is calculated from the ratio of the amount of dry matter and the total mass of the lean liquor. Formula 4.2.1 b shows the calculation. The mass flow of LignoBoost lignin after

drying equals \dot{m}_{LBL} , as it is assumed that all water is removed by drying. The mass flow of this dryer water flow results therefore from the difference between the mass of the filter cake and that of the LignoBoost lignin and amounts to 355.34 kg/h.

$$DS_{LL} = \frac{\dot{m}_{BL/h} \cdot \frac{DS_{BL}}{100} - \dot{m}_{LBL}}{\dot{m}_{BL/h} - \dot{m}_{cake}} = \frac{12500 \frac{kg}{h} \cdot 0.3 - 829.13 \frac{kg}{h}}{12500 \frac{kg}{h} - 1184.47 \frac{kg}{h}} = 829.13 \frac{kg}{h} \quad (4.2.1 \text{ b})$$

4.2.2 Lignin Pyrolysis

In chapter 4.2.2, the mass flows of the pyrolysis following the LignoBoost process are modelled. Product distributions of the experiments by de Wild et al. are the basis to estimate the mass flows of the presented process model [87]. The cited experiments are already described in detail in chapter 3.2.

It is assumed that the pyrolysis converts 39 % of LignoBoost lignin to biochar, 17 % to gases and 44 % to biooil. These 44 % of liquid refer to: 15 % water, 8 % phenolic monomers, 19 % oligomeric phenols and 2 % other light organic substances are produced. For the process model presented, this results in a production of 365 kg/h biooil (2919 t/y), 323 kg/h biochar and 141 kg/h non-condensable gases. The individual fractions of the biooil are 66 kg/h monomeric phenols, 158 kg/h pyrolytic lignin, 124 kg/h water, and 17 kg/h light organic substances. Figure 84 shows the calculated process flows of the model in the form of a Sankey diagram.

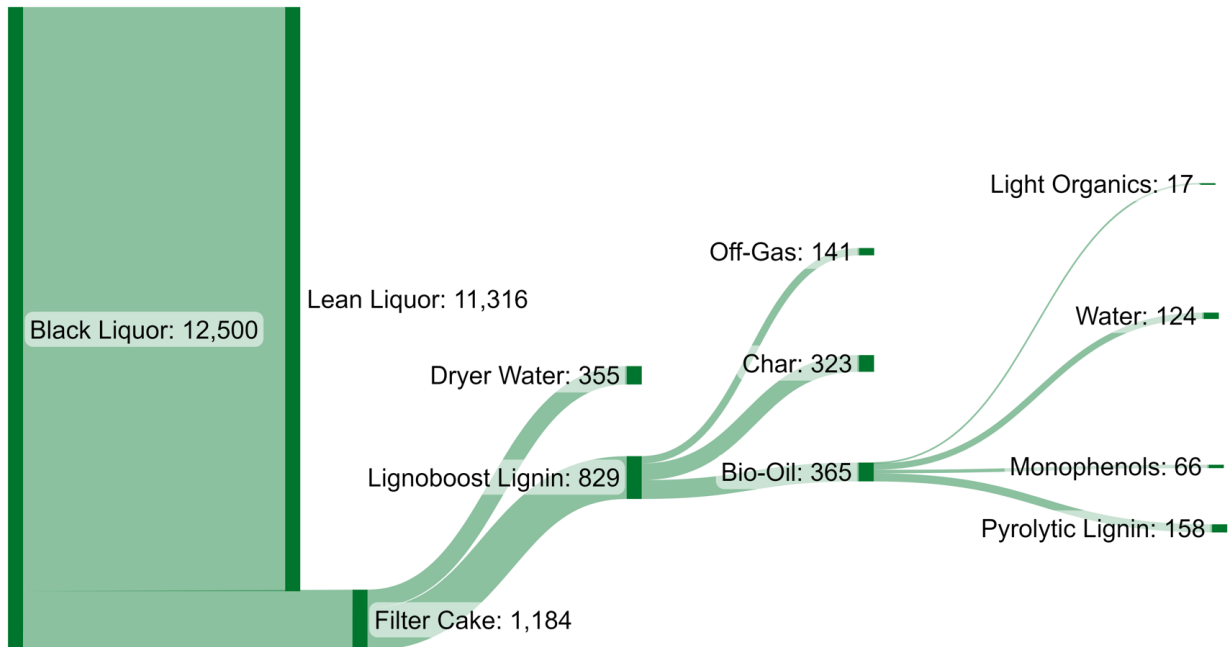


Figure 84: Sankey diagram of calculated process streams in kg/h

4.2.3 Chemicals and water consumption

In Chapter 4.2.3, the demand for chemicals for the process of lignin precipitation from kraft black liquor with subsequent flash pyrolysis is determined. The required process chemicals are CO_2 , H_2SO_4 , and water. CO_2 is obtained from the off gas of the pyrolysis and used to acidify the BL. Sulfuric acid is used to acidify the redissolved filter cake, as well as the wash water to pH 2.5. It is assumed that 220 kg of CO_2 , and 175 kg of H_2SO_4 are required per tonne of LignoBoost lignin produced. The requirement for wash water is estimated to 2 m³ per tonne of LignoBoost Lignin [142]. This results in a required quantity of 182.4 kg CO_2 , 145.1 kg/h H_2SO_4 , and 1.66 m³ of water based on the LignoBoost lignin production of 829 kg/h. All calculated process flows as well as the chemical requirements are shown in Figure 85.

Table 11 shows the annual demand for chemicals and water. Based on the amount of 100 kt/a black liquor, the production of lignin and bio-oil as well as the demand for H_2SO_4 , CO_2 and H_2O are shown. Since 100 kt/a are chosen for the calculation of the model, these values are equivalent to percentages.

Table 11: Annual chemicals and water consumption

black liquor [kt/a], [%]	lignin [kt/a] , [%]	biooil [kt/a] , [%]	CO_2 [kt/a] , [%]	H_2SO_4 [kt/a] , [%]	H_2O [kt/a] , [%]
100	6.63	2.92	1.46	1.16	13.28

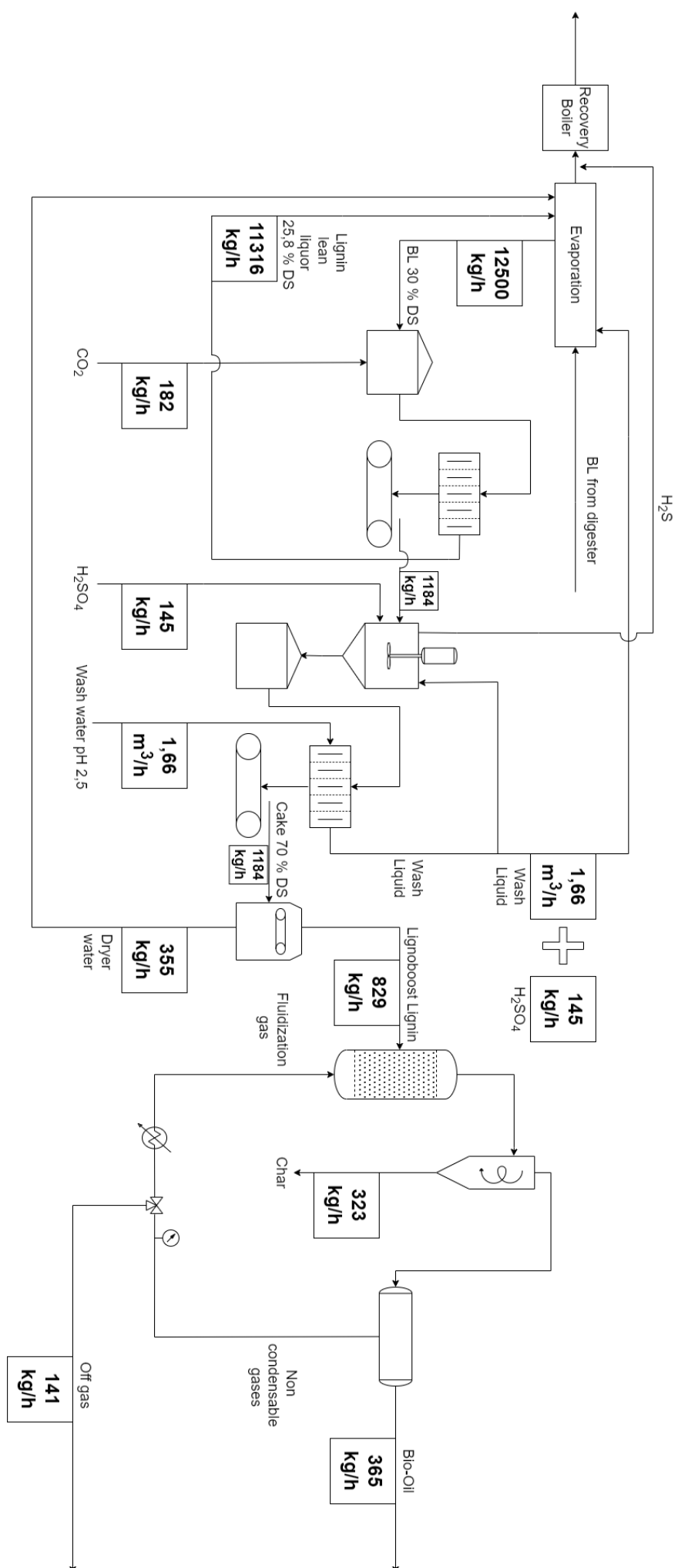


Figure 85: Mass flows of the modelled process

4.3 Energy consumption

In 4.3, the thermal energy needs in the process are modelled. In particular, it concerns drying of lignin, pyrolysis, evaporation of washing water, condensation and cooling of pyrolysis vapours, and combustion of biochar and gas.

The following assumptions are made for all calculations in this chapter. All heat capacities are constant in the considered temperature interval. The same applies to vaporization enthalpies. All processes are considered to be isobaric, and a steady state is assumed. Thermodynamic mixing effects are not taken into account. The whole process is considered perfectly insulated, so there are no heat losses and the heat transfer during condensation is ideal. The effect of the cooling and reheating of non-condensable gases on the total heat flows of the process are neglected. This assumption can be made since an ideal loss-less condenser is assumed.

4.3.1 Drying of lignin

The heat flow of the LignoBoost lignin drying is modelled in chapter 4.3.1. The calculation is based on the relationship shown in equation 4.3.1 a [143]. The given equation describes the relationship between the change in thermal energy ΔQ and the change in temperature ΔT of a substance. C_p is the specific heat capacity of the heated substance for isobaric state changes and m the mass.

$$\Delta Q = c_p \cdot \Delta T \cdot m \quad (4.3.1 \text{ a})$$

In the process considered, the filter cake has a temperature of 80 °C and consists of 70% DS. This filter cake is then dried to absolute dryness. Drying is modelled as heating the cake to 100°C and then evaporating the water at 100°C. For this, the specific vaporization enthalpy (Δh_v) of water must be considered. It is assumed that the specific heat capacity of LignoBoost lignin corresponds to that of wood. The constants used are given in Table 12.

Table 12: Physical constants of water and wood

constant	value	source
specific heat capacity of water	$c_{p,\text{water}} = 4.184 \text{ kJ/kgK}$	[144]
specific vaporization enthalpy	$\Delta h_{v,\text{water}} = 2257 \text{ kJ/kg}$	[144]
specific heat capacity of wood	$c_{p,\text{LBL}} = 1.36 \text{ kJ/kgK}$	[145]

In equations 4.3.1 b-d, the calculation of the amount of heat required to dry the filter cake which results in 237.3 kW is given.

$$Q_{\text{Drying}} = c_{p,\text{water}} \cdot \dot{m}_{w \text{ in cake}} \cdot \Delta T + c_{p,\text{wood}} \cdot \dot{m}_{\text{DS in cake}} \cdot \Delta T + \dot{m}_{w \text{ in cake}} \cdot \Delta h_{v,\text{water}} \quad (4.3.1 \text{ b})$$

$$Q_{Drying} = 4.184 \frac{kJ}{kgK} \cdot 355.34 \frac{kg}{h} \cdot 20K + 1.36 \frac{kJ}{kgK} \cdot 829.13 \frac{kg}{h} \cdot 20K + 355.34 \frac{kg}{h} \cdot 2257 \frac{kJ}{kg} \quad (4.3.1 \text{ c})$$

$$Q_{Drying} = 854 \frac{MJ}{h} = 237.3 \text{ kW} \quad (4.3.1 \text{ d})$$

4.3.2 Pyrolysis

In chapter 4.3.2, the thermal energy demand of pyrolysis is estimated. A simple method of quantifying the heat demand of a pyrolysis process is to use the pyrolysis enthalpy h_p . The pyrolysis enthalpy, which is analogous to the evaporation enthalpy, correlates to the thermal energy demand of the process based on material constants and the mass of the feed. The heating of the biomass to pyrolysis temperature is included in h_p [146]. Equation 4.3.2 a formulates the relationship between the amount of heat and the pyrolysis enthalpy.

$$Q_p = h_p \cdot \dot{m} \quad (4.3.2 \text{ a})$$

Reyes et al. show that lignin ($h_{p,Lig} = 0.86 \text{ MJ/kg}$) has a lower pyrolysis enthalpy at 500 °C compared to hemicellulose (1.43 MJ/kg) and cellulose (1.21 MJ/kg). The energy input of pyrolysis is therefore lower for lignin than for wood pyrolysis [147]. Inserting $h_{p,Lig}$ and \dot{m}_{LBL} (829.13 kg/h) into equation 4.3.2 a, results in a heat quantity of 713.05 MJ/h which corresponds to 198.07 kW.

4.3.3 Evaporation of washing water

For the LignoBoost process, it is necessary to heat water to 80 °C to wash the filter cake at the appropriate temperature. The washing water is then fed to the evaporators of the kraft process and is evaporated there. It is assumed that fresh water with a temperature of 10 °C is first heated to 80 °C and after washing of the filter further to 100 °C. A relationship analogous to equation 4.3.1 b can be established to determine the heat demand of this process step, this can be seen in equations 4.3.3 a-c. $C_{p,w}$ and $h_{v,w}$ data is listed in chapter 4.3.1. The mass flow of wash water \dot{m}_w is 1658.3 kg/h. This data is deduced from the mass balance. In chapter 4.2.3 this is given as 1.66 m³/h. This results in a heat requirement for heating and evaporating of the wash water of 1213.1 kW.

$$Q_{vap} = c_{p,w} \cdot \dot{m}_w \cdot \Delta T + \dot{m}_w \cdot \Delta h_v \quad (4.3.3 \text{ a})$$

$$Q_{vap} = 4.184 \frac{kJ}{kgK} \cdot 1658.3 \frac{kg}{h} \cdot 90K + 1658.3 \frac{kg}{h} \cdot 2257 \frac{kJ}{kg} \quad (4.3.1 \text{ b})$$

$$Q_{vap} = 4367.2 \frac{MJ}{h} = 1213.1 \text{ kW} \quad (4.3.1 \text{ c})$$

4.3.4 Condensation of pyrolysis vapours

Chapter 4.3.4 deals with the estimation of the heat fluxes that are needed for the cooling and condensation of the pyrolysis vapours. It is assumed that the condenser operates without losses. Furthermore, it is assumed that the specific heat capacities and the enthalpies of evaporation of the components are constant over the entire temperature range. In the case of condensable vapours, cooling of the vapour phase, condensation, and cooling of the liquid phase take place. The condensable vapours are assumed to behave like a pure substance. They are therefore assigned a common boiling point as well as a common specific heat capacity.

Heat flow calculations are performed analogously to equation 4.3.1 b. The condensation temperature of the vapor phase is assumed to be 92.2 °C, as this is the bubble point of LCBM pyrolytic vapours. As stated above, the specific heat capacity of the vapour as well as the resulting liquid phase is equal. They are estimated at 2.48 kJ/kgK. The enthalpy of condensation is assumed to be -1312.9 kJ/kg [148].

Pyrolysis vapours are first cooled from 500 °C to 92.2 °C ($\Delta T_1 = -407.8$ K). Condensation takes place at 92.2 °C. The resulting biooil is then cooled down to 20 °C ($\Delta T_2 = -72.2$ K). Equation 4.3.4 a summarizes this cooling and condensation process.

$$Q_{Cond} = c_{p,vap} \cdot \dot{m}_{vap} \cdot \Delta T_1 + \dot{m}_{vap} \cdot \Delta h_{cond} + c_{p,biooil} \cdot \dot{m}_{biooil} \cdot \Delta T_2 \quad (4.3.4 a)$$

Since the mass flow of the vapor phase is equal to the mass flow of the biooil phase ($\dot{m}_{vap} = \dot{m}_{biooil} = 364.82$ kg/h) and the specific heat capacity of both phases is assumed to be the same, the expression simplifies to equation 4.3.4 b. Equations 4.3.4 c and d show the calculation of the amount of heat released during condensation. During the condensation of the pyrolysis vapours, 253.68 kW of heat energy are transferred to the cooling water.

$$Q_{Cond} = c_{p,biooil} \cdot \dot{m}_{biooil} \cdot (\Delta T_1 + \Delta T_2) + \dot{m}_{biooil} \cdot \Delta h_{cond,biooil} \quad (4.3.4 b)$$

$$Q_{Cond} = 2.48 \frac{kJ}{kgK} \cdot 364.82 \frac{kg}{h} \cdot (-480K) + 364.82 \frac{kg}{h} \cdot (-1312.9 \frac{kJ}{kg}) \quad (4.3.4 b)$$

$$Q_{Drying} = -913.25 \frac{MJ}{h} = -253.68 kW \quad (4.3.4 c)$$

4.3.5 Energy supply by process byproducts

Estimating the amount of heat released during combustion of the resulting biochar and gas phase is described in Chapter 4.3.5.

For the combustion of the two products, it is assumed that the boiler efficiency is 85 % [145,146]. The amount of heat released is calculated by multiplying the respective specific heating values and the mass flows. For biochar a lower heating value of 25.51 MJ/kg is assumed [151]. The assumed gas component concentrations [152] and the associated heating values [153] are listed in Table 13.

Table 13: Off gas composition and heating values

	mass fraction	lower heating value [MJ/kg]
CH ₄	0.179	50
C ₂ H ₄	0.021	47.8
C ₂ H ₆	0.021	47.2
CO ₂	0.368	0
CO	0.411	10.16

The weighted average of the heating values for the gas phase is 15.12 MJ/kg. Equation 4.3.5 a shows the calculation of the heat quantity of the combustion of the biochar. The heat quantity of the gas combustion is estimated with equation 4.3.5 b.

$$Q_{Comb,biochar} = -\dot{m}_{biochar} \cdot HV_{biochar} = -323.36 \frac{kg}{h} \cdot 25.51 \frac{MJ}{kg} = -2291.36 kW \quad (4.3.5 a)$$

$$Q_{Comb,gas} = -\dot{m}_{gas} \cdot HV_{gas,avg} = -140.95 \frac{kg}{h} \cdot 15.12 \frac{MJ}{kg} = -595.12 kW \quad (4.3.5 b)$$

The determined heat quantities including the boiler efficiency of 85 % are -1947.66 kW for biochar and -505.85 kW for gas.

4.3.6 Energy balance

The heat quantities calculated in chapter 4.3 are presented and compared collectively in chapter 4.3.6.

Table 14 shows the heat flows associated with the respective sub-processes. A distinction is made between endothermic and exothermic processes, and the sum of the process energies is shown.

Table 14: Heat fluxes of modelled unit operations

	process	heat flux [kW]
endothermic processes	drying of lignin	237.3
	wash water evaporation	1041.6
	pyrolysis	198.07
	sum of endothermic processes	1477.0
exothermic processes	condensation of pyrolysis vapours	-253.7
	burning of char	-1947.7
	burning of gas	-505.9
	sum of exothermic processes	-2707.3
	total	-1230.33

The balance over all calculated thermal energy flows shows that -1230.33 kW of thermal energy is released if all streams are optimally used and under highly simplified model conditions. It should be noted that the effects on the recovery boiler of the power plant have not yet been taken into account. The withdrawal of lignin from the black liquor reduces the dry matter content. As a result, less fuel is available for the boiler, which leads to reduced heat production. In chapter 4.4, the costs of the process are estimated considering the reduced recovery boiler heat production.

4.4 Cost estimation

Chapter 4.4 provides a rough cost estimate for the modelled process.

The cost estimate is based on operating costs only. It does not include material costs, installation costs or other investment costs. Personnel costs, electricity costs, maintenance costs or other such expenditures also excluded in this estimation. The focus is on thermal energy and chemical costs. Currently, due to the aftermath of the Corona pandemic and the Ukraine crisis, the prices of electricity, gas and oil are subject to unpredictable fluctuations [154]. The additional thermal energy required for the production of one ton of biooil is quantified. This thermal energy related process cost estimation can be used to adapt to future changes in energy prices.

4.4.1 Cost of process chemicals

The running costs of the chemicals, calculated in chapter 4.4.1 are expected to be relatively low in comparison to the energy related costs. The required CO₂ is withdrawn from the off gas of the pyrolysis and the washing water is also available without charge. A price of 180 €/t is assumed H₂SO₄ [155]. Per ton of biooil produced, the demand of H₂SO₄ therefore is 397.5 kg. This results in costs of 72 € for H₂SO₄.

4.4.2 Thermal energy related costs

The implementation of the presented process leads to a reduction of the usable heat in the recovery boiler of the kraft process. In chapter 4.4.2, This reduction of heat output is quantified by calculating the combustion of the withdrawn LignoBoost lignin, since this amount corresponds to the reduction of the dry matter that would otherwise be fed to the boiler. For the production of one ton of biooil, 2,273 kg of lignin are processed. According to Demuner et al., the calorific value of KL is 27 MJ/kg [82]. This results in a heat of combustion of -61371 MJ. Expressed differently, this results in -17.05 MWh of thermal energy.

The total energy of -1230.33 kW calculated in table 13 represents the power output of the modelled process. Equations 4.4 a-c show the calculation of the resulting amount of energy in respect to one ton of biooil produced.

$$\frac{Q}{kg \text{ biooil}} = -1230.33 \text{ kW} \cdot \frac{3600s}{364.82 \text{ kg biooil}} = -12140.75 \frac{kJ}{kg \text{ biooil}} \quad (4.4 \text{ a})$$

$$-12140.75 \frac{kJ}{kg \text{ biooil}} = -12140.75 \frac{MJ}{ton \text{ biooil}} \quad (4.4 \text{ b})$$

$$\frac{-12140.75 \frac{MJ}{ton \text{ biooil}}}{3600 \frac{s}{h}} = -3.37 \frac{MWh}{ton \text{ biooil}} \quad (4.4 \text{ c})$$

The difference between the two processes is therefore 13.68 MWh/t biooil produced. To compare this value, the cost of 13.68 MWh of energy can be calculated using the current price of natural gas (34.95 €/MWh) [156]. 13.68 MWh of thermal energy, which is obtained from the combustion of natural gas, currently (27.06.2023) cost 478.12 €.

4.4.3 Process costs – summary

In chapter 4.4.3 the costs of process chemicals as well as the thermal energy costs are summarized. Table 15 shows the costs related to the production of one ton of biooil.

Table 15: Cost estimation of biooil

cost factor	demand ^a	price	Cost ^a
H ₂ SO ₄	397.5 kg	180 €/t	72 €
thermal energy	13.68 MWh	34.95 €/MWh ^b	478 €
sum			550 €

a... based on the production of one ton biooil b... natural gas price [156]

As can be seen in Table 15, the estimated cost of the biooil is 550 €/t. The costs given relate to biooil with a water content of 34 %. For water-free biooil, the cost can be estimated, using the product distribution of biooil presented in Figure 84 to 834.35 €/t. It should be noted that the modelled process is related to an existing kraft plant. Therefore, the price of biooil is highly dependent on energy prices.

As a comparison, it can be stated that Inayat et al. quote costs of various biomass originated pyrolysis oils in the range between 0.55 and 3.2 €/L, with most pyrolysis oils in the range between 1-1.5 €/L [157]. Since the present cost estimate only refers to the thermal energy and the chemicals used, actual costs are higher.

5 Conclusion

In this work, the process of lignin pyrolysis is investigated. First, a literature study is carried out to highlight the current state of the art and, furthermore, a process model is created to evaluate a pyrolysis process implemented in a kraft process.

In this master thesis, basic information on lignin pyrolysis is collected. It shows parallels to the pyrolysis of conventional biomass pyrolysis. In lignin pyrolysis, liquefaction rates of less than 50 % are achieved [81]. It is shown that temperature, residence time and heating rate are important influencing factors for efficient liquefaction. In principle, the shortest possible residence time and the fastest heating rate are necessary for optimal liquefaction. Optimal temperature for liquefaction is between 500-650 °C [136]. High biooil production rate does not mean that the biooil is suitable as a source of monomeric phenols. In fact, there is a trend for high liquefaction rates to be accompanied by high proportions of oligomers [106]. In most cases, the yield of monomeric phenols is roughly 5-10 %, and that of oligomers between 15 and 25 %, based on the feed quantity of the lignin used [88].

The state of the technology of lignin pyrolysis is not yet comparable with the pyrolysis of LCBM. For pyrolysis of LCBM, feed quantities of more than 4000 kg/h are achieved [67]; in terms of lignin pyrolysis, the largest installations operate at approximately 0.6 kg/h [87]. Furthermore, there are lignin handling complications. The melting of lignin leads to blockages in the feed system so that no further material can be introduced. Additionally, molten lignin leads to agglomerates with the heat transfer material of the reactors. These agglomerations lead to the fact that the reactor bed is no longer fluidised effectively, therefore the heat transfer and the pyrolysis efficiency decrease [112].

The optimisation potential of lignin pyrolysis has been analysed. Based on analysed influencing factors, optimisation possibilities become apparent. The choice of biomass and the pulping process have an impact on the chemical properties and molecular size distributions of the technical lignins, which in turn have an impact on biooil yield and composition. Hardwood contains 10-25 % lignin, which is characterised by a high proportion of G-type monophenols. In addition, hardwood has more B-O-4 bonds on average. Softwood contains 25-35 % lignin and consists of varying amounts of G-, S- and H-type monophenol.

In order to optimise lignin pyrolysis, in addition to the selection of the biomass and the pulping process, chemical, physical or biological pre-treatment of lignins can also be carried out. Viable methods are mainly those, that reduce the molecular masses, as smaller lignin molecules can be liquefied more efficiently [124]. Furthermore, the use of different catalysts as well as co-pyrolysis with hydrogen-rich substrates such as LDPE are potential optimisation options [74].

In addition to the literature research, the implementation of a lignin precipitation from the black liquor of a kraft process is modelled. With a feed quantity of 100,000 t/y black liquor, a biooil quantity of 365 kg/h can be produced which translates to 2.92 kt/y. The extraction of the lignin reduces the dry matter in the black liquor, which results in a reduced heat recovery from the recovery boiler of the kraft plant. This reduction in the amount of heat recovered, in addition to the costs of the process chemicals required for the precipitation of the lignin, leads to estimated biooil costs of 550 €/t.

6 Appendix

6.1 Literature

1. Dahl CF (1884) Process of manufacturing cellulose from wood. US Pat. Off. <https://patents.google.com/patent/US296935A>
2. Beckham G (2018) Lignin Valorization: Emerging Approaches. In: Beckham GT (ed) Energy and Environment Series. Royal Society of Chemistry, p 528
3. Öhman F, Wallmo H, Theliander H (2007) A novel method for washing lignin precipitated from kraft black liquor – Laboratory trials. Nord Pulp Pap Res J 22:9–16
4. Öhman F, Theliander H, Norgren M, et al (2005) Method for separating lignin from a lignin containing liquid/slurry. Eur. Pat. Off.
5. Serena G, Josipa B (2021) Durability of wood – integration of experimental and numerical approach Behind the Research. Eng Technol Res
6. Leisola M, Pastinen O, Axe DD (2012) Lignin -Designed Randomness. BIOcomplexity 2012:1–11. <https://doi.org/10.5048/bio-c.2012.3>
7. Francisco-Fernández M, Tarrío-Saavedra J, Naya S, et al (2017) Statistical classification of early and late wood through the growth rings using thermogravimetric analysis. J Therm Anal Calorim 127:499–506. <https://doi.org/10.1007/s10973-016-5917-5>
8. Bailey IW, Kerr T (1935) The visible structure of the secondary cell wall and its significance in physical and chemical investigations of tracheary cells and fibers. Arnold Arboretum, Harvard Univ 16:273–300
9. Rytioja J, Hildén K, Yuzon J, et al (2014) Plant-Polysaccharide-Degrading Enzymes from Basidiomycetes. Microbiol Mol Biol Rev 78:614–649. <https://doi.org/10.1128/mmbr.00035-14>
10. Donaldson L (1985) Within- and between-tree variation in lignin concentration in the tracheid cell wall of *Pinus radiata*. New Zeal J For Sci 15:361–369
11. Zhong R, Ye ZH (2015) Secondary cell walls: Biosynthesis, patterned deposition and transcriptional regulation. Plant Cell Physiol 56:195–214. <https://doi.org/10.1093/pcp/pcu140>
12. Rowell R, Pettersen R, Tshabalala M (2012) Cell Wall Chemistry. In: Handbook of

Wood Chemistry and Wood Composites, Second Edition. pp 33–72

13. Amboss (2023) glykosidic bond.
<https://www.amboss.com/de/wissen/Kohlenhydrate#Zb7211e78113c24b48e9760b262a18304>. Accessed 22 Aug 2023
14. Moon RJ, Martini A, Nairn J, et al (2011) Cellulose nanomaterials review: Structure, properties and nanocomposites. *Chem Soc Rev* 40:3941–3994.
<https://doi.org/10.1039/c0cs00108b>
15. Naz S, Ahmad N, Akhtar J, et al (2016) Management of citrus waste by switching in the production of nanocellulose. *IET Nanobiotechnology* 10:395–399.
<https://doi.org/10.1049/iet-nbt.2015.0116>
16. Ioelovich M (2021) Preparation, characterization and application of amorphized cellulose—a review. *Polymers (Basel)* 13:. <https://doi.org/10.3390/polym13244313>
17. Fernandes AN, Thomas LH, Altaner CM, et al (2011) Nanostructure of cellulose microfibrils in spruce wood. *Proc Natl Acad Sci U S A* 108:.
<https://doi.org/10.1073/pnas.1108942108>
18. Festucci-Buselli RA, Otoni WC, Joshi CP (2007) Structure, organization, and functions of cellulose synthase complexes in higher plants. *Brazilian J Plant Physiol* 19:1–13.
<https://doi.org/10.1590/s1677-04202007000100001>
19. Tredenick EC, Farquhar GD (2021) Dynamics of Moisture Transport in Plant Cuticles: The Role of Cellulose. Preprint(PP)
20. Hu L, Du M, Zhang J (2018) Hemicellulose-Based Hydrogels Present Status and Application Prospects: A Brief Review. *Open J For* 08:15–28.
<https://doi.org/10.4236/ojf.2018.81002>
21. Pettersen RC (1984) The chemical composition of wood. In: Rowell R (ed) *The Chemistry of Solid Wood, Advances in Chemistry*. American Chemical Society
22. Candolle MAP de (1815) *Theorie elementaire de la botanique, ou exposition des principes de la classification naturelle et de l'art de decrir et d'etudier les vegetaux*. Paris, Deterville
23. Witzler M, Alzagameem A, Bergs M, et al (2018) Lignin-derived biomaterials for drug release and tissue engineering. *Molecules* 23:1–23.
<https://doi.org/10.3390/molecules23081885>
24. Zinov'ev D V., Sole P (2004) Lignins: Natural polymers from oxidative coupling of 4-

hydroxyphenylpropanoids

25. Obst JR, Kirk TK (1988) Isolation of lignin. *Methods Enzymol* 161:3–12.
[https://doi.org/10.1016/0076-6879\(88\)61003-2](https://doi.org/10.1016/0076-6879(88)61003-2)
26. Balakshin M, Capanema EA, Zhu X, et al (2020) Spruce milled wood lignin: linear, branched or cross-linked? *R Soc Chem* 22:3985–4001.
<https://doi.org/10.1039/d0gc00926a>
27. Liu Q, Luo L, Zheng L (2018) Lignins: Biosynthesis and biological functions in plants. *Int J Mol Sci* 19:. <https://doi.org/10.3390/ijms19020335>
28. BioBase BioBase GmbH. <https://biobase.at/ueber-bio-base/>. Accessed 10 Sep 2022
29. Bajwa DS, Pourhashem G, Ullah AH, Bajwa SG (2019) A concise review of current lignin production, applications, products and their environment impact. *Ind Crops Prod* 139:111526. <https://doi.org/10.1016/j.indcrop.2019.111526>
30. Bridgwater A V., Meier D, Radlein D (1999) An overview of fast pyrolysis of biomass. *Org Geochem* 30:1479–1493. [https://doi.org/10.1016/S0146-6380\(99\)00120-5](https://doi.org/10.1016/S0146-6380(99)00120-5)
31. Mboowa D (2021) A review of the traditional pulping methods and the recent improvements in the pulping processes. *Biomass Convers Biorefinery*.
<https://doi.org/10.1007/s13399-020-01243-6>
32. Ma J, Li Q, Wu Y, et al (2021) Elucidation of ligninolysis mechanism of a newly isolated white-rot basidiomycete *Trametes hirsuta* X-13. *Biotechnol Biofuels* 14:.
<https://doi.org/10.1186/s13068-021-02040-7>
33. Rico A, Rencoret J, Del Río JC, et al (2014) Pretreatment with laccase and a phenolic mediator degrades lignin and enhances saccharification of Eucalyptus feedstock. *Biotechnol Biofuels* 7:1–14. <https://doi.org/10.1186/1754-6834-7-6>
34. Cabrera MN (2017) Pulp Mill Wastewater: Characteristics and Treatment. *Biol Wastewater Treat Resour Recover*. <https://doi.org/10.5772/67537>
35. Watt C, Burgess H (1854) Improvement in the manufacture of paper from wood. US Pat. Off.
36. Rahman M, Avelin A (2020) A review on the modeling, control and diagnostics of continuous pulp digesters. *Processes*. <https://doi.org/10.3390/pr8101231>
37. Dernegård H, Brelid H, Theliander H (2017) Characterization of a dusting lime kiln - A mill study. *Nord Pulp Pap Res J* 32:25–34. <https://doi.org/10.3183/npprj-2017-32-01-p025-034>

38. Aro T, Fatehi P (2017) Production and Application of Lignosulfonates and Sulfonated Lignin. *ChemSusChem* 10:1861–1877. <https://doi.org/10.1002/cssc.201700082>
39. Chakar FS, Ragauskas AJ (2004) Review of current and future softwood kraft lignin process chemistry. *Ind Crops Prod* 20:131–141. <https://doi.org/10.1016/j.indcrop.2004.04.016>
40. Gellerstedt G (2015) Softwood kraft lignin: Raw material for the future. *Ind Crops Prod* 77:845–854. <https://doi.org/10.1016/j.indcrop.2015.09.040>
41. Crestini C, Lange H, Sette M, Argyropoulos DS (2017) On the structure of softwood kraft lignin. *Green Chem* 19:4104–4121. <https://doi.org/10.1039/c7gc01812f>
42. Svensson S (2008) Minimizing the sulphur content in Kraft lignin. Mälardalen University College
43. Zakzeski J, Bruijninx PCA, Jongerius AL, Weckhuysen BM (2010) The catalytic valorization of lignin for the production of renewable chemicals. *Chem Rev* 110:3552–3599. <https://doi.org/10.1021/cr900354u>
44. Hubbe MA, Alén R, Paleologou M, et al (2019) Lignin recovery from spent alkaline pulping liquors using acidification, membrane separation, and related processing steps: A review. *BioResources* 14:2300–2351. <https://doi.org/10.15376/biores.14.1.2300-2351>
45. Kienberger M, Maitz S, Pichler T, Demmelmayer P (2021) Systematic review on isolation processes for technical lignin. *Processes* 9:. <https://doi.org/10.3390/pr9050804>
46. Zhu W (2015) Precipitation of Kraft Lignin Yield and Equilibrium, PhD Thesis
47. Fredrik Ö, Theliander H (2007) Filtration properties of lignin precipitated from black liquor. *Tappi J* 6:3–9
48. ÖHMAN F, THELIANDER H, NORGREN M, et al (2006) Method for seperating lignin from a lignin containing liquid/slurry WO2006038863
49. Välimäki E, Niemi P, Haaga K (2010) A case study on the effects of lignin recovery on recovery boiler operation. *Asian Pap 2010 - New Appl Technol Conf Proc*. <https://doi.org/10.13140/2.1.1777.5046>
50. ÖHMAN F, THELIANDER H, TOMANI P, AXEGARD P Method for seperating lignin from black liquor WO2006031175
51. Valmet (2022) Valmet- Lignin extraction with LignoBoost.

- <https://www.valmet.com/pulp/other-value-adding-processes/lignin-extraction/>. Accessed 7 Dec 2022
52. Tomani P (2010) The lignoboost process. *Cellul Chem Technol* 44:53–58
 53. Timmerfors JG (2020) Wood Chips for Kraft and Sulfite Pulping Evaluation of Novel Forest-Industrial Drum Chipping Technology. Umeå University
 54. Gopalakrishnan K, Kim S, Ceylan H (2010) Chapter 12: Lignin recovery and utilization. In: *Bioenergy and Biofuel from Biowastes and Biomass*. pp 247–274
 55. Ruwoldt J (2020) A Critical Review of the Physicochemical Properties of Lignosulfonates: Chemical Structure and Behavior in Aqueous Solution, at Surfaces and Interfaces. *Surfaces* 3:622–648. <https://doi.org/10.3390/surfaces3040042>
 56. Vaidya AA, Murton KD, Smith DA, Dedual G (2022) A review on organosolv pretreatment of softwood with a focus on enzymatic hydrolysis of cellulose. *Biomass Convers Biorefinery*. <https://doi.org/10.1007/s13399-022-02373-9>
 57. Kleinert T, Tayenthal K (1932) Process of decomposing vegetable fibrous matter for the purpose of the simultaneous recovery both of the cellulose and of the incrusting ingredients. US Pat. Off.
 58. Grand View Research (2019) Lignin Market Size, Share & Trends Analysis Report By Product (Ligno-Sulphonates, Kraft, Organosolv), By Application (Macromolecule, Aromatic), By Region, And Segment Forecasts, 2020 - 2027. <https://www.grandviewresearch.com/industry-analysis/lignin-market>. Accessed 10 Nov 2022
 59. Lv X, Li Q, Jiang Z, et al (2018) Structure characterization and pyrolysis behavior of organosolv lignin isolated from corncob residue. *J Anal Appl Pyrolysis* 136:115–124. <https://doi.org/10.1016/j.jaap.2018.10.016>
 60. Mäki E, Saastamoinen H, Melin K, et al (2021) Drivers and barriers in retrofitting pulp and paper industry with bioenergy for more efficient production of liquid, solid and gaseous biofuels: A review. *Biomass and Bioenergy* 148:. <https://doi.org/10.1016/j.biombioe.2021.106036>
 61. Fredheim GE, Braaten SM, Christensen BE (2002) Molecular weight determination of lignosulfonates by size-exclusion chromatography and multi-angle laser light scattering. *J Chromatogr* 942:191–199
 62. Ludmila H, Michal J, Andrea Š, Aleš H (2015) Lignin, potential products and their market value. *Wood Res* 60:973–986

63. Raza M, Inayat A, Ahmed A, et al (2021) Progress of the pyrolyzer reactors and advanced technologies for biomass pyrolysis processing. *Sustain* 13:1–42. <https://doi.org/10.3390/su131911061>
64. Encinar JM, González JF (2008) Pyrolysis of synthetic polymers and plastic wastes. Kinetic study. *Fuel Process Technol* 89:678–686. <https://doi.org/10.1016/j.fuproc.2007.12.011>
65. Huber GW, Iborra S, Corma A (2006) Synthesis of transportation fuels from biomass: Chemistry, catalysts, and engineering. *Chem Rev* 106:4044–4098. <https://doi.org/10.1021/cr068360d>
66. Chen Y, Zhang X, Chen W, et al (2017) The structure evolution of biochar from biomass pyrolysis and its correlation with gas pollutant adsorption performance. *Bioresour Technol* 246:101–109. <https://doi.org/10.1016/j.biortech.2017.08.138>
67. Hu X, Gholizadeh M (2019) Biomass pyrolysis: A review of the process development and challenges from initial researches up to the commercialisation stage. *J Energy Chem* 39:109–143. <https://doi.org/10.1016/j.jechem.2019.01.024>
68. Dimitriadis A, Chrysikou LP, Meletidis G, et al (2021) Bio-based refinery intermediate production via hydrodeoxygenation of fast pyrolysis bio-oil. *Renew Energy* 168:593–605. <https://doi.org/10.1016/j.renene.2020.12.047>
69. Oh SJ, Choi GG, Kim JS (2017) Production of acetic acid-rich bio-oils from the fast pyrolysis of biomass and synthesis of calcium magnesium acetate deicer. *J Anal Appl Pyrolysis* 124:122–129. <https://doi.org/10.1016/j.jaap.2017.01.032>
70. García-Pérez M, Chaala A, Pakdel H, et al (2006) Multiphase structure of bio-oils. *Energy and Fuels* 20:364–375. <https://doi.org/10.1021/ef050248f>
71. Tessarolo NS, dos Santos LRM, Silva RSF, Azevedo DA (2013) Chemical characterization of bio-oils using comprehensive two-dimensional gas chromatography with time-of-flight mass spectrometry. *J Chromatogr A* 1279:68–75. <https://doi.org/10.1016/j.chroma.2012.12.052>
72. Rasul MG, Jahirul MI, Science W (2012) Recent Developments in Biomass Pyrolysis for Bio-Fuel Production : Its Potential for Commercial Applications Pyrolysis Process Description Pyrolysis classification. *Recent Res Environ Geol Sci Recent* 256–265
73. Meier D, Faix O (1999) State of the art of applied fast pyrolysis of lignocellulosic materials - A review. *Bioresour Technol* 68:71–77. [https://doi.org/10.1016/S0960-8524\(98\)00086-8](https://doi.org/10.1016/S0960-8524(98)00086-8)

74. Yu D, Hui H, Ding G, et al (2021) Enhancement of aromatics production from catalytic co-pyrolysis of walnut shell and LDPE via a two-step approach. *J Anal Appl Pyrolysis* 157:. <https://doi.org/10.1016/j.jaap.2021.105216>
75. Li Z, Li N, Yi W, et al (2017) Design and operation of a down-tube reactor demonstration plant for biomass fast pyrolysis. *Fuel Process Technol* 161:182–192. <https://doi.org/10.1016/j.fuproc.2016.12.014>
76. Hervy M, Weiss-Hortala E, Pham Minh D, et al (2019) Reactivity and deactivation mechanisms of pyrolysis chars from bio-waste during catalytic cracking of tar. *Appl Energy* 237:487–499. <https://doi.org/10.1016/j.apenergy.2019.01.021>
77. Garcia-Nunez JA, Pelaez-Samaniego MR, Garcia-Perez ME, et al (2017) Historical Developments of Pyrolysis Reactors: A Review. *Energy and Fuels* 31:5751–5775. <https://doi.org/10.1021/acs.energyfuels.7b00641>
78. Bioenergy Concept (2020) Ablative Fast Pyrolysis Plant. [https://bioenergy-concept.com/ablative-fast-pyrolysis/#:~:text=In ablative pyrolysis%2C heat is,volatile components \(bio-oil\)](https://bioenergy-concept.com/ablative-fast-pyrolysis/#:~:text=In%20ablative%20pyrolysis%20heat%20is%20volatile%20components%20(bio-oil).). Accessed 17 May 2023
79. Campuzano F, Brown RC, Martínez JD (2019) Auger reactors for pyrolysis of biomass and wastes. *Renew Sustain Energy Rev* 102:372–409. <https://doi.org/10.1016/j.rser.2018.12.014>
80. Yang J, Blanchette D (2008) Modelling, Scale-up and Demonstration of a Vacuum Pyrolysis Reactor. In: *Progress in Thermochemical Biomass Conversion*. Quebec, pp 1296–1311
81. Singh-Morgan A, Puente-Urbina A, Van Bokhoven J (2022) Technology Overview of Fast Pyrolysis of Lignin: Current State and Potential for Scale-Up. *ChemSusChem* 15:. <https://doi.org/10.1002/cssc.202200343>
82. Demuner IF, Gomes FJB, Coura MR, et al (2021) Determination of chemical modification of eucalypt kraft lignin after thermal treatment by Py-GC–MS. *J Anal Appl Pyrolysis* 156:. <https://doi.org/10.1016/j.jaap.2021.105158>
83. Margellou AG, Lazaridis PA, Charisteidis ID, et al (2021) Catalytic fast pyrolysis of beech wood lignin isolated by different biomass (pre)treatment processes: Organosolv, hydrothermal and enzymatic hydrolysis. *Appl Catal A Gen* 623:. <https://doi.org/10.1016/j.apcata.2021.118298>
84. Cui Y, Wang W, Chang J (2019) Study on the product characteristics of pyrolysis lignin with calcium salt additives. *Materials (Basel)* 12:. <https://doi.org/10.3390/ma12101609>

85. Choi HS, Meier D (2013) Fast pyrolysis of Kraft lignin - Vapor cracking over various fixed-bed catalysts. *J Anal Appl Pyrolysis* 100:207–212.
<https://doi.org/10.1016/j.jaap.2012.12.025>
86. Ghysels S, Dubuisson B, Pala M, et al (2020) Improving fast pyrolysis of lignin using three additives with different modes of action. *Green Chem* 22:6471–6488.
<https://doi.org/10.1039/d0gc02417a>
87. De Wild PJ, Huijgen WJJ, Gosselink RJA (2014) Lignin pyrolysis for profitable lignocellulosic biorefineries. *Biofuels, Bioprod Biorefining* 8:645–657.
<https://doi.org/10.1002/bbb.1474>
88. De Wild PJ, Huijgen WJJ, Heeres HJ (2012) Pyrolysis of wheat straw-derived organosolv lignin. *J Anal Appl Pyrolysis* 93:95–103.
<https://doi.org/10.1016/j.jaap.2011.10.002>
89. Bayerbach R, Meier D (2009) Characterization of the water-insoluble fraction from fast pyrolysis liquids (pyrolytic lignin). Part IV: Structure elucidation of oligomeric molecules. *J Anal Appl Pyrolysis* 85:98–107. <https://doi.org/10.1016/j.jaap.2008.10.021>
90. Bayerbach R, Nguyen VD, Schurr U, Meier D (2006) Characterization of the water-insoluble fraction from fast pyrolysis liquids (pyrolytic lignin). Part III. Molar mass characteristics by SEC, MALDI-TOF-MS, LDI-TOF-MS, and Py-FIMS. *J Anal Appl Pyrolysis* 77:95–101. <https://doi.org/10.1016/j.jaap.2006.02.002>
91. Kloekhorst A, Wildschut J, Heeres HJ (2014) Catalytic hydrotreatment of pyrolytic lignins to give alkylphenolics and aromatics using a supported Ru catalyst. *Catal Sci Technol* 4:2367–2377. <https://doi.org/10.1039/c4cy00242c>
92. Zheng S, Liu H, He Y, et al (2023) Combustion of biomass pyrolysis gas: Roles of radiation reabsorption and water content. *Renew Energy* 205:864–872.
<https://doi.org/10.1016/j.renene.2023.02.013>
93. Sharma RK, Wooten JB, Baliga VL, et al (2004) Characterization of chars from pyrolysis of lignin. *Fuel* 83:1469–1482. <https://doi.org/10.1016/j.fuel.2003.11.015>
94. Mistar EM, Alfatah T, Supardan MD (2020) Synthesis and characterization of activated carbon from *Bambusa vulgaris striata* using two-step KOH activation. *J Mater Res Technol* 9:6278–6286. <https://doi.org/10.1016/j.jmrt.2020.03.041>
95. Chua YW, Yu Y, Wu H (2019) Structural changes of chars produced from fast pyrolysis of lignin at 100–300 °C. *Fuel* 255:115754. <https://doi.org/10.1016/j.fuel.2019.115754>
96. Zhang C, Shao Y, Zhang L, et al (2020) Impacts of temperature on evolution of char

- structure during pyrolysis of lignin. *Sci Total Environ* 699:134381.
<https://doi.org/10.1016/j.scitotenv.2019.134381>
97. Cheng F, Li X (2018) Preparation and application of biochar-based catalysts for biofuel production. *Catalysts* 8:1–35. <https://doi.org/10.3390/catal8090346>
98. Barrow CJ (2012) Biochar: Potential for countering land degradation and for improving agriculture. *Appl Geogr* 34:21–28. <https://doi.org/10.1016/j.apgeog.2011.09.008>
99. Schmidt H-P (2012) 55 Uses of Biochar. *Ithaka J* 25:13–25
100. Kawamoto H (2017) Lignin pyrolysis reactions. *J Wood Sci* 63:117–132.
<https://doi.org/10.1007/s10086-016-1606-z>
101. Zhao Y, Zhang H, Zong P, et al (2021) Evaluation of pyrolysis characteristics and product distribution of black liquor using Py-GC/MS and down tube reactor: Comparison with lignin. *Fuel* 292:120286. <https://doi.org/10.1016/j.fuel.2021.120286>
102. Liu WJ, Jiang H, Yu HQ (2015) Development of Biochar-Based Functional Materials: Toward a Sustainable Platform Carbon Material. *Chem Rev* 115:12251–12285.
<https://doi.org/10.1021/acs.chemrev.5b00195>
103. Bai X, Kim KH, Brown RC, et al (2014) Formation of phenolic oligomers during fast pyrolysis of lignin. *Fuel* 128:170–179. <https://doi.org/10.1016/j.fuel.2014.03.013>
104. Zhou S, Garcia-Perez M, Pecha B, et al (2013) Effect of the fast pyrolysis temperature on the primary and secondary products of lignin. *Energy and Fuels* 27:5867–5877.
<https://doi.org/10.1021/ef4001677>
105. Hoekstra E, van Swaaij WPM, Kersten SRA, Hogendoorn KJA (2012) Fast pyrolysis in a novel wire-mesh reactor: Design and initial results. *Chem Eng J* 191:45–58.
<https://doi.org/10.1016/j.cej.2012.01.117>
106. Yu J, Wang D, Sun L (2021) The pyrolysis of lignin: Pathway and interaction studies. *Fuel* 290:120078. <https://doi.org/10.1016/j.fuel.2020.120078>
107. Debiagi PEA, Gentile G, Pelucchi M, et al (2016) Detailed kinetic mechanism of gas-phase reactions of volatiles released from biomass pyrolysis. *Biomass and Bioenergy* 93:60–71. <https://doi.org/10.1016/j.biombioe.2016.06.015>
108. El-Shall MS (2008) Polymerization in the gas phase, in clusters, and on nanoparticle surfaces. *Acc Chem Res* 41:783–792. <https://doi.org/10.1021/ar7001396>
109. Carlroth (2023) Boiling Point of Guaiacol-Carlroth.
<https://www.carlroth.com/at/de/aromatische-bausteine/guajacol/p/7308.1>. Accessed 23

Jun 2023

110. Carlroth (2023) Boiling Point Phenol.
<https://www.carlroth.com/at/de/viskositaetsbestimmung/phenol/p/0040.2>. Accessed 23 Jun 2023
111. Chen Y, Li C, Zhang L (2023) Journal Pre-proof. Interaction of the lignin-/cellulose-derived char with volatiles of varied origin: Part of the process for evolution of products in pyrolysis. *Chemosphere*. <https://doi.org/10.1016/j.chemosphere.2023.139248>
112. Nowakowski DJ, Bridgwater A V., Elliott DC, et al (2010) Lignin fast pyrolysis: Results from an international collaboration. *J Anal Appl Pyrolysis* 88:53–72.
<https://doi.org/10.1016/j.jaap.2010.02.009>
113. Dictionary C (2023) Value chain - Cambridge Dictionary.
<https://dictionary.cambridge.org/dictionary/english/value-chain>. Accessed 10 Jun 2023
114. Suota MJ, da Silva TA, Zawadzki SF, et al (2021) Chemical and structural characterization of hardwood and softwood LignoForce™ lignins. *Ind Crops Prod* 173:1–14. <https://doi.org/10.1016/j.indcrop.2021.114138>
115. Wang W, Liu Y, Wang Y, et al (2022) Energy Conversion and Management : X The influence of solvent on the pyrolysis of organosolv lignins extracted from willow. *Energy Convers Manag X* 13:100139. <https://doi.org/10.1016/j.ecmx.2021.100139>
116. Karthäuser J, Biziks V, Frauendorf H, et al (2022) Vacuum Low-Temperature Microwave-Assisted Pyrolysis of Technical Lignins. *Polymers (Basel)* 14:3383. <https://doi.org/10.3390/polym14163383>
117. Huang X, Yin H, Zhang H, et al (2022) Pyrolysis characteristics, gas products, volatiles, and thermo–kinetics of industrial lignin via TG/DTG–FTIR/MS and in–situ Py–PI–TOF/MS. *Energy* 259:. <https://doi.org/10.1016/j.energy.2022.125062>
118. Daniel D, Khachatryan L, Astete C, et al (2019) Bioresource Technology Reports Sulfur contaminations inhibit depolymerization of Kraft lignin. *Bioresour Technol Reports* 8:100341. <https://doi.org/10.1016/j.biteb.2019.100341>
119. Shafaghat H, Sirous P, Ro D, et al (2017) Journal of Industrial and Engineering Chemistry In-situ catalytic pyrolysis of lignin in a bench-scale fixed bed pyrolyzer. *J Ind Eng Chem* 54:447–453. <https://doi.org/10.1016/j.jiec.2017.06.026>
120. Borella M, Casazza AA, Garbarino G, et al (2022) A Study of the Pyrolysis Products of Kraft Lignin. *Energies* 15:. <https://doi.org/10.3390/en15030991>

121. Li T, Yin Y, Wu S, et al (2020) Effect of pre-acetylation of hydroxyl functional groups by choline chloride/acetic anhydride on subsequent lignin pyrolysis. *Bioresour Technol* 317:. <https://doi.org/10.1016/j.biortech.2020.124034>
122. Fan Y, Lei M, Zhang Z, et al (2021) Unmasking radical-mediated lignin pyrolysis after benzyl hydroxyl shielding. *Bioresour Technol* 342:. <https://doi.org/10.1016/j.biortech.2021.125944>
123. Ahmad Z, Paleologou M, Xu CC (2021) Oxidative depolymerization of lignin using nitric acid under ambient conditions. *Ind Crops Prod* 170:. <https://doi.org/10.1016/j.indcrop.2021.113757>
124. Marathe PS, Westerhof RJM, Kersten SRA (2019) Fast pyrolysis of lignins with different molecular weight : Experiments and modelling. *Appl Energy* 236:1125–1137. <https://doi.org/10.1016/j.apenergy.2018.12.058>
125. Zhang L, Choi C, Machida H, Norinaga K (2021) Production of light hydrocarbons from organosolv lignin through catalytic hydrogenation and subsequent fast pyrolysis. *J Anal Appl Pyrolysis* 156:. <https://doi.org/10.1016/j.jaap.2021.105096>
126. Gordobil O, Herrera R, Poohphajai F, et al (2021) Impact of drying process on kraft lignin: Lignin-water interaction mechanism study by 2D NIR correlation spectroscopy. *J Mater Res Technol* 12:159–169. <https://doi.org/10.1016/j.jmrt.2021.02.080>
127. Majeke BM, Collard F-X, Tyhoda L, Görgens JF (2021) The synergistic application of quinone reductase and lignin peroxidase for the deconstruction of industrial (technical) lignins and analysis of the degraded lignin products. *Bioresour Technol* 319:. <https://doi.org/10.1016/j.biortech.2020.124152>
128. Majeke BM, Collard F çX, Tyhoda L, Görgens JF (2022) The Application of Enzymatic Pretreatment with Subsequent Pyrolysis to Improve the Production of Phenols from Selected Industrial (Technical) Lignins. *Waste and Biomass Valorization*. <https://doi.org/10.1007/s12649-021-01656-y>
129. Cao X, Shao L, Huang W, et al (2021) Thermal degradation of lignins fractionated by gradient acid precipitation. *J Anal Appl Pyrolysis* 157:. <https://doi.org/10.1016/j.jaap.2021.105200>
130. Pienihäkkinen E, Lindfors C, Ohra-Aho T, et al (2021) Fast Pyrolysis of Hydrolysis Lignin in Fluidized Bed Reactors. *Energy and Fuels* 35:14758–14769. <https://doi.org/10.1021/acs.energyfuels.1c01719>
131. Xie T, Zhao L, Yao Z, et al (2023) Co-pyrolysis of biomass and polyethylene: Insights

- into characteristics, kinetic and evolution paths of the reaction process. *Sci Total Environ* 897:165443. <https://doi.org/10.1016/j.scitotenv.2023.165443>
132. Kumar A, Biswas B, Saini K, et al (2021) Py-GC/MS study of prot lignin with cobalt impregnated titania, ceria and zirconia catalysts. *Renew Energy* 172:121–129. <https://doi.org/10.1016/j.renene.2021.03.011>
133. Vichaphund S, Wimuktiwan P, Soongprasit C, et al (2021) Aromatic and aliphatic production of catalytic pyrolysis of lignin using ZSM-5/Al-SBA-15 catalyst derived from high-calcium fly ash. *Energy Reports* 7:232–247. <https://doi.org/10.1016/j.egyr.2021.07.127>
134. Wang S, Li Z, Yi W, et al (2021) Renewable aromatic hydrocarbons production from catalytic pyrolysis of lignin with Al-SBA-15 and HZSM-5: Synergistic effect and coke behaviour. *Renew Energy* 163:1673–1681. <https://doi.org/10.1016/j.renene.2020.10.108>
135. Fang Y, Yin L, Yang H, et al (2021) Catalytic mechanisms of potassium salts on pyrolysis of β -O-4 type lignin model polymer based on DFT study. In: *Proceedings of the Combustion Institute*. Elsevier Ltd, pp 3969–3976
136. Fan L, Zhang Y, Liu S, et al (2017) Bio-oil from fast pyrolysis of lignin: Effects of process and upgrading parameters. *Bioresour Technol* 241:1118–1126. <https://doi.org/10.1016/j.biortech.2017.05.129>
137. Jiang G, Nowakowski DJ, Bridgwater A V. (2010) Effect of the temperature on the composition of lignin pyrolysis products. *Energy and Fuels* 24:4470–4475. <https://doi.org/10.1021/ef100363c>
138. Trinh TN, Jensen PA, Sárossy Z, et al (2013) Fast pyrolysis of lignin using a pyrolysis centrifuge reactor. *Energy and Fuels* 27:3802–3810. <https://doi.org/10.1021/ef400527k>
139. Olsson MR (2009) Simulations of Evaporation Plants in Kraft Pulp Mills Including Lignin Extraction and Use of Excess Heat
140. Zhu W, Theliander H (2011) Equilibrium of lignin precipitation. 16th Int Symp Wood, Fiber Pulping Chem - Proceedings, ISWFPC 1:195–199
141. Hu Z, Du X, Liu J, et al (2016) Structural Characterization of Pine Kraft Lignin: BioChoice Lignin vs Indulin AT. *J Wood Chem Technol* 36:432–446. <https://doi.org/10.1080/02773813.2016.1214732>
142. Per Tomani (2010) Lignin extraction from black liquor from 43rd Pulp and Paper International Congress & Exhibition (Innventia)

143. Uni München Thermodynamic equations, collection of Uni München.
https://www.cup.uni-muenchen.de/pc/lamb/lehre/PCI_Lehramt/Homework/Formelsammlung.pdf. Accessed 27 Jun 2023
144. The Engineering Toolbox (2023) thermodynamic constants of water.
https://www.engineeringtoolbox.com/specific-heat-capacity-water-d_660.html. Accessed 27 Jun 2023
145. Samarasekara L, Coorey R (2011) Thermal capacity as a function of moisture content of Sri Lankan wood species : Wheatstone bridge method Thermal capacity as a function of moisture content of Sri Lankan wood species : Wheatstone bridge method
146. Daugaard DE, Brown RC (2003) Enthalpy for pyrolysis for several types of biomass. *Energy and Fuels* 17:934–939. <https://doi.org/10.1021/ef020260x>
147. Reyes L, Abdelouahed L, Mohabeer C, et al (2021) Energetic and exergetic study of the pyrolysis of lignocellulosic biomasses, cellulose, hemicellulose and lignin. *Energy Convers Manag* 244:114459. <https://doi.org/10.1016/j.enconman.2021.114459>
148. Atsonios K, Panopoulos KD, Bridgwater A V., Kakaras E (2015) Biomass fast pyrolysis energy balance of a 1kg/h test rig. *Int J Thermodyn* 18:267–275.
<https://doi.org/10.5541/ijot.5000147483>
149. Vakkilainen EK, Ahtila P (2011) Modern method to determine recovery boiler efficiency. *O Pap* 72:58–65. <https://doi.org/10.13140/2.1.3487.3606>
150. Bureska-Joleska L (2017) Influence of coal quality to the boiler efficiency and opportunity for its improvement. *Termotehnika* 43:59–65.
<https://doi.org/10.5937/termoteh1704059b>
151. Park S, Jae J, Farooq A, et al (2019) Continuous pyrolysis of organosolv lignin and application of biochar on gasification of high density polyethylene. *Appl Energy* 255:113801. <https://doi.org/10.1016/j.apenergy.2019.113801>
152. Margellou AG, Lazaridis PA, Charisteidis ID, et al (2021) Catalytic fast pyrolysis of beech wood lignin isolated by different biomass (pre)treatment processes: Organosolv, hydrothermal and enzymatic hydrolysis. *Appl Catal A Gen* 623:118298.
<https://doi.org/10.1016/j.apcata.2021.118298>
153. The Engineering Toolbox (2023) heating values of fuel gases.
https://www.engineeringtoolbox.com/heating-values-fuel-gases-d_823.html. Accessed 27 Jun 2023

154. euronews.next (2023) Energy crisis in Europe: Which countries have the cheapest and most expensive electricity and gas?
<https://www.euronews.com/next/2023/03/29/energy-crisis-in-europe-which-countries-have-the-cheapest-and-most-expensive-electricity-a>. Accessed 27 Jun 2023
155. Christoph G, Thomas T (2022) personal message from the 28th of July, Metadynea, BioBase
156. Trading Economics (2023) EU Natural Gas. In: EU Nat. Gas.
<https://tradingeconomics.com/commodity/eu-natural-gas>. Accessed 27 Jun 2023
157. Inayat A, Ahmed A, Tariq R, et al (2022) Techno-Economical Evaluation of Bio-Oil Production via Biomass Fast Pyrolysis Process : A Review. Front Energy Res 9:1–9.
<https://doi.org/10.3389/fenrg.2021.770355>

6.2 List of figures

Figure 1: Macro to micro-scale structures of wood [5].....	2
Figure 2: Cross section of a tracheid cell of <i>siparuna bifida</i> [8]	3
Figure 3: Cell layers of a plant cell - schematic representation [9]	3
Figure 4: Macromolecular interconnections of cellulose, hemicelluloses and lignin in secondary walls [6].....	4
Figure 5: β -(1-4) glycosidic bond of β -D-glucopyranose units [14]	5
Figure 6: Intramolecular (thin dotted) and intermolecular (dotted) hydrogen bonds of cellulose chains [14].....	6
Figure 7: Schematics of a cellulose microfibril with regions of crystallinity and amorphous structure [14]	6
Figure 8: Molecular structure of a O-acetyl-galactoglucomannan type hemicellulose [20]	7
Figure 9: Molecular structure of a O-acetyl-(4-O-methylglucorono)xylan type hemicellulose [20].....	8
Figure 10: Molecular structure of monolignols and their corresponding fragments in lignin [23]	9
Figure 11: Molecular weight distribution of spruce wood MWL [26].....	10
Figure 12: Structural model of spruce MWL [26].....	11
Figure 13: Simplified flow sheet of a Kraft pulp mill [36].....	14
Figure 14: Reaction mechanism of an alkaline β -O-4 bond break in non-phenolic units [39].	15
Figure 15: Reaction mechanism of a sulfidolytic β -O-4 bond break in phenolic units [39]	16
Figure 16: Competing reactions on a quinone methide [39].....	17
Figure 17: Hypothetical Kraft lignin model structure [43].....	18

Figure 18: Lignin recovery with H ₂ SO ₄ treatment [44]	19
Figure 19: Lignin precipitation with CO ₂ from softwood black liquor with varying pH and IS [46]	19
Figure 20: Specific filtration resistance dependence on precipitation temperatures at pH 9.7 [47]	20
Figure 21: Schematic diagram of a LignoBoost process [44]	21
Figure 22: Simplified flow sheet of a magnesium-based bisulfite process [54]	23
Figure 23: Sulfonation mechanism in acidic sulfite pulping (pH 1-5) [38]	23
Figure 24: Sulfonation mechanism in neutral sulfite pulping (pH 5-7) [38]	24
Figure 25: Possible liginosulfonate structure [55]	25
Figure 26: Schematics of an organosolv process with lignin precipitation [56]	26
Figure 27: Estimation of the structure of lignin isolated from maize cob residues by THF/H ₂ O organosolv pre-treatment [59]	27
Figure 28: Overview of technically relevant lignin separation methods [55]	27
Figure 29: Bio-oil yield and chemical characteristics of pyrolysis products [30]	29
Figure 30: bio-oil from ablative flash pyrolysis [68]	32
Figure 31: microscopic image of SWBR bio-oil at 25°C. a) phase contrast b) polarized light [70]	33
Figure 32: GCMS analysis of corncob pyrolysis bio-oil [69]	33
Figure 33: Laboratory scale fixed bed reactor [74]	34
Figure 34: Bubbling fluidised bed reactor [67]	35
Figure 35: Circulating fluidised bed reactor [67]	36
Figure 36: Rotating cone reactor [67]	37
Figure 37: Ablative reactor [67]	38
Figure 38: Auger reactor [67]	39
Figure 39: Evacuated pyrolysis system [63]	39
Figure 40: Lignin pyrolysis process scheme [81]	42
Figure 41: Representatives of monomeric product groups of lignin pyrolysis [82]	44
Figure 42: GC-MS of lignin pyrolysis biooil [83]	47
Figure 43: Model of an exemplary PL molecule [89]	48
Figure 44: Molecular size distribution of PL measured with MALDI-TOF and SEC	49
Figure 45: BET surface area of oxidative and pyrolytic lignin chars [93]	50
Figure 46: SEM micrographs of kraft lignin and pyrolytic biochar at 250-350 °C [93]	51
Figure 47: SEM micrographs of kraft lignin and pyrolytic biochar at 450-750 °C [93]	52

Figure 48: Biochar structure [97]	53
Figure 49: Dissociation energies of frequent substructures in lignin molecules in kcal/mol [100]	54
Figure 50: TGA analysis of pyrolysis of Japanese cedar MWL [100]	55
Figure 51: α -O-4 and β -O-4 cleavage related radical chain reaction mechanism [100]	56
Figure 52: Representation of opposing primary lignin pyrolysis reactions [102]	57
Figure 53: Monomer substitution changes in the secondary phase of lignin pyrolysis [100] ..	58
Figure 54: Degradation mechanism of radical catechol monomers [100]	59
Figure 55: Molecular size distributions of biooils of different pyrolysis temperatures [104]	60
Figure 56: Biooil yield of lignin pyrolysis with heating rate of 8000 °C/s, residence time of 15-25 ms, and cooling of vapours to -100°C [104]	60
Figure 57: Simplified schematic of possible reactions in lignin pyrolysis [100, 104]	62
Figure 58: LIBRA Lignin pyrolysis setup [87]	64
Figure 59: Blocked feed screws caused by molten lignin. left: Bridgewater et al. [112] right: de Wild et al. [88]	66
Figure 60: Single valve with funnel (left) and push rod (right) [112]	67
Figure 61: Deposits on ESP body [112]	67
Figure 62: Value chain - Lignin pyrolysis	69
Figure 63: Product distributions of three different lignins, pyrolyzed at 500 °C [87]	72
Figure 64: Product distribution of lignins pyrolyzed at 500 °C in a fixed bed reactor [119]	72
Figure 65: Product distribution of PKL and acetylated PKL [121]	74
Figure 66: Lignin pyrolysis after benzyl hydroxyl shielding [122]	74
Figure 67: Product distribution of pyrolysis of MWL, DOL and PSL [122]	75
Figure 68: Molecular size distributions of KL before and after oxidative depolymerisation [123]	76
Figure 69: Correlation between molecular weight and biooil yield in lignin pyrolysis [124]	77
Figure 70: Identified products of EOL and HEOL pyrolysis in H ₂ atmosphere at 850 °C [125]	78
Figure 71: Hydrolytic demethylation [82]	79
Figure 72: Proportions of phenolic groups in biooil [82]	79
Figure 73: Photographs of KL 25 and KL 55 [126]	80
Figure 74: Pyrolysis product distributions of enzymatically treated lignins [128]	81
Figure 75: Relative contents of pyrolysis products of KL, LpH6, LpH4 and LpH2 [129]	82
Figure 76: Pyrolytic product yields of lignins with varying carbohydrate content [130]	83
Figure 77: Reaction mechanism for co-pyrolysis (TSCCP) of lignin and LDPE [74]	84

Figure 78: Product distributions of catalytic pyrolysis experiments [119]	85
Figure 79: Biooil products from catalytic pyrolysis of lignin [119].....	85
Figure 80: Product yields from organosolv pyrolysis in a wire mesh reactor [104]	87
Figure 81: Yield dependencies on residence time in lignin pyrolysis [138]	88
Figure 82: Influencing factors of lignin pyrolysis	91
Figure 83: Lignin precipitation from kraft black liquor with subsequent flash pyrolysis	94
Figure 84: Sankey diagram of calculated process streams in kg/h	96
Figure 85: Mass flows of the modelled process	98

6.3 List of tables

Table 1: Comparison of relevant aspects of technical lignins	28
Table 2: Categorization of pyrolytic processes [65]	30
Table 3: Properties of bio-oil [67]	32
Table 4: Product distributions of lignin pyrolysis.....	45
Table 5: Results of BFB pyrolysis at 500 °C [88].....	46
Table 6: Relative content of chemical groups in lignin biochars [95]	53
Table 7: Product distributions of LIBRA pyrolysis results of wheat straw organosolv lignin [87]	65
Table 8: Challenges of lignin pyrolysis	66
Table 9: Catalysts in use for lignin pyrolysis.....	86
Table 10: Model parameters for LignoBoost process	95
Table 11: Annual chemicals and water consumption	97
Table 12: physical constants of water and wood	99
Table 13: Off gas composition and heating values	102
Table 14: Heat fluxes of modelled unit operations.....	103
Table 15: cost estimation of biooil	105